Delft University of Technology & Norwegian University of Science and Technology

Model-free Positioning Control of a Payload by use of Wires

Thesis report

M.T. Bron

TU Delft NTNU Boskalis

Model-free Positioning Control of a Payload by use of Wires

Thesis report

by

M.T. Bron

in partial fulfillment of the requirements of the degree of
Master of Science in

Offshore & Dredging Engineering at the Delft University of Technology
Technology- Wind Energy at the Norwegian University of Science and Technology

To be publicly defended on Tuesday the 30th of August 2022 at 10:30

Student number TU Delft: 4473051
Student number NTNU: 557417
Project duration: January, 2022 – August, 2022
Thesis committee:

prof. dr. ir. A.V. Metrikine,	TU Delft, chairman
dr. ir. E. Lourens,	TU Delft, supervisor
prof. dr. ir. D.T. Nguyen,	NTNU, supervisor
prof. dr. ir. Z. Gao,	NTNU, co-supervisor
ir. P.M. Jacobs,	Boskalis
ir. R. Beindorff,	Boskalis

TU Delft NTNU Boskalis

Preface

This report represents the final deliverable in order to obtain a degree in Offshore & Dredging Engineering at the Delft University of Technology (TU Delft) and Technology-Wind Energy at the Norwegian University of Science and Technology (NTNU).

For this research, I would like to thank several people. First, I would like to thank my TU Delft supervisor, Eliz-Mari Lourens, for her effort and guidance throughout the project. In addition, I want to thank my chairman, Andrei Metrikine, for his valuable critical feedback. Your sense of humour and cheerfulness always made me feel at ease during the progress meetings. Furthermore, I would like to thank David Domingos for the interesting and useful discussions.

This research project is performed under the guidance of Boskalis. From Boskalis, I would first of all like to thank Peter Jacobs. Peter, as my direct supervisor, your help and feedback were essential for this study. For you, it was the first time supervising a MSc thesis student, but this was unnoticeable. You were always available for questions and helped me when needed. You have a critical eye which led to exciting and enjoyable discussions during our weekly meetings. I would also like to thank Ruud Beindorff for his guiding role as co-supervisor. I am thankful for your positivity, constructive criticism and support.

From the NTNU, I would like Dong Trong Nguyen and Zhen Gao for their guidance. Both of you have supported me during my literature study in Trondheim, and I appreciate how you continued showing this commitment during my period in the Netherlands. Zhen, you always gave me helpful feedback on the content and the structure of my work. One year ago, I barely had any knowledge of control engineering, and one of my thesis goals was to improve my knowledge in this field. Therefore, I would like to thank Dong; your passion and great expertise in control engineering were vital for this thesis.

Finally, I would like to thank my family, Emilie, fellow EWEM students, and everyone that has supported me throughout these years.

M.T. Bron
Delft, August 2022

Abstract

With the highly increased interest in offshore wind turbines and their technologies, the sector has witnessed rapid development in the past decade. For installed offshore wind turbines, there has been a lot of research conducted in the field of aero-, hydro- and structural dynamics, wind turbine-control, operation & maintenance, foundations and moorings. The research field of offshore wind turbine installation is on the other hand relatively new, and the studies regarding this topic are limited. The lifting of heavy objects is one of the most commonly performed offshore installation operations and has become more challenging due to the trend of increasingly larger and heavier payloads. Especially for substantial waves, the pendular motions of the payload may cause operations to be halted.

This thesis performs a study on a positioning control strategy for a complex lifting control scenario, i.e., position-keeping of a complex-shaped 6-DOF payload using a floating vessel equipped with multiple tugger winches. As the system is highly complex and contains non-linear and time-varying dynamic phenomena, it is an impracticable task to formulate a model that meticulously describes the actual system. For this reason, a fully integrated simulation model in Orcaflex has been used to capture the non-linear dynamic behaviour of the system.

The preassembly operation of a Jacket Lifting Tool on a monohull vessel is adopted as a case study to verify the proposed control strategy. Two scenarios are considered -installation and decommissioning- for which an outrigger configuration is used to position the tugger winches. Due to the difference in setpoint (i.e. the desired position) in the two scenarios, the proposed controller is solely implemented in the decommissioning scenario. Damping tuggers, the current state-of-the-art when it comes to motion mitigation, is considered suitable in the installation scenario.

The proposed controller does not consider the state–space equations of the system and only relies on real-time motion and tension measurements of the vessel and suspended payload. In addition, the controller considers the system's velocity tension and power limitations. The controller's impact is evaluated based on the positional error and verified by the peak reduction in the power spectral density spectra of the simulations. Despite its simple form, results show a significant reduction in the positional error, and therefore the possibility to extend the working conditions of the installation vessel. To improve the controller's performance it is recommended to involve derivative control, consider payload motion prediction and to optimise the tugger winch configuration. For further studies, experimental testing is needed to verify the effectiveness of the control scheme as it could appear that the controller does not exhibit similar performance in the real system. However, it is deemed unlikely that the latter would occur as a sensitivity study regarding measurement error indicates a stable response of the controller.

Contents

Nomenclature

Abbreviations

Abbreviation	Definition
BL1	Bokalift 1
DoF	Degree of Freedom
DP	Dynamic positioning
JLT	Jacket Lifting Tool
LC1	Load Case 1
LC2	Load Case 2
SWL	Safe Working Load
STD	Standard Deviation

Symbols

Symbol	Definition	Unit
A	amplitude damping profile	[kN]
b_c	critical damping coefficient	[$\frac{\text{kN}\cdot\text{s}}{\text{m}}$]
d	damping coefficient	[-]
e_l	length error	[m]
e_p	positional error	[m]
e_T	tension error	[kN]
f	wave frequency	[Hz]
f_p	spectral peak frequency (=$\frac{1}{T_p}$)	[Hz]
g	gravitational constant	[m/s^2]
k	stiffness coefficient	[-]
$k_{p,l}$	proportional gain (length error)	[-]
$k_{p,T}$	proportional gain (tension error)	[-]
K_i	integral gain	[-]
l	length of tugger line	[m]
l_d	desired length of tugger line	[m]
m	mass	[kg]
H_s	Significant wave height	[m]
i	index of a tugger winch	[-]
p_0	position of payload bottom centre	[m]
p_b	position of the base point	[m]
p_c	position of the connecting point	[m]
p_{cd}	desired position of the connecting point	[m]
p_d	desired position	[m]
P	power	[W]
r	winch radius	[m]
R	range damping profile	[m/s]
S_{JS}	JONSWAP wave spectrum	[m^2/Hz]
T	tension	[kN]
T_d	desired tension	[s]
T_p	wave peak period	[s]
T_w	wave period	[s]

Symbol	Definition	Unit
T_z	zero-upcrossing period	[s]
u	winch velocity	[m/s]
w	work	[MJ]
Δz_{ct}	vertical crane tip displacement	[m]
α	slope (tension-velocity profile)	[(kn·s)/m]
α_{JS}	Generalised Philip's constant	[-]
ϵ	strain $(= 5 \cdot \left(H_s^2 f_p^4 / g^2\right) \cdot (1 - 0.287 \ln \gamma) \cdot \pi^4)$	[-]
θ	wave direction	[deg]
σ	spectral width parameter	[-]
γ	Peak enhancement factor	[-]
ω	winch rotation speed	[rad/s]
ω_n	natural frequency	[Hz]
ζ	damping coefficient ratio	[-]

List of Figures

List of Tables

1 Introduction

In the 2015 Paris Agreement on climate change, 195 countries agreed to limit the global average temperature rise to a maximum 2 °C above pre-industrial levels. In addition, all countries concurred to bring greenhouse gas emissions to zero within the second half of the 21st century. Energy production is responsible for 73.2% of global greenhouse gas emissions and will be the focal area for climate change mitigation efforts [42]. At the same time, the global energy demand has been increasing over the last decades due to an increase in world population in combination with technological and economic developments [20]. This trend is likely to continue in the coming years. The total final energy consumption is estimated to increase by 1.4 - 1.7% per year from 2020 to 2030. The exact percentage will largely depend on the global energy efficiency and electrification developments. In order to reach the climate targets and meet the global energy demand, new energy sources are to be implemented. The shift from hydrocarbons to renewable energy as the primary energy supplier is known as the energy transition. One of the most promising renewable energy sources is offshore wind energy. Offshore wind energy offers many benefits in comparison to onshore wind. For example, no horizon pollution, higher wind speeds and less fluctuating amounts of energy are produced. Furthermore, offshore space is practically unlimited, making it suitable for developing large (>100 turbines) wind farms. This allows for large-scale development of renewable energy, a goal many European countries pursue.

1.1. Lifecycle of an offshore wind farm

The lifecycle of a OWF consist of 5 main stages:

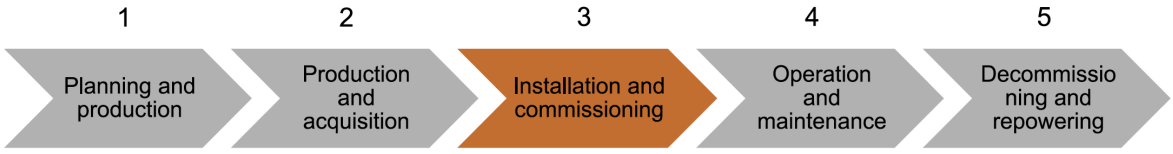

Figure 1.1: Lifecycle stages of an OWT [23]

1. **Planning and production**
   This can also be called the ”scoping” stage. The site selection and preparation of a formal consent application take place. The metocean data and seabed conditions are analysed, and an environmental impact assessment induced by the chosen wind turbine type is carried out.
2. **Production and acquisition**
   The second stage refers to the manufacturing/production of the WTs, moorings and cables.
3. **Installation and commissioning**
   In this stage, the installation of the OWTs takes place. This includes the installation of the cables, foundation, tower, nacelles and blades. Depending on the chosen installation method, installation vessels and handling equipment are needed. The most suitable installation method for an OWF depends on the foundation types, site conditions, and available equipment [23].

4. **Operation and maintenance**
   Stage 4 includes health monitoring, inspection and maintenance of the OWF. The lifetime of wind turbines is approximately 20 years. At the end of this lifespan, the developer must decide whether to decommission or re-power the OWF.
5. **Decommissioning and repowering**
   In the last stage, the OWF is decommissioned (complete removal of the OWF) or re-powered. Re-powering means that the wind turbines get updated by either replacing older turbines with new ones or swapping out the parts in the original turbines with new, more efficient technologies. If they are re-powered, the cycle starts again.

This study will focus on third stage: *Installation and commissioning*.

1.2. Offshore wind farm installation

An offshore wind farm installation includes the installation of the cables, foundation, tower, nacelles and blades. Depending on the chosen installation method, installation vessels and handling equipment are needed. The most suitable installation method for an offshore wind farm strongly depends on the foundation types, site conditions, and available equipment [23]. This study will focus on the foundation installation with the Bokalift 1, a heavy lifting vessel of Boskalis. More details and information about this vessel is given in Appendix F.

The foundation used for offshore wind farms mostly depends on the water depth of the specific site [47]. Bottom-fixed offshore wind turbines dominate the current offshore wind energy market [22] where monopiles and jackets are the most used foundations. Monopiles are, in general most cost-effective for shallow waters (<30m) and are the most used substructure type in the offshore wind industry (80.5%). At medium water depths (30-60m), monopiles become economically and/or technically infeasible. At medium water depths, multi-member support structures are used. These come in a variety of designs, depending on the application. The most commonly used multi-member support structure is the jacket foundation. The production costs of multi-member support structures are relatively high. They are composed of many tubular elements that are (generally) connected in the welded nodes. On the other hand, the substructure requires relatively little steel to manufacture. Despite storage and logistics challenges [23], jacket-supported OWTs are the second most used foundation (9.9%), and its share has been increasing in the past years [48]. The higher share of jacket foundations follows the trend of offshore wind farms being placed in deeper waters. At the end of 2015, the average water depth of grid-connected wind farms was 27.1m. In 2020 this average increased to 36m. One of the reasons for this is the better wind conditions further offshore.

1.3. Jacket foundation

A *jacket foundation* is a multi-membered construction generally built from three or four legs connected by bracing, see Figure 1.2. Jacket foundations used for OWTs are based on designs adapted from the offshore petroleum industry according to Manwell [30]. The top of the jackets features a transition piece that can be connected to the shaft of an OWT. Jackets are fabricated on shore, brought to the site, and lowered, by crane, into place. The legs of the substructure can be attached to small diameter suction buckets or soil piles to anchor the structure to the seabed [47]. Because of the ”see-through” appearance of the substructure, they are less sensitive to hydrodynamic loads than other substructure types. The cross-braced structure and its large footprint result in a stiff foundation type.

Figure 1.2: Jacket foundation

1.3.1. Seabed placement

A jacket substructure can be fixed to the seabed by three methods: pre-pile driving, post-pile driving or suction buckets.

Pre-pile driving
The most commonly used jacket foundation installation is the *pre-pile installation* method, shown in Figure 1.3. The process starts with stabbing the anchor piles into an installation frame, a template structure that ensures that the piles are installed vertically, in the right place and distance from each other. Then the hammering procedure starts. This procedure drives the piles into the soil. The jacket is subsequently lifted from a barge or crane vessel. In order to make optimum use of the space on the deck, jackets are sometimes transported horizontally by a barge. In that case, the jacket must be upended first (unlike Figure 1.3). Afterwards, the substructure is lowered and mated with the pre-installed piles. To ease the mating, the legs of jackets have different lengths. The piles' inclination, position and heading are essential factors that influence successful mating. Underwater sensors are usually used to provide real-time decision support [23]. Finally, the annulus is filled with grout and left to cure before installing the wind turbine. The annulus is the area between two concentric objects, in this case, between the anchor pile and the pile sleeve in the jacket.

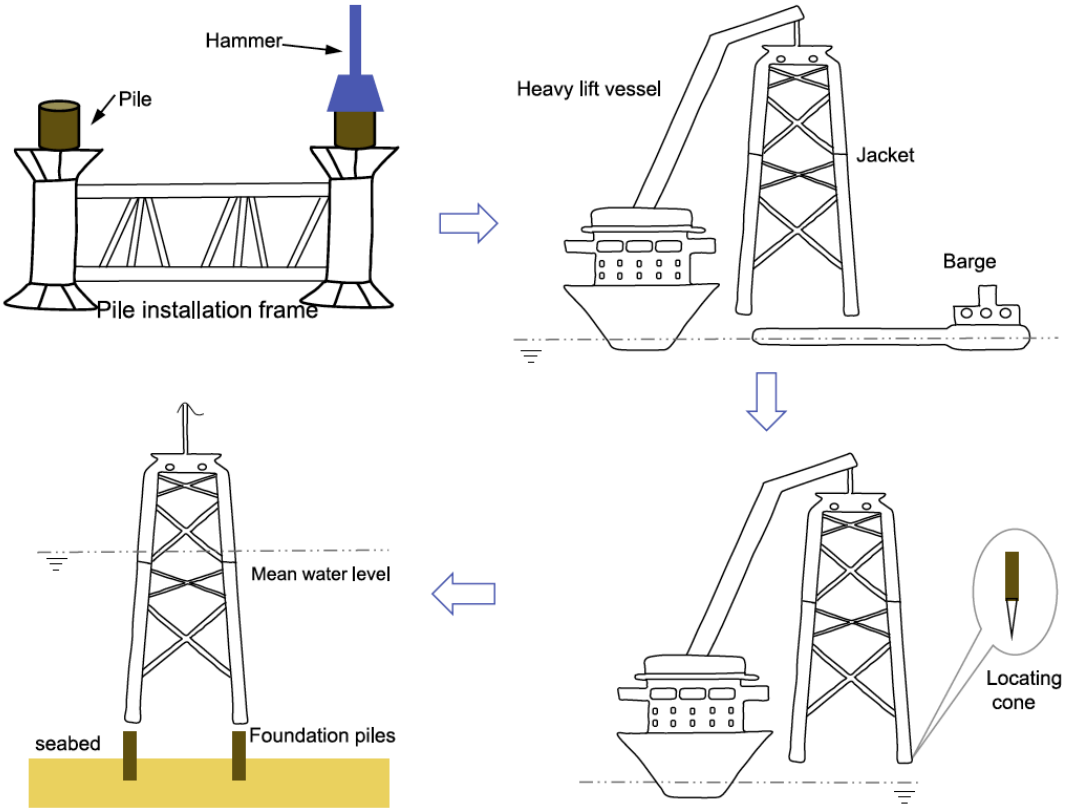

Figure 1.3: Key steps of a jacket installation (pre-pile driving) [23]

Post-pile driving
Post-pile driving method is an alternative way to fix the jacket to the seabed. Foundation piles are used here as well, but as the name implies, they are now hammered into the seabed after placing the jacket. The pin piles are driven (or lowered into pre-drilled sockets) through a sleeve on the jacket legs. Post-pile driving seems more convenient than pre-pile driving as it would require fewer installation steps. Nevertheless, pre-piling is used more often since it has the advantage of decoupling the piling and jacket installation, reducing the vessel costs to be used for piling and maximising the use of deck space of the main jacket installation vessel [6].

Suction bucket
A *suction bucket* is a well-known technology in the oil and gas industry that potentially lowers the installation costs because less equipment and no pile driving is needed [6]. They are normally made from steel or concrete and installed using the principles of suction. The pressure difference between the

inside of the bucket and the water leads to the structure being installed without the use of mechanical force. The buckets can be (re)moved by pumping air back into them. This technology is currently a solution for soil conditions unsuitable for monopiles. An advantage of using suction buckets for a jacket is that the jacket can be installed in a single lifting and assembly process, resulting in a reduced construction time and the associated costs. In addition, suction buckets produce much less underwater noise during installation than pile driving. The noise produced by pile driving can reach such high levels that marine animals are at risk of disturbance, injury, or even death [3]. A downside is that it can only be installed for certain soil conditions, preferably sand or clay that is neither too dense or hard nor too loose or soft.

Suction buckets have not been widely used with offshore wind turbines so far. Nevertheless, they are, according to Oh et al.[37] the most promising solution and will become more common in the future. Besides jackets, they can also be applied as part of a mooring system for floating support structures.

1.3.2. Jacket Lifting Tool

Regardless of which seabed positioning method is used, a jacket must be lifted from the vessel into the water when installing the jacket. In a jacket decommissioning operation, the lifting operation can be thought of contrariwise. A Jacket Lifting Tool (JLT) is used for jacket lifting and is the coupling mechanism between the crane hook and the jacket. It is used during loading, unloading, installation and (could be used for) decommissioning of jacket foundations. The JLT is remotely controlled, which ensures no need for the crew to access the top of the jacket. The tool has six clamps that will jointly lift the substructure. To reduce tilt, the JLT is equipped with a Center of Gravity (CoG) adjustment system [14]. A pre-mounted guide frame on the jacket flange is used for the mating process of the JLT and the jacket. The guiding frame ensures that no clamps of other fixtures are required. In addition, precision will be maintained regarding the alignment of the tool relative to the jacket.

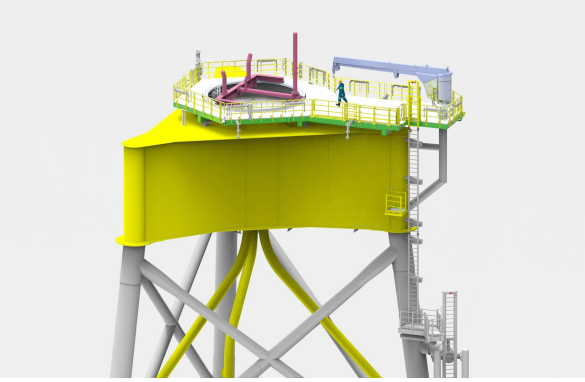

Figure 1.4: Guide frame is pre-mounted on jacket flange [14]

Figure 1.5: JLT attached to jacket [14]

1.4. Problem Definition

Although the overall installation duration varies depending on the project specifications, a jacket's installation time is generally longer compared to a monopile installation, as it involves more steps. Floating crane vessels have the potential to reduce the installation time compared to conventional jack-up vessels significantly. However, a monohull vessel is much more sensitive to the wave motions, which can result in undesired excitation of the lifted object. Especially when the system is exposed to a sea state with a wave frequency close to the resonance frequency of the pitch and roll mode, the rotational motions of the vessel become significant. The same applies to the pendular motions of the payload. Boskalis received reports of lifting operations of 'relatively light' payloads (<200t) causing problems because of severe pendular motions. These motions can entail safety risks and thereby negatively affect the workability of the operation. An example of such a lightweight payload is the Jacket Lifting Tool (JLT). This study will focus on the lifting operation of JLT with a floating crane vessel.

Tugger winches can be utilised to limit the pendular motion of a suspended payload. However, as

a tugger line can only provide nonnegative tension in one direction, the complete control of the movements of a suspended payload by tugger lines is only possible if the tugger lines come from all six degrees of freedom relative to the payload. For example, see Figure 1.6; one can observe two tugger lines connected to the JLT before its mated to the jacket. In this case, if the JLT is moving towards the tugger lines, the tugger lines cannot compensate for this. Furthermore, the tugger winches are commonly situated on deck and the vessel's crane. As the crane usually rotates during a lifting operation, it could easily entangle obstructions on the deck.

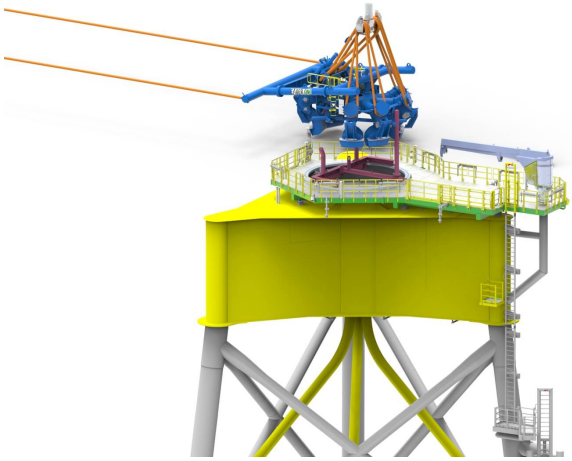

Figure 1.6: JLT with two tugger lines attached [14]

Multiple studies have been carried out to actively mitigate the pendular motions of a suspended payload with the use of active tugger winches. Several *model-based* control methods for designing a anti-swing controller have been developed, such as PID control [45], LQR control [1], robust adaptive control [39], neural adaptive control [49] [27], and fuzzy sliding mode control [35]. One of the most important prerequisites of model-based control is the existence of a detailed mathematical description of the system in question. In other words, the controllers are designed as if the model of the system is exact. This point limits the flexibility of model-based controllers as they are most likely to perform poorly under new circumstances. The system to be controlled, a suspended payload (i.e. the JLT) coupled to a floating crane vessel, is highly complex and contains nonlinear and time-varying dynamic phenomena. Madadi [29] indicates that "in practice often the mathematical description of the system can not be given easily or modelled accurate enough". All the earlier mentioned studies therefore used simplified models. As a consequence, generality of the systems is lost, and the controllers become impracticable to implement in the real system.

To summarise, monohull crane vessels are sensitive to wave excitation. During a lifting operation, this could lead to undesired pendular motions of a payload, resulting in a less efficient and more dangerous operation. The use of tugger winches is used to limit these motions. Many studies regard active tugger control as a valuable addition with much potential. However, tugger lines only work in one direction, and offshore operations entail challenging configuration constraints. In addition, offshore lifting operations are complex dynamic processes which operate under different conditions, including system variations and sea-state alterations. Using model-based control in a complex system causes the model to be an approximation of the actual system. The mismatch between the real system and model, the so-called model error, may cause the performance of the control scheme to deteriorate.

1.5. Objectives

Model-free control methods are utilised as an efficient alternative to avoid the demanding and complex modelling procedures that come with model-based control described in the previous section. Model-free control does not require an accurate mathematical model of the system (i.e. state-space equations). More information about model-free control is given Section 2.2.

The main objective of this thesis is to propose a model-free control scheme for tugger winches to reduce

the undesired (pendular) motions of a payload during a lifting operation. The goal of the control scheme is to keep the suspended payload at the desired position while considering the vessel's response to first-order wave loads and the operational limits of the system. An offshore JLT lifting operation by the Bokalift 1 (BL1), a heavy lifting vessel of Boskalis, is adopted as a case study, in which two scenarios are considered: installation and decommissioning.

To achieve the objective, the following tasks are arranged for each load case:

- Integrate a model-free control scheme in the simulation model of the JLT lifting operation where multiple actuators, in the form of tugger winches, are used to keep the payload at its desired position.
- Propose a configuration of multiple tugger winches suitable for the lifting operation and its corresponding control scheme.
- Analyse, tune and improve the model-free control schemes.
- Identify the effects of the operational winch limitations on the system's performance.

1.6. Research Questions

To fulfil the main research objective, the following research question is stated:

What is the impact of the proposed model-free control strategies on the dynamic behaviour of a complex-shaped 6-DOF payload?

The sub-research questions are the following:

- What are the relevant motion modes of the system, and to what extent do they influence the positional error?
- What are the system's limitations, and how do they affect the tugger winch performance?

1.7. Methodology

This section describes the approach to answer the research questions.

The relative position between the JLT bottom centre and foundation top centre affects the successful operational rate (i.e. workability), and the corresponding relative velocity influences the impact force. Therefore, the target is to achieve an anti-swing control scheme that stabilises the payload in the air above the jacket flange centre and maintains the position to achieve a smooth mating operation. The standard deviation (STD) of the positional error (e_p) is employed as the criteria to evaluate the performance of the proposed control strategy. Since the STD of the position is always proportional to the STD of the velocity and motion maxima, it affects both the success rate and impact force of an operation [24]. The e_p is defined as

$$e_p = |p_d - p_0| = (x_d - x_0)^2 + (y_d - y_0)^2 \tag{1.1}$$

where p_d is the desired position in the horizontal plane, i.e. top of the centre of the jacket flange, and p_0 is the horizontal position of (the bottom centre of) the JLT, see Figure 1.7.

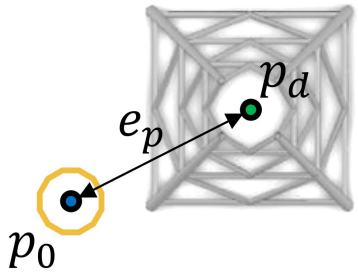

Figure 1.7: Illustration of the positional error (top view)

First, the fundamental introductory knowledge on offshore lifting, environmental loading of offshore structures and motion control is reviewed, which can be found in the Appendix. Next, the dynamics of the uncontrolled system are analysed (time and frequency domain). Then, a tugger winch configuration is proposed, which considers the tugger winch problems described in the Problem Definition (Section 1.4). As all real control systems are non-linear, the system is accessed in the time domain. A state-of-the-art Orcaflex model of the proposed configuration is used to efficiently capture the inherently non-linear response of the system. A suitable model-free controller is integrated into the model by the use of a Python script. As OrcaFlex uses embedded Python, it can execute an external Python code during an OrcaFlex time-domain simulation. Time domain simulations in a diverse range of dynamic marine systems are conducted to tune and evaluate the effectiveness and sensitivity of the proposed *control strategy*[1]. The control strategy is to be tuned in a data-driven iterative way. Finally, the impact of the control strategy is determined by comparing the dynamics of the model with and without the proposed control strategy and the current state-of-the-art of pendular motion mitigation. The results are verified with frequency response analysis using the Fast Fourier Transform (FFT) method to obtain the power spectrum density (PSD). The power spectrum is a measure of how much of the energy associated with the time-dependent behaviour (such as oscillations) is stored in each mode. Finally, the stability of the controller is evaluated by performing a sensitivity study regarding measurement error.

[1] model-free control scheme + tugger winch configuration

1.8. Report structure

The outline of this thesis is as follows:

- Chapter 1: The current chapter discusses the overall overview and scope of this thesis, including the main challenges and problems.
- Chapter 2: The second chapter provides a review of tugger winch dynamics. In addition, it describes the two different model-free control approaches used in this study.
- Chapter 3: The third chapter the thesis provides detailed insight into the setup of the Orcaflex models.
- Chapter 4: This chapter focuses on the dynamics of the uncontrolled system. The vessel and payload's motions are analysed separately. In addition, a modal analysis is performed to verify the motions observed in the time domain.
- Chapter 5: This chapter introduces the proposed control strategies. The configuration and control scheme are discussed separately. Moreover, the impact of the tugger winches on the motion modes is analysed.
- Chapter 6: The sixth chapter validates the effectiveness of the control strategies. In this chapter, various time-domain simulation results are compared with the uncontrolled scenario.
- Chapter 7: Finally, in the last chapter, the summary and conclusion of this study are discussed. Furthermore, final remarks and recommendations for future work are outlined.

This thesis research is conducted under Boskalis Offshore Heavy Lifting (BOHL), a subsidiary of Boskalis specialised and involved in installing and decommissioning offshore structures. The expertise of the team members of this subsidiary will provide guidance to fulfill the research objective.

2

Tugger winch control

A tugger winch is commonly used marine equipment that uses a drum to wind wire rope or chain to tow or lift heavy objects. For example, to haul in and haul out the anchor lines. Tugger winches are usually installed on the ship's cargo deck or at the crane. A simplified winch illustration is given in Figure 2.1.

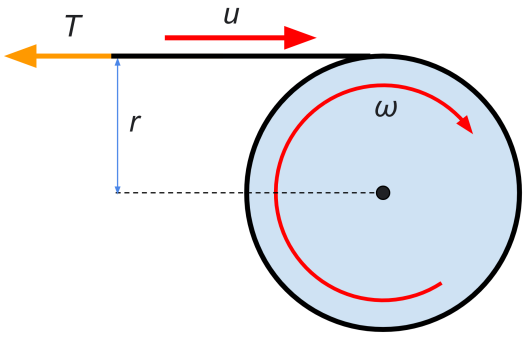

Figure 2.1: Simplified winch illustration

When hauling in, the winch is limited by its power capacity. The power in Watt of the winch is given by:

$$P = T \cdot u \tag{2.1}$$

where T is the tension on the winch and u is the winch's velocity. Paying out does not require any power of the winch. In this case, the winch is limited by the capacity of the angular velocity. The maximum velocity of the winch depends on the maximum angular velocity (ω) and radius (r) of the winch:

$$u = \omega \cdot r \tag{2.2}$$

A tugger line can only provide nonnegative tension and therefore only resist tension rather than compression. In the case of horizontal motions of the crane tip, the payload will follow and be accelerated by the tugger lines. Therefore, the load in the tugger line is proportional to the mass of the payload. A slack-taut alternating phenomenon may occur in a tugger line when the attached object's motion is drastic. This phenomenon is unfavourable as it will significantly increase the dynamic tension in the line. Consequently, it increases the wear and tear of the line and the risk of failure. An instantaneously increased dynamic tension is defined as a *snap load* [40].To avoid snap loads, the tugger lines have a minimum tension greater than zero. The maximum allowable load in a tugger winch can be limited by the winch, lines, connecting point or other system parts. The limiting factor therefore differs per scenario.

2.1. Tugger lines

For a tugger winch system, either steel wire ropes or synthetic ropes can be used, depending on the type of operation. One can either use natural or synthetic fibres. Today, most ropes are made from synthetic fibres [13]. The threads are opposite to the strands to prevent the unlaying of ropes, see Figure 2.2. Certain ropes have a sleeve to keep the strands in the core together. This is makes it possible that the strands in the core can be arranged in parallel fashion, resulting in maximum tensile strength. Furthermore, the wear resistance of the sleeve (usually polyester) must be higher than the wear resistance of the core. Steel wire ropes on ships are used for station keeping (moored to the seabed or a jetty), lifting operations and niche-specific operations (for example, fishing and dredging). High-grade cables, polyamide, polyester, polyolefines and steel wire ropes are cable types commonly used on offshore vessels according to Dokkum [13]. In Appendix C, more details about these materials are given. Apart from the steel wire rope, all other wire ropes are made of synthetic fibres. Synthetic fibres are man-made fibres consisting of polymers that do not occur naturally, but are produced entirely in a chemical plant or laboratory. Usually, polymers are by-products of petroleum or natural gas. The problem with polymers is the ageing when exposed to light (mainly UV) and oxygen, causing loss of stiffness, strength and toughness, discolouration, and loss of gloss. This can be countered by additives: antioxidants, light stabilisers and fluorescent whitening agents.

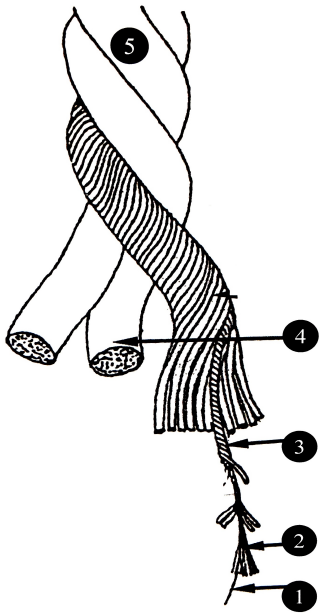

Figure 2.2: Rope composition (1 = Fiber, 2 = Thread, 3 = Rope yarn, 4 = Strand, 5 = 3-Strand rope) [13]

An important characteristic of polymeric materials is their viscoelastic behaviour. When mechanical stress is applied to a viscoelastic material such as a polymer, parts of the long polymer chain change positions. This movement or rearrangement is called *creep* and builds up a back stress [31]. The elastic energy is stored per unit volume [5]:

$$U = \int_0^{\sigma_{\text{max}}} \sigma d\varepsilon \approx \frac{1}{2} \frac{\sigma_{\text{max}}^2}{E} \tag{2.3}$$

When the back stress is the same magnitude as the applied stress, the material no longer creeps. When the original stress is removed, the accumulated back stresses will cause the polymer to return to its original form. The unloading curve differs from the loading curve, resulting in a hysteresis loop. The difference between the two curves represents the amount of energy that is dissipated during the load cycle, see Figure 2.3. The energy is lost as heat (dotted area) [26]:

$$\Delta U = \oint \sigma de \tag{2.4}$$

The damping, or mechanical loss coefficient is therefore:

$$d = \frac{\Delta U}{2\pi U} \tag{2.5}$$

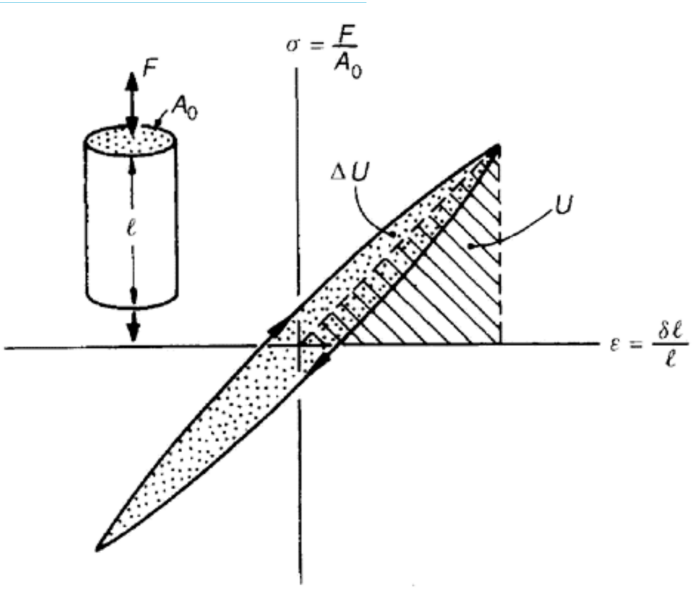

Figure 2.3: The loss coefficient d measures the fractional energy dissipated in a stress-strain cycle [5]

The Kelvin-Voigt model can be used to explain the creep behaviour of polymers [17]. The model consists of an elastic spring (Hooke's law) and viscous dashpot (Newton's law). Figure 2.4 and 2.5 illustrate a linear spring and viscous dashpot, and their corresponding stress-strain relations are given by Equation 2.6 and 2.7.

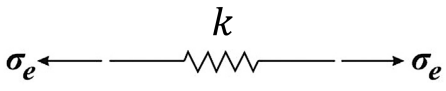

Figure 2.4: Linear spring

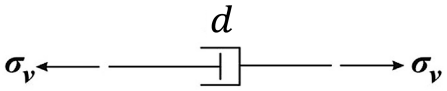

Figure 2.5: Dashpot

$$\sigma_e = k \cdot \epsilon_e \tag{2.6}$$

$$\sigma_v = k \cdot \epsilon_v \tag{2.7}$$

In which σ represents the applied stress and ϵ the captured strain, k the linear spring's stiffness and d the dashpot's damping coefficient. Elastic and viscous behaviour is denoted by the subscripts e and v, respectively. The spring and dashpot are connected in parallel, and the Kelvin-Voigt model can be evaluated as presented in Equation 2.8.

$$\begin{aligned} \varepsilon &= \varepsilon_e = \varepsilon_v \\ \sigma &= \sigma_e + \sigma_v \end{aligned} \tag{2.8}$$

Substituting Equation 2.6 and 2.7 into Equation 2.8 results in the following equation for the total stress of the model based on its component's coefficients [17]:

$$\sigma = k\varepsilon_e + d\frac{\mathrm{d}\varepsilon_v}{\mathrm{d}t} \quad \xrightarrow{\varepsilon=\varepsilon_e=\varepsilon_v} \quad \sigma = k\varepsilon + d\frac{\mathrm{d}\varepsilon}{\mathrm{d}t} \tag{2.9}$$

As mentioned before, tugger lines often consist of polymers. For this reason, the tension of a tugger line is described similarly:

$$T = k\varepsilon + d\frac{\mathrm{d}\varepsilon}{\mathrm{d}t} \tag{2.10}$$

The strain (ε) can be obtained by determining the difference between the unstretched (l_0) and stretched length (l). The damper in the given wire model works to reduce the tension, which means its direction is opposite to the relative elongation changing rate.

Taking the time derivative of ε gives the wire strain rate ($\frac{\mathrm{d}\varepsilon}{\mathrm{d}t}$):

$$\varepsilon = \frac{l - l_0}{l_0} \quad \rightarrow \quad \frac{\mathrm{d}\varepsilon}{\mathrm{d}t} = \frac{1}{l_0}\left(\frac{\mathrm{d}l}{\mathrm{d}t} - \frac{\mathrm{d}l_0}{\mathrm{d}t}\right) \tag{2.11}$$

where the length of the wire (l) can be obtained by the positions of the connecting point (p_c) and base point (p_b):

$$l = |p_b - p_c| \tag{2.12}$$

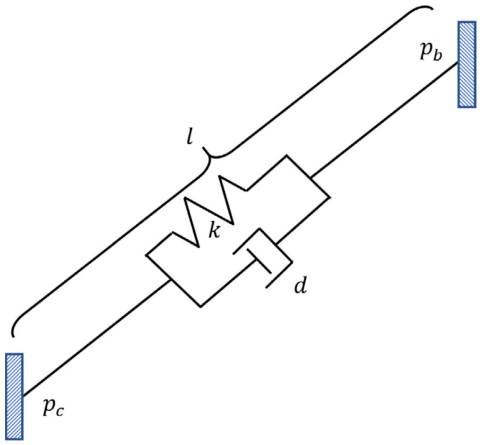

Figure 2.6: Diagram of a lift wire.

2.2. Model-free control

Model-free control is an alternative technique to control complex systems in which the accurate mathematical model of the system (i.e. state-space equations) is not required. For this reason, model-free control approaches can be a suitable solution to pursue high performance using solely the data collected from the input and output of the system. The key advantage of this approach lies in the fact that the unknown parts of the system, which might be highly nonlinear and time-varying, are taken into account [34].

To address undesired motions of the payload, actively controlled tugger winches with the use of a model-free control scheme will be used. Two relevant model-free control schemes have been used and modified to achieve this goal. One controller is the current state-of-the-art for pendular motion mitigation in offshore lifting operations. The control scheme is proposed by Meskers and Dijk [32] and aims to damp out energy from the pendular movement. In this study, tuggers controlled by this control scheme will be referred to as *damping tuggers*. The other control scheme proposed by Ren et al. [41] can be used to keep or bring a mass to a specific position. Tuggers controlled by Ren et al.'s control scheme will be referred to as *positioning tuggers*. In LC1, the damping tuggers will be used. For LC2, a modified combination of both control schemes is proposed. The damping control scheme is a proportional controller and the positioning control scheme is a proportional-integral controller. More information about these types of controllers can be found in the Appendix B.

2.2.1. Damping tuggers

The swinging motion of a lifted object is a resonance problem and can be reduced by adding damping, which the damping tuggers can achieve. Meskers and Dijk [32] performed analytical and experimental tests where the effectiveness of this concept was proven. This proportional controller monitors the tension, determines the tension error (e_T) and tries to minimise this error by proportionally paying-in or paying-out the tugger line with a certain winch velocity (u). e_T is the difference in actual tension (T) of the wire and the desired (pre-)tension (T_d):

$$e_T = T - T_d \tag{2.13}$$

The line is paid-out when e_T is positive and paid-in when negative. As a result, the tension fluctuates around the desired tension. The tension fluctuation causes dissipation of energy and thus dampens the payload's motion. In Figure 2.7, an overview of the damping control system can be found.

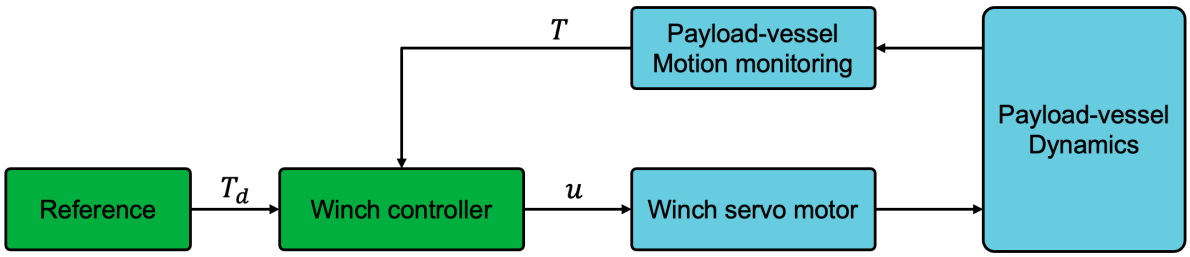

Figure 2.7: Overview of the damping controller

The magnitude of the controller's output value (i.e. winch velocity) depends on the tension-velocity profile. Meskers and Dijk [32] used a linear profile in their research, which will also be used for this study. The profile depends on three variables; the pre-tension (T_d), amplitude (A) and range (R). An example of a tension-velocity profile with all notations is illustrated in Figure 2.8. The higher A, the longer the controller allows tension build-up. Therefore, A should not be higher than the pre-tension, as it would cause the lines to fall slack. As the tension increases, the tugger lines provide a more significant force opposite to the direction of the payload's pendular motion. In addition, more strain (ε) will take place, so more energy can be dissipated due to creep (see Figure 2.3). The maximum allowable tension of the system limits A and can be found by Equation 2.14.

$$A_{max} = \frac{T_{max} + T_{min}}{2} \tag{2.14}$$

When keeping A constant, an increase in range (R) leads to an increase in the system's responsiveness (i.e. a higher u for a given e_T). The optimal value depends on the vessel and payload dynamics and can be found from time domain simulations.

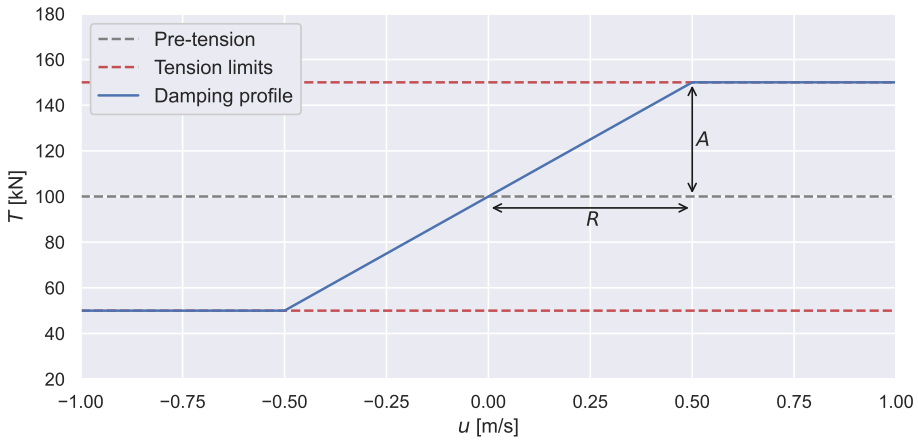

Figure 2.8: Overview of a random linear tension-velocity profile(R=0.5m/s, A=50kN)

A and R together determine the slope of the tension-velocity profile, hence the proportional gain ($k_{p,T}$) of the controller. When the tension reaches its limits, the winches switch to constant tension (CT) mode. The pulling force of the line is measured by a load cell and is monitored by a control system. If this value differs from the desired value, the winch will either haul in or haul out the line to maintain the desired value. A perfect CT mode keeps a constant tension in the lines, ensuring minimal effects on the system's dynamics [32].

$$u_{=} \begin{cases} \text{CT-mode} & \text{for} \quad T < T_{min} \\ e_T \cdot k_{P,T} & \text{for} \quad T_{min} \leq T \leq T_{max} \\ \text{CT-mode} & \text{for} \quad T > T_{max} \end{cases} \tag{2.15}$$

$$k_{P,T} = \frac{R}{A} \tag{2.16}$$

The unit of $k_{P,T}$ is $\frac{\text{m}}{\text{kN}\cdot\text{s}}$, hence indicating the inverse of the actual damping (b) induced by the tugger lines. In other words, $k_{P,T}^{-1} = b$. The damping coefficient (ζ) can express the amount of damping the tuggers exert on the system [2]. For a damped harmonic oscillator with mass m, damping coefficient c, and spring constant k, the damping coefficient can be expressed by:

$$\zeta = \frac{b}{b_c} = \frac{1}{b_c \cdot k_{P,T}} \tag{2.17}$$

in which the critical damping (b_c) can be obtained by:

$$b_c = 2\sqrt{km} = 2m\omega_n \cdot \tag{2.18}$$

It should be noted that the unit of the natural frequency (ω_n) is in rad/s.

- A *critically damped* system has a ζ of 1. It represents the minimum amount of damping which results in a displaced system returning to its original position without oscillation. It therefore has no overshoot and has the fastest rise and settle time.
- If ζ>1, the system is classified as *overdamped*. It also has no overshoot but has slower rise and settle times. This may be desired, or it may prove to be problematic. An overdamped system will return to its ideal state more slowly, which can benefit systems where overshooting is problematic.
- A 0<ζ<1 is referred to as an *underdamped* system and exhibits a fast rise time, but it overshoots the ideal state. The magnitude of the overshooting oscillation will diminish over time until it is no more. Therefore it may take some time for the system to settle. However, with the right amount of damping, it can settle faster than critically damped or overdamped systems. Therefore an overdamped system can be beneficial if the goal is achieving a stable state quickly. However, if the overshooting causes problems, an underdamped system is not recommended.

Examples of transient responses for all three cases of damping (critically damped, overdamped and underdamped) are illustrated in Figure 2.9.

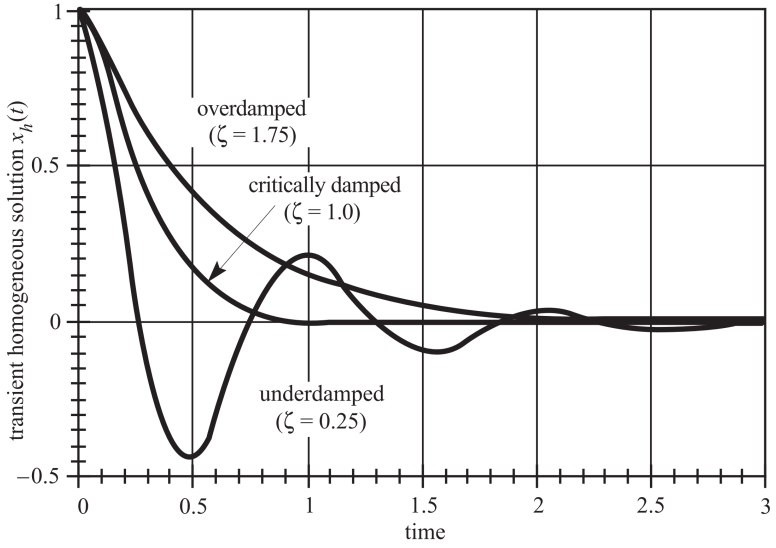

Figure 2.9: Transient response of second-order systems [2]

2.2.2. Positioning tuggers

A positioning control scheme is used to coordinate an object with the use of multiple wires to a specific point. The proposed positing control scheme (introduced in Section 5.4.1) is inspired on the model-free control scheme presented by Ren et al. [41]. In the study, the authors consider a catamaran installation vessel with multiple cranes lifting a large, heavy payload, see Figure 2.11. The controller was designed to lift a payload with multiple tuggers and hold it in a specified position. An overview of the control scheme is given in Figure 2.10.

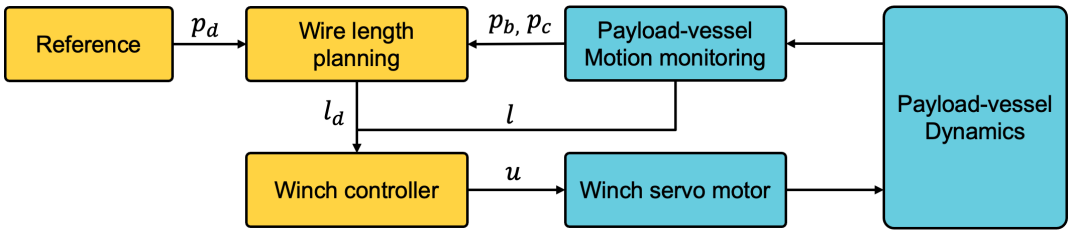

Figure 2.10: Overview of the positioning controller

First, the measurement system determines the position of the payload. The controller's setpoint is the desired position (p_d) which comes the reference module. In the study, p_d is assumed to be constant in the global reference system:

$$p_d = \begin{bmatrix} X_d \\ Y_d \\ Z_d \end{bmatrix} \tag{2.19}$$

Subsequently, the wire length planning module calculates the desired wire lengths. The desired length (l_d) of the lift wire is given by:

$$l_d(t) = |p_{cd}(t) - p_b(t)| \tag{2.20}$$

where p_b is the position of the winch. The desired position of the connection point (p_{cd}) of the tugger line is given by:

$$p_{cd}(t) = p_d + p_c - p_0 - K_i \int_0^t (p_0(\tau) - p_d(\tau))\, d\tau \tag{2.21}$$

p_0 is the position of the concerned point (bottom centre of the JLT), p_c is the tugger line's connecting point, and $K_i \in \mathbb{R}^{3\times3}$ is a positive diagonal matrix to be tuned. The integral gain K_i eliminates any steady-state error caused by the wire elongation.

Finally, the winch controller controls the corresponding winch servo motors to change the wire lengths by hauling them in or out. The winch velocity (u_i) is determined based on the length error (e_l):

$$u = -k_p \cdot e_l \tag{2.22}$$

where

$$e_l = l - l_{d,} \tag{2.23}$$

and k_p>0 is a proportional control gain to be tuned.

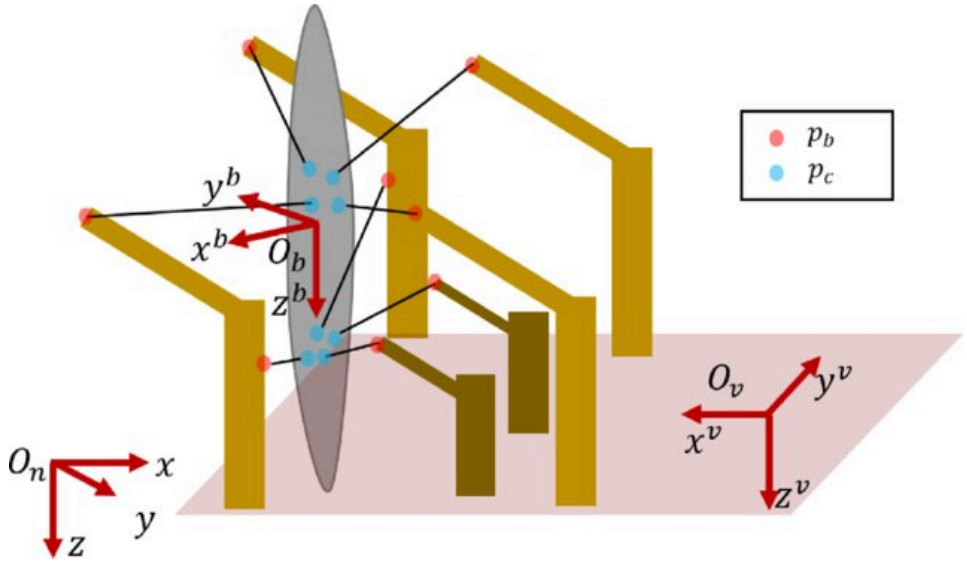

Figure 2.11: Lifting configuration used in the case-study by Ren et al. [41]

3

Model definition

In this study, many time domain Orcaflex simulations are performed to analyse the system's dynamics and tune the control strategies. OrcaFlex is a dynamic analysis software programme that encompasses a large variety of objects and features which enable assessing complex systems and applications through a mathematical model. The finite element analysis tool makes it able to model the non-linear response of the system in both the time and frequency domain and is used primarily for offshore engineering. This chapter describes how the Orcaflex models are set up.

3.1. General properties

3.1.1. System of units

For all calculations of the model, SI units are applicable.

3.1.2. Simulation time

All time domain simulations last 1100s, with a time step of 0.01s. The first 100s are removed to avoid startup effects.

3.1.3. Constants and conventions

The important constants used for the analysis are given in Table 3.1:

Table 3.1: Constants used in the study

Constant	Symbol	Value	Unit
Water density	ρ_{water}	1.025	t/m^3
Air density	ρ_{air}	0.00129	t/m^3
Gravitational acceleration	g	9.81	m/s^2

3.1.4. Coordinate system and vessel notations

The following global coordinate system is applicable:

- The X-axis is defined as positive from the stern to the bow of the vessel
- The Y-axis is defined as positive from the Center Line to Port Side
- The Z-axis is defined as positive upwards from the waterline

Besides a global coordinate system, two local coordinate systems are used in the analyses. The origin of the vessel's coordinate system can be found at the same X and Y coordinates as the origin of the global coordinate system. The Z-coordinate is located at the baseline of the vessel. The local coordinate system of the payload is defined as follows:

- The x-axis is positive in the side-lead direction (towards the vessel's Port Side).
- The y-axis is positive in the off-lead direction (away from the crane)

- The z-axis is defined as positive upwards from the centre of the JLT

The global and local coordinate systems, together with the environmental angles of attack with respect to the vessel, are shown in Figure 3.1

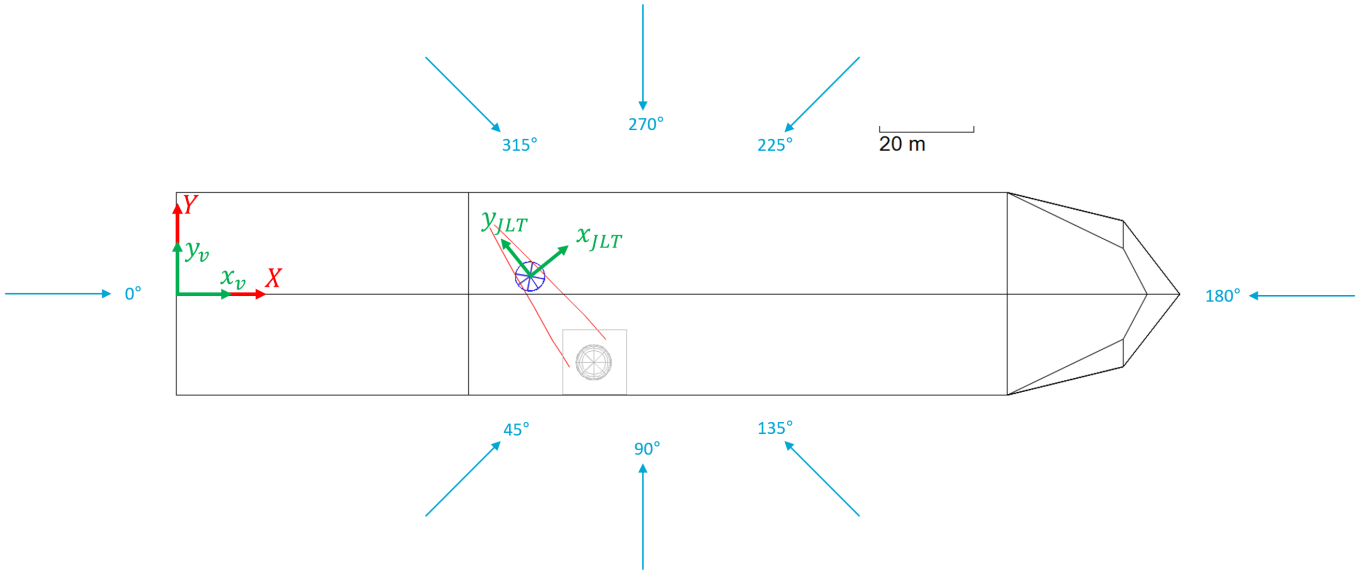

Figure 3.1: Environmental angles of attack and axis

The six fundamental vessel motions have been visualised in Figure 3.2.

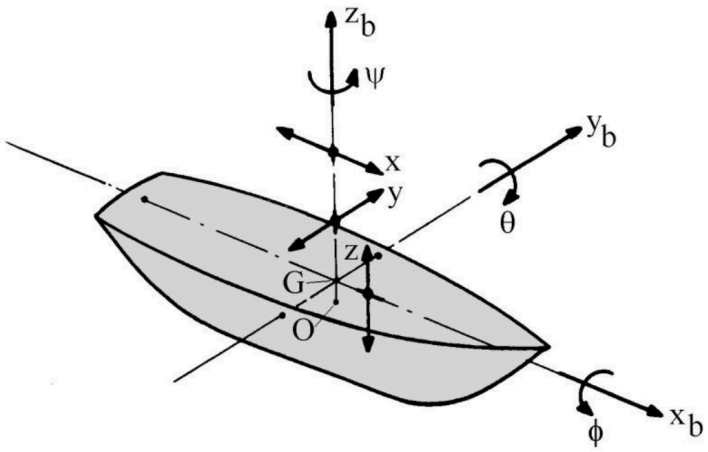

Figure 3.2: Definition of vessel Motions in six DoF [25]

A floating body, such as a ship, can be regarded as rigid but moving body. Any ship motion is build up from six degrees of freedom (DOF). The DOF is a set of independent displacements and rotations that give a complete overview of the displaced position and orientation the body [46]. The DOF of a steadily translating vessel are the following:

Translational motions

- Surge in the longitudinal x-direction, positive forwards
- Sway in the lateral y-direction, positive to port side
- Heave in the vertical z-direction, positive upwards

Rotational motions

- Roll about the x-axis, positive right turning
- Pitch about the y-axis, positive right turning
- Yaw about the z-axis, positive right turning

The static angular offset about the X and Y-axis are called the heel and trim, respectively. It is attempted to begin all simulations art zero heel and zero trim for the most optimal results and weather thresholds.

3.2. Load cases

As JLT lifting operation takes place during the installation and decommissioning of a jacket, the following two load cases (LCs) with corresponding models will be analysed:

- **LC1**: JLT lift-on on jacket positioned on the deck (see Figure 3.3)
- **LC2**: JLT lift-on on jacket positioned on the seabed (see Figure 3.4)

The Bokalift 1 (BL1) is suitable for transportation and the installation of jackets. The jacket is therefore lifted from the BL1 into the water. As the jacket is on deck, the jacket's position (and therefore p_d) is constant in the body-fixed reference system (of the vessel) and variable in the global coordinate system. In LC2 the jacket foundation has already been installed. When the jacket is decommissioned, the jacket must be lifted out of the sea. The jacket is positioned on the seabed and does not move. Hence, p_d is variable in the local coordinate system (of the vessel) and constant in the global coordinate system.

The configuration differences in the LCs are the crane orientation and the length of the hoist tackles. Both of these affect the motion modes of the system. The motion modes of the uncontrolled system will be discussed in Chapter 4.

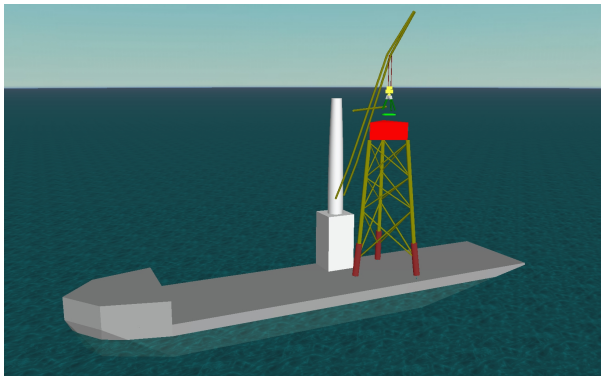

Figure 3.3: Load case 1 Orcaflex model

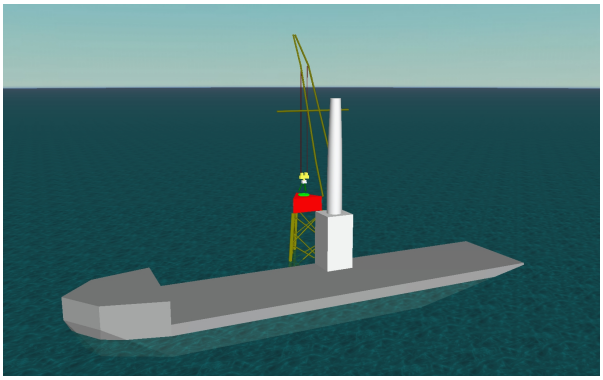

Figure 3.4: Load case 2 Orcaflex model

3.3. Objects

3.3.1. Vessel

In 2017 Boskalis converted the heavy cargo vessel Finesse into the heavy lifting vessel Bokalift 1 (BL1). With a 6,300 m^2, open deck, dynamic positioning capabilities (DP2) and an anti-heeling system, the BL1 is well-suited for transport and installation projects on offshore wind farms, oil and gas fields, and decommissioning projects. The large deck of 165 meters by 43 meters makes it possible to transport multiple large objects (such as jackets) on deck. Therefore barges, which have substantially lower workability, are not required. The BL1 can accommodate 150 persons, and a helicopter deck is available for offshore transfers. The dimensions and general properties of the vessel are summarised in Table 3.2. All different views of the Orcaflex models of the BL1 can be found in the Appendix in Figure D.2.

Figure 3.5: The Bokalift 1 [9]

In Orcaflex, vessels type objects are used to model ships. They are rigid bodies whose hydrodynamic properties are defined by the load Response Amplitude Operator (RAO) and hydromechanical reaction forces (added mass and damping) for each of the six DoF. Therefore, the motions of the vessel result from all forces acting on it, including forces exerted on the vessel by, for example, the load in the crane. The BL1 is modelled as a vessel where the hydrodynamic properties were calculated (by Boskalis) in the three-dimensional diffraction programme AQWA at a typical operational draft at zero heel and trim and at a water depth of 44m. The computer programme AQWA is based on linear potential theory. Therefore, the software has not taken into account any additional viscous nonlinear damping on the roll motion. According to Fossen [15], marine craft commonly have a reduction of 0.5% in the natural frequency. Therefore, to account for the viscous component of the roll damping, a roll damping of 0.5% of the critical roll damping has been considered.

The dynamic positioning (DP) system compensates for the second-order wave drift forces. Therefore the vessel's mean horizontal position and heading are stabilised. The details about the DP system are neglected since it is not the main focus of the present study. The DP system of the BL1 is modelled with four spring lines constraining the vessel in the surge, sway and yaw motions. The stiffness of the springs is chosen in such a way that the natural period does not interfere with wave excitation periods (T_{surge}, T_{sway} & T_{yaw} >40s). As a result, the low-frequency motions do not interfere with the vessel's first-order motions, which strongly occur in the range of wave periods.

Table 3.2: Vessel properties [8]

Parameter	Value	Unit
Length overall	216	m
Breadth	43	m
Depth moulded	13	m
Operating draft	8-9	m
Cargo deck area	6,300	m^2
Maximum deck load	15,000	t
Mass	57,440	t

3.3.2. Crane

The BL1 is equipped with a 3,000-ton revolving Huisman crane and is therefore capable of lifting jacket foundations of the vessel's deck. Other general properties of the crane are summarised in Table 3.3. In Orcaflex, the crane is assumed to be rigid. The boom makes an angle of 45 and 90 degrees with respect to the X-axis for LC1 and LC2, respectively. All different views of the Orcaflex models of the BL1, together with the crane's orientation, can be found in the Appendix in Figure D.2.

Table 3.3: Crane properties [19]

Parameter	Value	Unit
Crane lifting capacity	3,000	t
Min radius	16	m
Max radius	72	m
Lift height above deck	90	m
Crane house height	71	m
Footprint	14x14	m
Mass	2,630	t

3.3.3. Payload

The payload consists of the crane hook and the jacket lifting tool (JLT) connected to each other by a rigging configuration. Relevant properties of the payload can be found in Table 3.4. In Figure 3.6 an example of a jacket installation with the use of a JLT is given in which all parts of the payload are indicated.

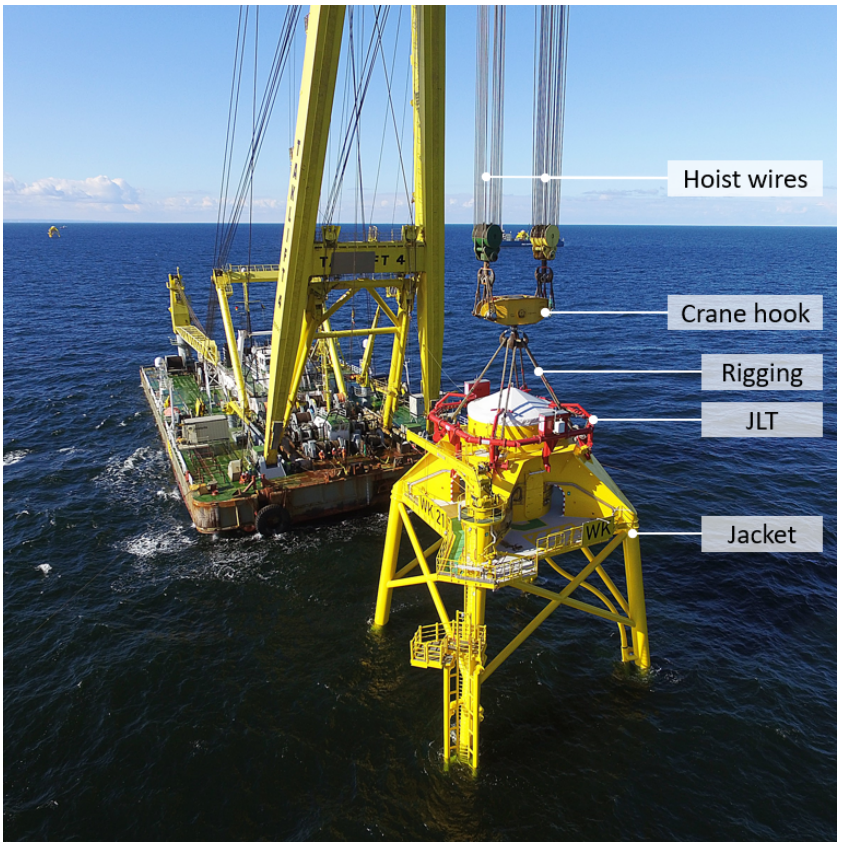

Figure 3.6: Jacket Installation with indicated payload parts

The JLT and the crane hook are modelled as a 6D buoy object in Orcaflex. 6D buoys are rigid bodies with all six degrees of freedom (translation and rotation). They have mass, volume, hydrodynamic and contact properties. With the use of diffraction- or Morison-type formulation, the hydrodynamic forces acting on the 6D buoy can be defined. The lifting operation of a JLT does not include hydrodynamic loads as it does not interact with the water.

Table 3.4: payload properties [8]

Parameter	Value	Unit
Mass crane hook	120	t
Mass JLT	65	t
Footprint JLT	6x8	m

3.3.4. Tackles

The hoist consists of two tackles, both consisting of 14 parts (called falls). The wire type is steel wire rope. The unstretched length of the tackles is constant during the lifting operation. Both lengths can be found in Table 3.5.

Table 3.5: Hoist tackle length per load case [8]

Parameter	Value	Unit
Tackle length (LC1)	14	m
Tackle length (LC2)	56	m

3.4. Environmental conditions

This section covers the weather-related input for the time-domain analysis.

3.4.1. Waves

The wave climate is represented by the significant wave height (H_s) and peak period (T_p). Stationary irregular sea states may be described by the power spectral density function of the vertical sea surface displacement, the so-called *wave spectrum*. The parametric spectrum models are empirical expressions where user-defined parameters are used to fit ocean surface elevation measurements [16]. Such models are used to simulate realistic ocean waves without measurement data, but can also be adapted to fit specific data. The most suitable wave spectrum depends on the geographical area with local bathymetry and severity of the sea state. For North Sea conditions, the *Joint North Sea Wave Observation Project* (JONSWAP) spectrum is the most appropriate spectrum to use [12]. A JONSWAP spectrum is suitable for fetch-limited (or coastal) wind-generated seas and is the assumed sea-state in this study. The IEC [21] standards recommends the following formulation for the JONSWAP spectrum:

$$S_{\mathrm{JS}}(f) = \frac{\alpha_{\mathrm{JS}} g^2}{(2\pi)^4} f^{-5} \exp\left(-\frac{5}{4}\left(\frac{f}{f_p}\right)^{-4}\right) \gamma^{\exp\left(-0.5\left(\frac{f-f_p}{\sigma \cdot f_p}\right)^2\right)} \tag{3.1}$$

where

$$\sigma = \begin{cases} 0.07 & \text{for } f \leq f_{\mathrm{p}} \\ 0.09 & \text{for } f > f_{\mathrm{p}} \end{cases} \tag{3.2}$$

The peak enhancement factor (γ) is obtained by the use of Equation 3.3.

$$\gamma = \begin{cases} 5 & \text{for} \quad \frac{T_{\mathrm{P}}}{\sqrt{H_{\mathrm{s}}}} \leq 3.6 \\ \exp\left(5.75 - 1.15\frac{T_{\mathrm{p}}}{\sqrt{H_{\mathrm{s}}}}\right) & \text{for} \quad 3.6 \leq \frac{T_{\mathrm{p}}}{\sqrt{H_{\mathrm{s}}}} \leq 5 \\ 1 & \text{for} \quad \frac{T_{\mathrm{P}}}{\sqrt{H_{\mathrm{s}}}} > 5 \end{cases} \tag{3.3}$$

The zero-upcrossing period (T_z) depends on T_p and γ through the following relationship:

$$T_z = T_p \sqrt{\frac{5+\gamma}{11+\gamma}} \tag{3.4}$$

According to O'Connor et al. [36], offshore wind farms in the North Sea have access levels of approximately 60-80% based on wave height access limit of a H_s of 1.5m. For larger waves, these installations

become too risky.

As the model has to simulate an installation scenario, a sea-state with a H_s=1.5m is utilised. To find out how the systems behave under different peak periods and wave directions (θ's), different circumstances will be considered by varying the T_p from 4-10s and θs from beam sea (90 deg) to head sea (180 deg). For conservatism, it is assumed there is no wave spreading.

3.4.2. Wind and current

Ren et al.'s [41] research indicates the motion of the suspended payload is dominated by the floating vessel as the influence of the turbulent wind field and current is limited. Therefore no wind and current have been used in the simulations.

3.4.3. Water depth

Jackets are installed at medium water depths (40-60m). Therefore a water depth of 44m is used in the analyses.

4

The uncontrolled system

First, the uncontrolled scenario of the system is analysed. In this case, no tugger lines are attached to the payload. Therefore, the JLT is free hanging, fully suspended in the crane, and can swing with no control forces correcting for these motions.

4.1. Modal analysis

In order to gain insight into the dynamic behaviour of the uncontrolled system, the natural frequencies (ω_n's) and periods (T_n's) of the system are obtained using a modal analysis in Orcaflex. Only the first-order wave loads are considered. As the natural modes are affected by the position of the crane and the length of the hoist wires the analysis is performed for both load cases. Only the relevant modes (i.e. modes with a natural frequency close to, or within, the range of the considered JONSWAP spectra) are given and analysed.

In Table 4.1, the modes and corresponding natural periods and frequencies of the coupled systems (LC1 & LC2) are given. As the payload is relatively light (<2% of the vessel's mass), the coupling's influence is very limited. The difference in roll period between LC1 and LC2 is because of the vessel's different loading conditions and therefore metacentric height. Furthermore, the pendulum modes of the system are significantly larger for LC2 due to the increase in the hoist tackles' length. The natural period of a simple pendulum is given by:

$$T_n = \frac{2\pi}{\omega} = 2\pi\sqrt{\frac{L}{g}} \tag{4.1}$$

where L is the length of the pendulum. However, the payload is not a simple pendulum as it consists of two complex-shaped masses connected by a rigging configuration. Nevertheless, by simplifying the payload, it can be determined whether the natural period provided by the modal analysis is in the expected order of magnitude. Therefore it is assumed that the L is the sum of the tackle length (Table 3.5) and half of the vertical rigging length (=$\pm$11m). Substituting this in Equation 4.1 results in a natural pendulum period of 8.88s and 15.77s for LC1 and LC2, respectively. These periods are in-line with pendulum mode periods found by the modal analysis in Orcaflex (see Table 4.1).

To get an overview of which ω_n falls within which sea state, the JONSWAP spectra (Equation 3.1) along with the natural frequencies are plotted and illustrated in Figure 4.1. What should be noted is that the pendulum modes in LC2 (Mode 1 & 2) fall outside the wave spectra of most of the concerned peak periods. One can therefore expect smaller pendular motions in LC2.

Table 4.1: Natural periods and frequencies of LC1 & LC2

	Mode	Load case 1		Load case 2	
		T_n [s]	ωn [Hz]	T_n [s]	ωn [Hz]
Vessel	Surge	207.12	0.005	209.51	0.005
	Sway	72.53	0.014	73.41	0.014
	Heave	8.89	0.112	8.93	0.112
	Roll	14.77	0.068	13.54	0.074
	Pitch	8.87	0.118	8.45	0.118
	Yaw	95.43	0.010	96.21	0.010
Payload	1: off-lead pendulum	8.41	0.119	17.24	0.058
	2: side-lead pendulum	7.88	0.127	15.23	0.066
	3: rotation	8.95	0.112	15.75	0.064
	4: off-lead double pendulum	3.88	0.258	4.32	0.231
	5: side-lead double pendulum	3.60	0.278	3.84	0.260
	6: rotation double pendulum	2.83	0.353	3.25	0.308

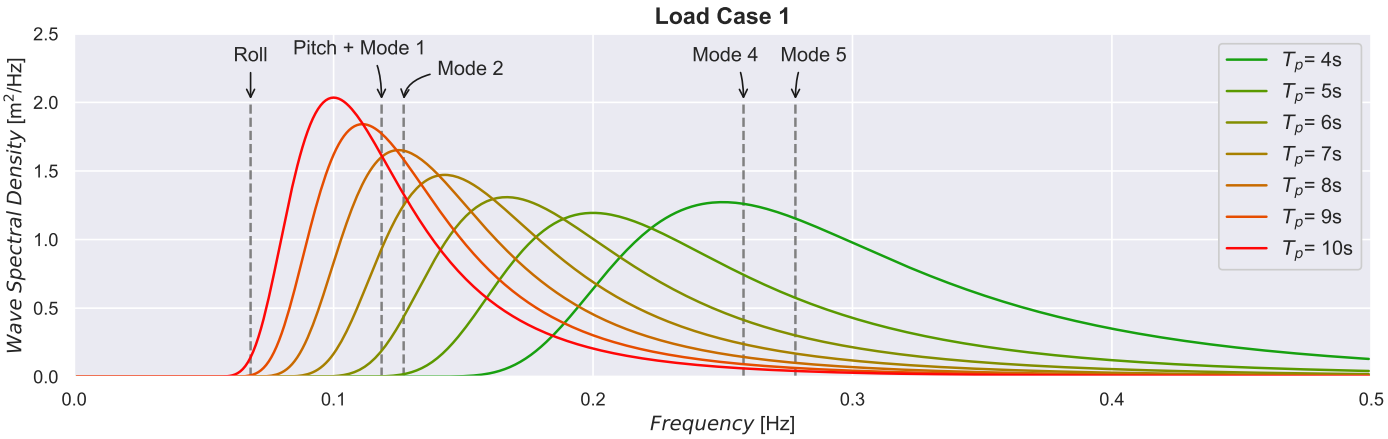

Figure 4.1: Jonswap spectra + natural frequencies (LC1, without tuggers)

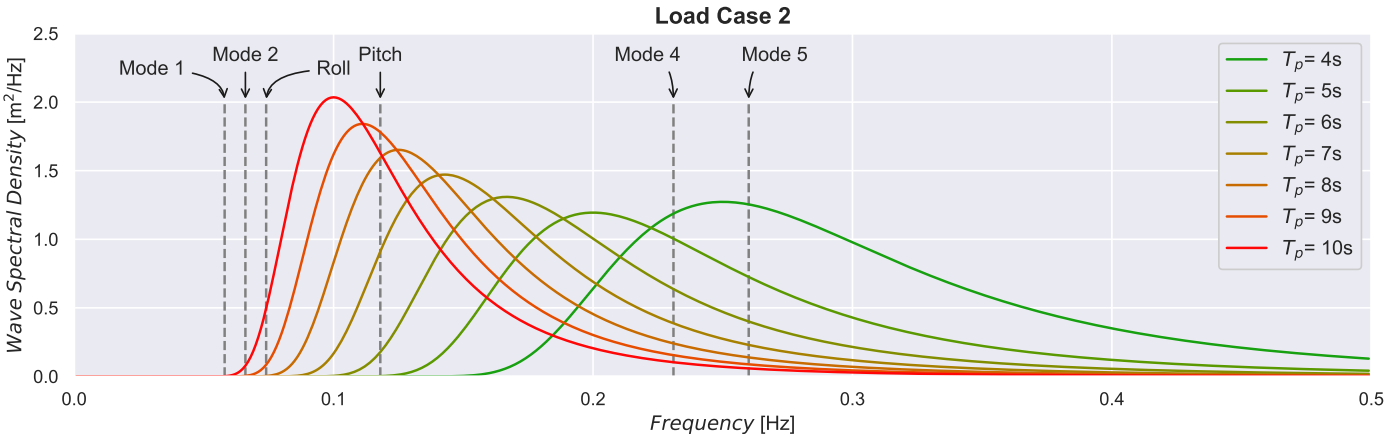

Figure 4.2: Jonswap spectra + natural frequencies (LC2, without tuggers)

4.2. Time-domain analysis

Multiple time-domain simulations for various sea states are analysed to gain insight into the dynamics of the uncontrolled systems. All choices regarding the Orcaflex model are given in Chapter 3. The maximum roll and pitch of the vessel will are analysed together with the standard deviation of the positional error. The results will be summarised using heat maps in which relatively high values are shown in red and relatively low in green.

Orcaflex has aborted some simulations in LC1. This occurred when the JLT excitation became too severe, and the software got a numerical error. In this case, extracting data from these simulations is impossible and therefore shown blank in the heat map plots. However, it can be assumed that the displacement is relatively high considering the observed trends. This is confirmed by looking at the system's dynamics in Orcaflex before the simulations crashed.

4.2.1. Vessel dynamics

The vessel dynamics are significantly influenced by both the wave peak period and the angle of attack of the waves, see Figures 4.3 and 4.4. The vessel is more prone to rolling than pitching. This is because of the greater water resistance to pitching than to rolling. For this reason, the vessel is generally more vulnerable to rotational motions when the sea is abeam; due to the shape of the vessel (length > breath), the wave loads will be higher.

The coupling between the vessel and payload is very limited. This is in line with the expectation as the payload is relatively light. Therefore, the vessel dynamics in both load cases are very close to each other. The severe roll motion for 9-10s can be explained by the natural periods of the modes found in the modal analysis of the system (see Table 4.1). In Figure 4.2, it can be seen that the roll mode falls within both wave spectra, which causes resonance motions. The pitch mode has a natural period even closer to the wave periods. Nevertheless, the motions are less severe compared to the roll motions.

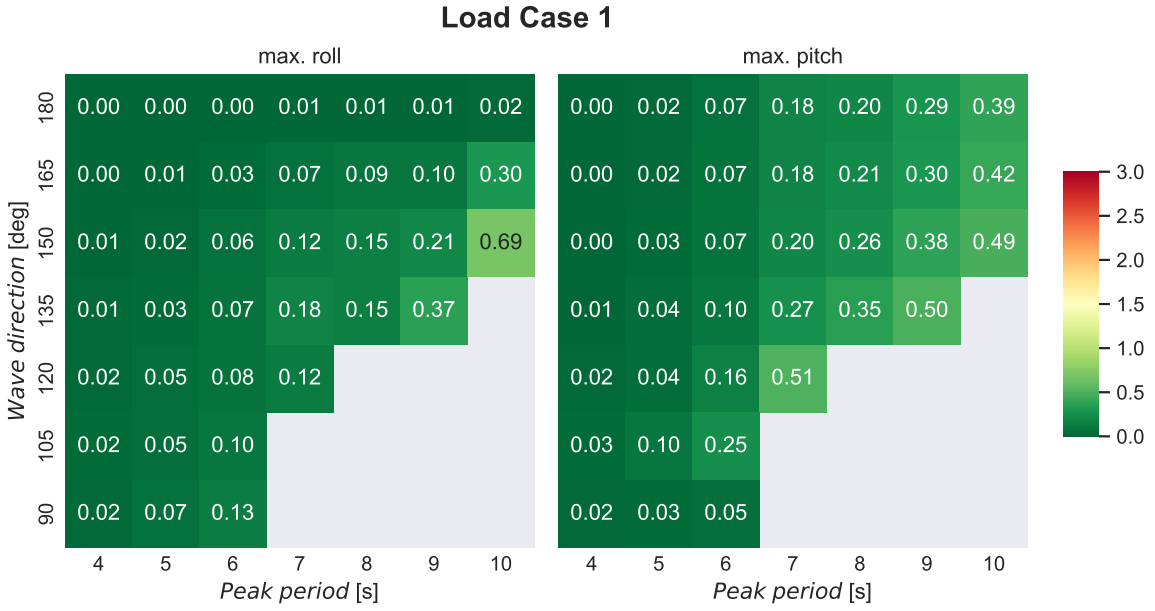

Figure 4.3: Vessel roll & pitch motions for the uncontrolled system (LC1)

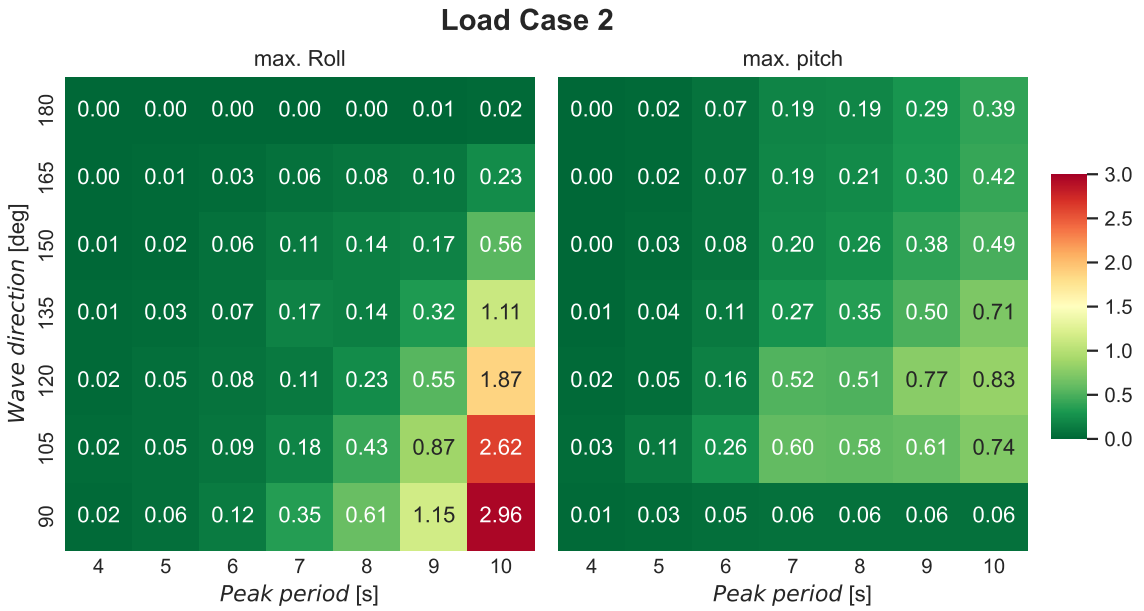

Figure 4.4: Vessel roll & pitch motions for the uncontrolled system (LC2)

4.2.2. Positional error

The positional error results of the uncontrolled scenario in LC1 and LC2 are given in Figure 4.5. The STD of the positional error is generally lower in LC2 compared to LC1. This also explains why no simulations crashed in LC2. Especially for peak periods <9s, a green-coloured heat map can be seen, which refers to relatively low values. The reason for this is the longer hoist tackle length in LC2. As mentioned in Section 4.1, a longer hoist tackle results in a larger natural period of the pendulum modes (see Equation 4.1). Consequently, the pendular movements of the payload are less sensitive to shorter wave periods.

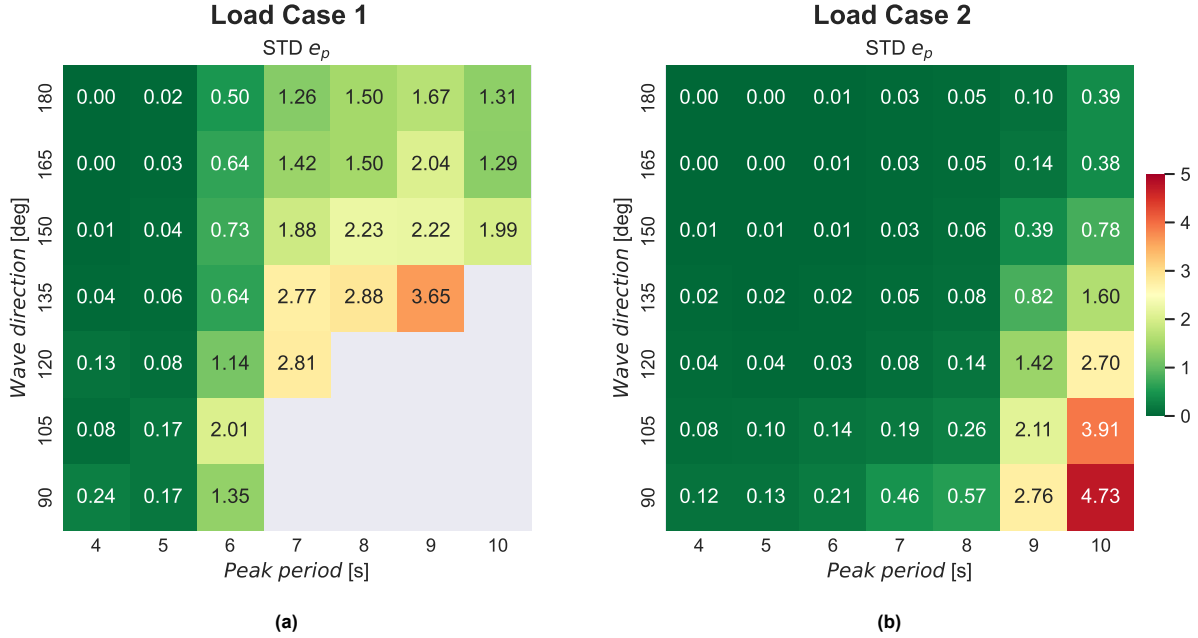

Figure 4.5: STD of e_p for the uncontrolled load cases

In LC1, the natural periods of the pendulum mode fall within the wave energy spectrum for most of the accessed wave peak periods, which causes resonance and thus an increase in e_p. In addition, in LC1, the two positions (bottom centre of the payload and the top of the jacket) that determine the positional error are variable over time in the global reference system. When they move in opposite directions, this leads to high(er) positional errors. In LC2, there is only one variable position as the desired position (top of the jacket) is constant. This also contributes to the relatively lower positional error in LC2. Finally, it can be observed that the positional error is highly coupled to the roll motions of the vessel. The pitch motions are less severe but have a minor influence on the positional error. This is because the crane is positioned more or less midships. Therefore the pitch has a limited effect on the crane tip motions, which drives the pendulum motion

5

Controlled system

A configuration and control scheme are proposed for both load cases, in which the goal is to keep the suspended payload at its desired position by controlling the winch velocity.

5.1. Configuration

The configuration must consider the tugger line challenges described in the Problem Definition (Section 1.4). Therefore the most important factors to consider are the position of the winch relative to the payload (i.e. the tugger line's angle of attack) and the configuration's applicability.

The relative position of the winch with regards to the payload depends on the winch position (base point p_b) and the position where the tugger lines attach to the payload (connecting point p_c). An improper arrangement of the tuggers lines may introduce instability problems and degrade the control performance. The design of the tugger winch positions is a very general and complex problem. Next to the position of the payload's centre of gravity, it depends on the winch capacities, payload shape, wire properties and much more according to Ren et al. [41]. Therefore, a feasible configuration is proposed in this study to give a general evaluation of the proposed control schemes.

The pendular motion of a payload can be divided into two types of movements: off-lead and side-lead. The side-lead is the hoist wire's rotation angle in the crane boom's lateral direction. Off-lead is the hoist wire's rotation angle in the crane boom's longitudinal direction. In order to compensate for both side-lead directions, two tugger lines attaching to both sides of the payload are needed. Illustrations of the off-lead and side-lead angles are given in Figure 5.1 and 5.2, respectively.

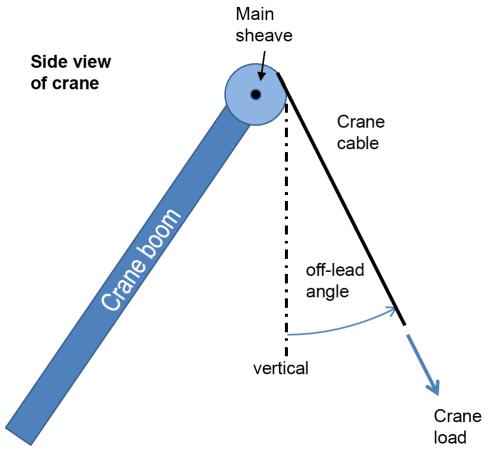

Figure 5.1: Off-lead angle [44]

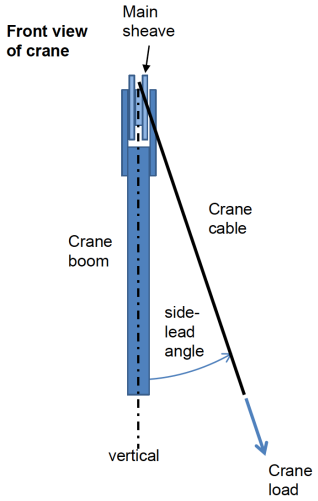

Figure 5.2: Side-lead angle [44]

Placing the tugger winches on deck is not a suitable solution for two reasons. First, the crane rotates during a jacket installation operation, and when the winches are fixed on deck, it causes a change in inclination angles of the tuggers, which complicates the tuning of a model-free controller. In addition, in this scenario, the lines are stretched across the deck, which causes safety risks for staff on deck and requires a lot of free deck space. An *outrigger configuration* is the proposed solution to this problem. An outrigger is a beam which extends horizontally from the crane boom. As the winches on the outrigger are attached to the payload at a specific angle (w.r.t. off-lead direction), they can provide a force in the side-lead direction. The tugger winches are set at a specific pre-tension to have a force (and therefore control) in both off-lead directions. The resulting inclination of the hoist wire creates the off-lead force in the opposite direction, creating the force equilibrium shown in Figure 5.3.

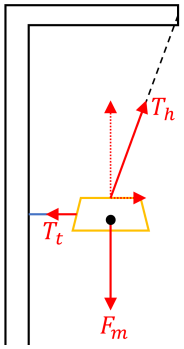

Figure 5.3: Equilibrium of forces with an applied pre-tension (side view of crane)

A narrower arrangement of the winches on the outrigger would lead to more off-lead compensation and vice versa for a wider arrangement with side-lead compensation. In this study, the location of the winch on the outrigger is indicated by the winch distance (l_w) and is iteratively set to 18m. It represents the distance of the two winches on the outrigger to the centre of the crane boom and is indicated in Figure 5.4.

Besides the two winches placed on the outrigger, the system has a third winch at the crane boom. The crane of the BL1 has a padeye every ten meters from which a tugger line can come. For LC1 & LC2, the third tugger line comes from a padeye located at a height where the tugger line declination angle is minimal, thereby maximizing the horizontal force vector. The three connecting points are positioned so that the tugger line points towards the centre of gravity of the payload in static equilibrium. Doing so reduces the chance of unwanted rotational motions of the payload as the moment arm to the CoG of the payload is very small.

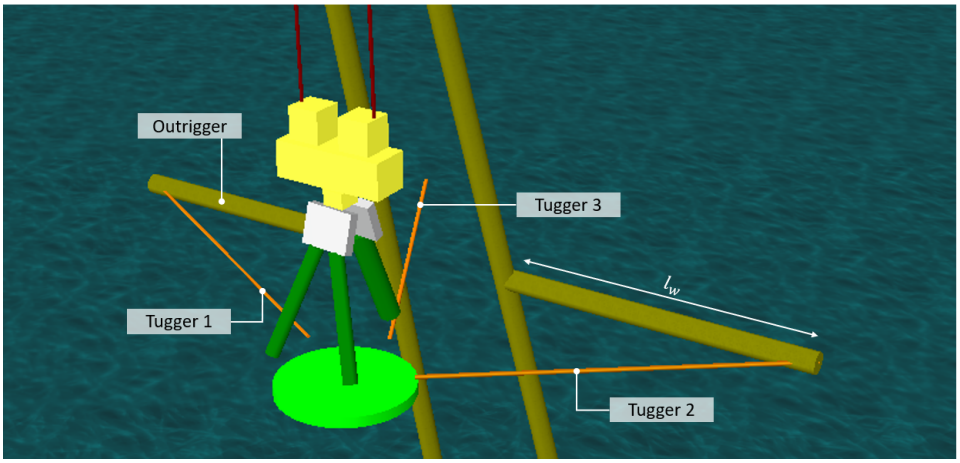

Figure 5.4: Outrigger configuration in Orcaflex

5.1.1. Modal analysis

The introduction of the tugger winch configuration affects the natural periods of the system. Especially the payload modes are affected. The vessel modes are barely influenced as the payload is relatively light. In general, the system becomes stiffer, resulting in shorter natural periods compared to the uncontrolled system (given earlier in Table 4.1). The natural periods and frequencies of all relevant modes, with the implemented tugger winch configuration, are given in Table 5.1. The JONSWAP spectra, along with the natural frequencies of the controlled system are illustrated in Figure 5.5 & 5.6.

Table 5.1: Natural periods and frequencies of LC1 & LC2 with tuggers

	Mode	Load Case 1		Load Case 2	
		T_n [s]	ωn [Hz]	T_n [s]	ωn [Hz]
Vessel	Surge	207.11	0.005	209.51	0.005
	Sway	72.53	0.014	73.41	0.014
	Heave	8.89	0.112	8.93	0.112
	Roll	14.60	0.069	12.92	0.077
	Pitch	8.54	0.117	8.44	0.118
	Yaw	95.42	0.010	96.16	0.010
Payload	1: off-lead pendulum	7.28	0.137	16.44	0.061
	2: side-lead pendulum	7.05	0.142	13.18	0.076
	3: rotation	4.55	0.220	4.77	0.210
	4: off-lead double pendulum	4.15	0.241	4.22	0.237
	5: side-lead double pendulum	3.59	0.279	3.76	0.266
	6: rotation double pendulum	2.88	0.347	2.77	0.362

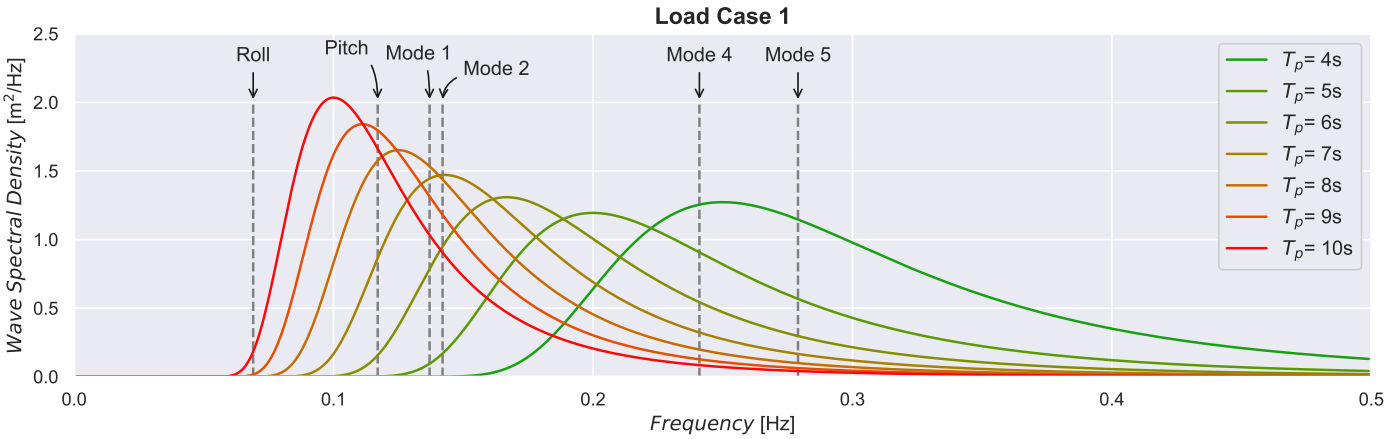

Figure 5.5: Jonswap spectra + natural frequencies (LC1, with tuggers)

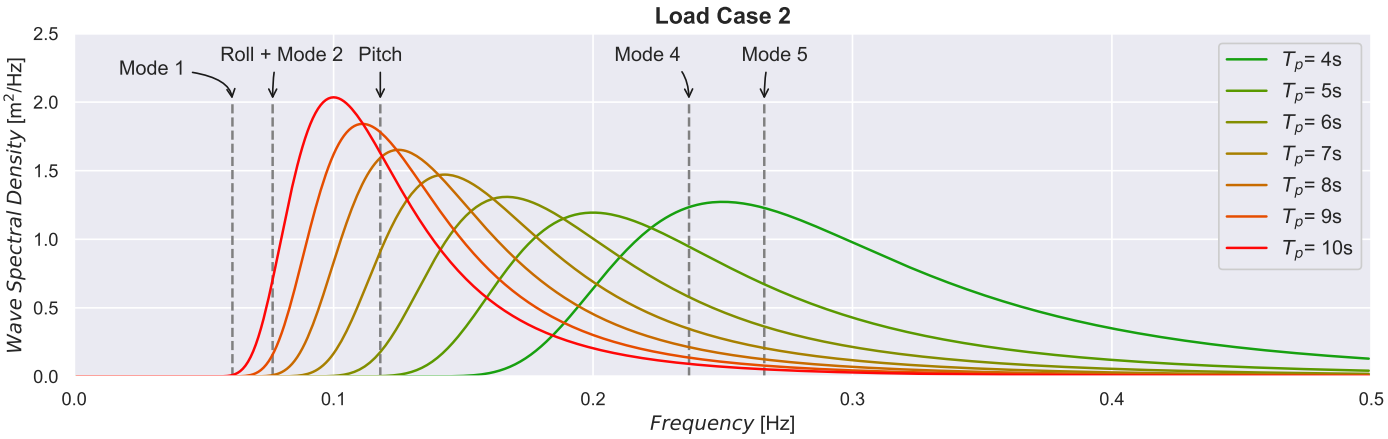

Figure 5.6: Jonswap spectra + natural frequencies (LC2, with tuggers)

5.2. Limitations

The winch will haul in or out when the tuggers are actively controlled. The system does have certain limitations that the controller must take into account. In this study, the velocity (u), tension (T) and power (P) capacity are considered. The winch limits of the BL1 are summarised in Table 5.2 and illustrated in Figure 5.7. The transparent coloured areas are tension-velocity combinations that exceed one or more of the system's limits.

In the considered system, the winch is responsible for maximum power and velocity. The maximum allowable tension is because of the padeyes on the crane boom. It is assumed that the winches and padeyes on the outrigger have the same limits as the ones on the crane boom.

Table 5.2: Winch limits of the BL1

Limit	Value	Unit
Max P	90	kW
Max. u	1.0	m/s
Max. T	220	kN
Min. T	10	kN

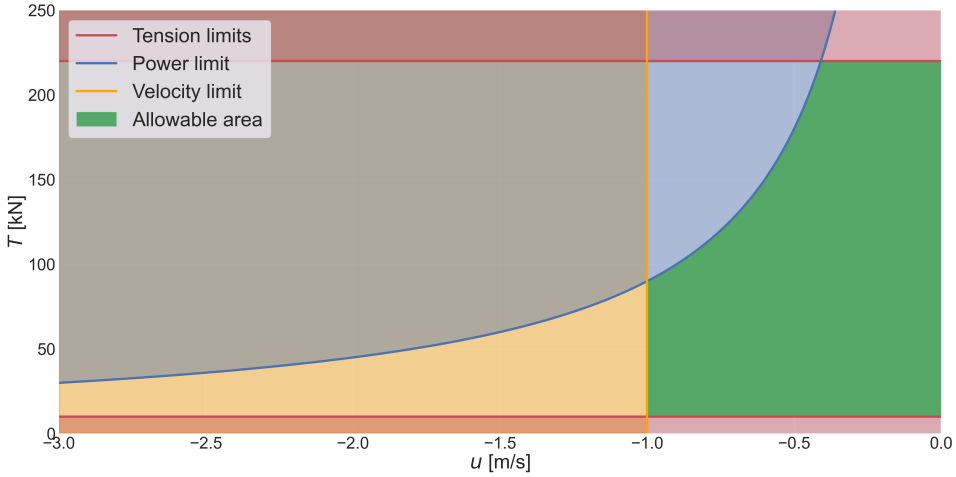

Figure 5.7: Tension-velocity graph illustrating the systems limits

5.3. Load Case 1: installation

LC1 represent the lifting operations during the installation phase. During this operation, the JLT must be lifted into the top of the jacket, which is positioned on the vessel's deck. A simplified 2D representation of the operation is shown in Figure 5.8.

5.3.1. Tugger control strategy

Since the desired position (p_d) is constant in the local coordinate system of the vessel, the positional error (e_p) would be zero in the case of a rigid system. A rigid system can be achieved if the tugger lines are kept at a constant length (and one neglects the wire elongations). In this case, the winch is put on a brake after applying a certain pre-tension, and the tugger lines behave as springs, with a stiffness equal to the stiffness of the tugger lines [32]. In case of vessel motions, the lifted object will follow and be accelerated by the tugger lines. Therefore, the load in the tugger line is proportional to the mass of the lifted object. As the allowable tension of the system is limited (Table 5.2), putting the tugger lines at fixed length mode cannot guarantee a safe lifting operation.

For this reason, the tuggers will operate as damping tuggers. This control scheme (see Section 2.2.1 & Figure 2.7) prevents tension limits from being exceeded while trying to keep the tension at the desired setpoint (i.e. the pre-tension). When controlling the tugger winch velocity with the damping control

scheme, the system will be limited by the velocity and power capacity of the winches. These limits have to be taken into account when tuning the control scheme. It is assumed that the tension of the lift wires is well estimated by sensors and observers. The observer design is neglected.

5.3.2. Tuning

The damping control scheme has a proportional gain ($k_{P,T}$) which has to be tuned. As shown in Figure 2.8, the slope depends on the tension-velocity profile's amplitude (A) and range (R). The control gain is, in fact, the inverse of the slope of the tension velocity profile and therefore indicates how much the tuggers damp the system. Therefore damping ratio (ζ) is used to express the control gain during the tuning process.

The tension limits determine the 'strength' of the system. When the load (i.e. tension) on the tugger lines become too high, the winches will haul out, and vice versa. This causes the payload to move and results in an increase in the positional error. An increase in the tension limit would therefore lead to a system that is more capable of keeping the payload at a fixed position in the vessel's reference system. So, the higher the amplitude of the tension-velocity profile (see Figure 2.8), the more force the tuggers can apply to keep the payload constant in the vessel's reference system. In addition, Antoci, Voor, and Roberts [4] research showed that a higher tension in wires leads to a higher axial stiffness of the system, which lowers the e_p. Therefore, the maximum possible amplitude is used and can be found with Equation 2.14, which results in a pre-tension of 115 kN and A=105 kN.

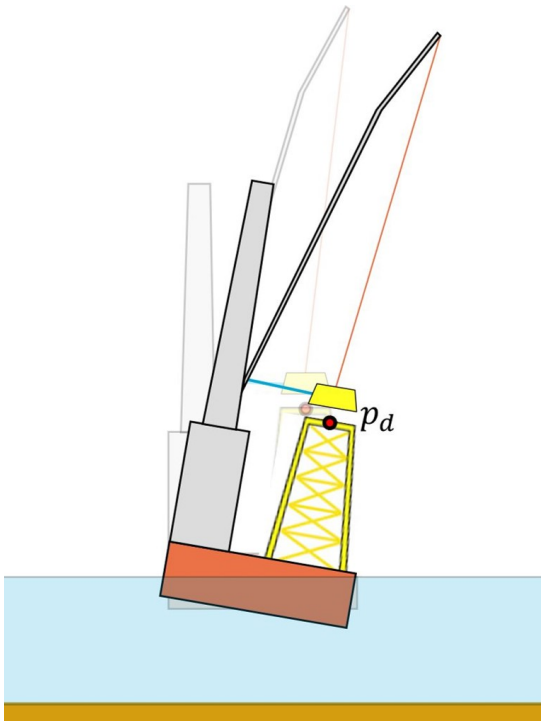

Figure 5.8: Simplified illustration of Load Case 1

The range (R) of the tension-velocity profile is limited by the maximum winch velocity (u_{max}) or power (P) capacity. With the use of linear algebra, the minimum $k_{P,T}$ that ensures the power limit is not exceeded is derived (see Appendix E) and given by Equation 5.1:

$$k_{pT,min} = \frac{4P_{max}}{T_d^2} \tag{5.1}$$

substituting the above equation in Equation 2.16 provides the equation to be used to find R_{max} when the winches are limited by their power capacity:

$$R_{max} = \frac{T_d^2}{4A \cdot P_{max}} \tag{5.2}$$

To check whether the found $k_{P,T}$ exceeds the velocity limit, R should be smaller than u_{max}. As shown in Figure 5.7, the R_{max} of the BL1 is limited by the maximum velocity of the winches. Therefore $R_{max} = u_{max}$ =1m/s.

The pendulum modes (off-lead and side-lead) are the main cause of the payload's positional error. In Table 5.1, the natural frequencies of these modes can be found. The pendulum mode has a natural frequency of $\pm$ 0.14 Hz. The critical damping for this mode is subsequently found by Equation 2.18 and results in 3.26E+05 $\frac{\text{kN·s}}{\text{m}}$. Figure 5.9 illustrates the damping ratio (ζ) corresponding to different R's of the tension-velocity profile. The R-$k_{P,T}$ relationship can be determined by Equation 2.16. The $k_{P,T}$ - ζ relationship is given by Equation 2.17.

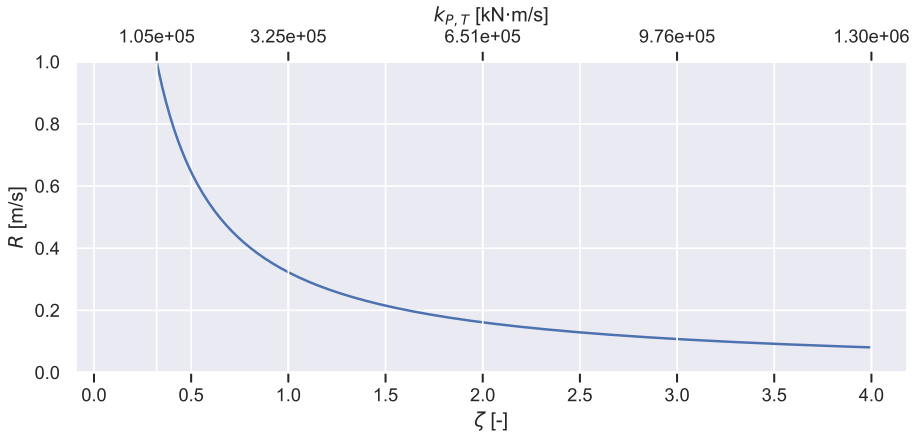

Figure 5.9: ζ and corresponding R values for a constant A=105kN

It must be noted that the ζ values indicate the amount of damping in the excitation direction (i.e. pendulum direction). As the dampers (i.e. tugger lines) have a variable incident angle with respect to the pendular motion, the damping efficiency is reduced. In addition, the displacement of the bottom centre of the JLT is not solely because of the pendular motions but also other modes, such as the double pendulum and rotational motions. A $\zeta = 1$ does therefore not indicate the payload being critically damped.

The optimal amount of damping to minimise the positional error is to be found in an iterative data-driven way. Multiple time domain simulations are performed and analysed. Since the control scheme must be suitable for rolling and pitching the ship, a bow quartering sea (θ= 135 deg) environment is accessed. The control strategy is assumed to be reasonable for other wave directions. As described in the methodology, the tuning will be based on the positional error, system limits and work.

Positional error
The positional error (e_p) of the simulations is analysed for different ζ's. The same range of ζ's has been accessed, as shown in Figure 5.9. The control scheme is tuned for T_p's causing the biggest installation problems (i.e. relatively large positional errors). Therefore the control scheme is tuned for peak period from 6-10s (see Figure 4.5). In Figure 5.10, the result of the simulations is illustrated.

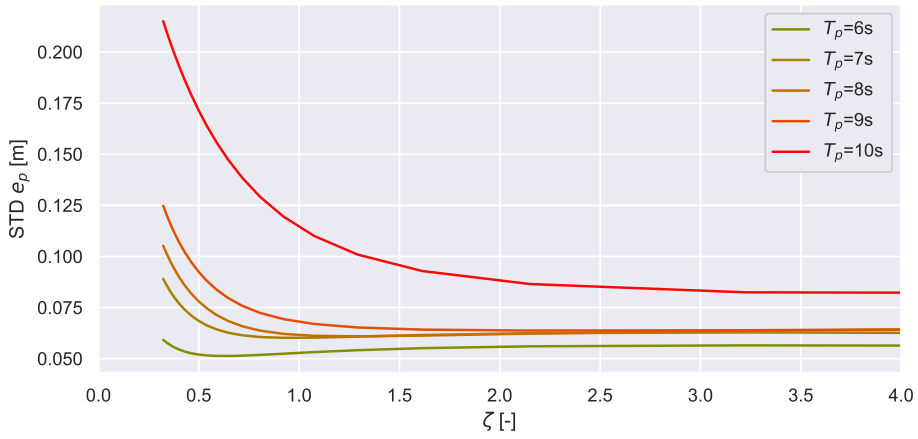

Figure 5.10: Positional error (e_p) for different damping ratios (ζ's)

As in uncontrolled scenario, an increase in T_p leads to an increase in e_p. It should be mentioned that compared to the uncontrolled scenario, the standard deviation of the positional error is already significantly lower for all different control gains (i.e. ζ's). In the uncontrolled scenario with a the same sea

state (θ=135 and T_p=6-10s) a STD e_p of 0.64-3.65m was observed (see Figure 4.5). With the damping tuggers, the values decreased to 0.05-0.20m, depending on the applied control gain.

For all T_p's, one can observe a similar trend; the STD of e_p becomes smaller for higher values of ζ and flattens out due to the exponential decaying R-ζ relationship, shown in Figure 5.9. As more resonance occurs for the higher T_p's, more damping is required before the somewhat constant STD of e_p is reached.

Generally, one can observe the smallest e_p for high ζ values. This is because a higher ζ results in a damping controller with a smaller R, i.e. a controller with less responsiveness to tension fluctuations. Consequently, the tuggers allow more tension build-up and the payload position is more constant in the vessel's reference system.

System limits
One of the perquisites of the controller is that it operates within the system's limitations. During the design of the different tension-velocity profiles, the tension and power limits of the system have already been taken into account. The controller switches to constant tension mode when the tuggers reach their tension limit. In this mode, the winch velocity limits can be exceeded. However, with the concerned sea states and control gains, the winches remained within their limits.

Total work
In Figure 5.11, the difference in total work of the control gains is given. As ζ increases, the winches will become less sensitive to tension fluctuations. This results in a more passive winch which therefore consumes less energy. The higher peak periods increase the excitation of the system. This logically causes an increase in tension fluctuations and therefore performed work of the winches.

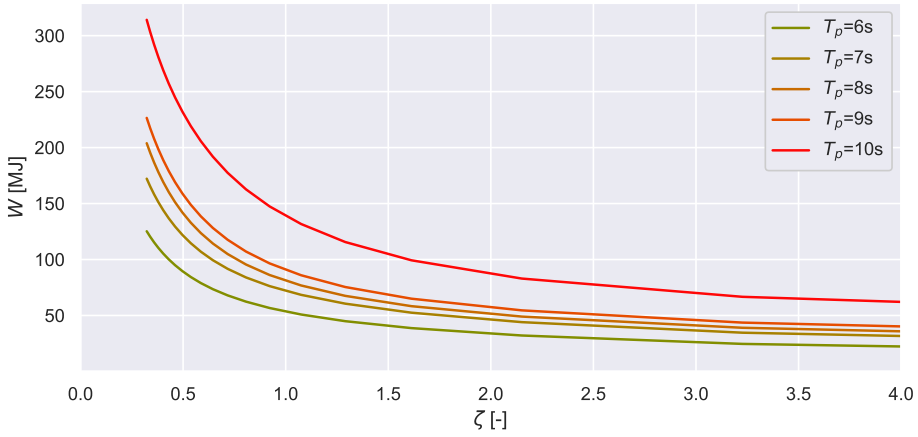

Figure 5.11: Total work (W) for different (ζ)'s

To conclude, in general a lower positional error and power consumption is observed for a damping controller with a high damping ratio. Therefore there has been chosen for a ζ of 3. The average positional error and work for all concerned peak periods are relatively low for this control gain. This corresponds to an R of $\pm$0.1 m/s, according to Figure 5.9.

5.4. Load case 2: decommissioning

LC2 represent the lifting operations during the decommissioning phase. During this operation, the JLT must be lifted into the top of the jacket, which is fixed on the seabed. A simplified 2D representation of the operation is shown in Figure 5.12.

5.4.1. Tugger control strategy

As the desired position (p_d) is constant in the global coordinate system, utilizing the tuggers as damping tuggers will not have the desired effect. The damping tugger control scheme reduces the payload movement in the local coordinate system. However, since p_d is constant in the global coordinate system (and therefore variable in the local coordinate system of the vessel), the positioning tuggers, introduced in Section 2.2.2, are expected to perform better than the damping tuggers in this scenario. Therefore a control scheme using the findings of Ren et al. [41] is used as a basis for the applied control scheme. It is assumed that the unstretched length of the lift wires are well estimated by sensors and observer. The observer design is neglected.

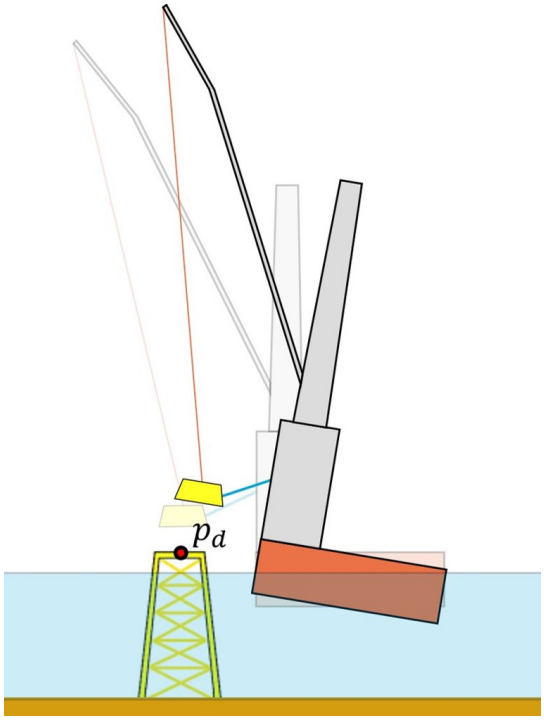

Figure 5.12: Simplified illustration of Load Case 2

The control scheme has been adjusted to ensure the positioning controller yields the desired results. The adjustments of the positioning tuggers are based on several reasons. As Ren et al. [41] considers a different lifting configuration (a catamaran vessel lifting a heavy payload), the definition of the the desired position is adjusted, and the K_i term is neglected. Furthermore, Ren et al. [41] evaluated the performance of the positioning tuggers based on the positional error and did not consider system limitations. Finally, some adjustments are implemented to ensure the positioning controller operates within the system's limitations. More details about the adjustments are given below.

Desired position

Ren et al. [41] designed the positioning controller for a catamaran vessel where all tuggers (36 in total) jointly lift a (heavy) payload. Therefore the desired position (p_d) was constant (Equation 5.3) in the global reference system. In addition, the tuggers are attached from all sides of the payload. Therefore, the payload's position could be controlled in the horizontal and vertical plane.

In the study, the hoist tackles have a fixed length and are responsible for lifting the payload. Consequently, it is impossible to control the payload in the vertical plane (i.e. heave compensate), as it would require the tugger winches to lift or lower the payload. Lifting the payload is not possible due to the tension limitations of the tuggers. Lowering is not possible due to the fixed length of the hoist wires. In this study, the tugger wires are responsible for controlling the horizontal position of the payload. The desired position (p_d) is therefore defined as:

$$p_d = \begin{bmatrix} X_d \\ Y_d \\ Z_d + \Delta z_{ct} \end{bmatrix} \tag{5.3}$$

where Δz_{ct} is the difference of the crane tip's Z-coordinate due to the rotational motions of the vessel in comparison to its static equilibrium (see Figure 5.13). Since p_d is variable in the vertical plane, enough safety margin between the Z_d and the jacket must be incorporated to prevent a collision between the two.

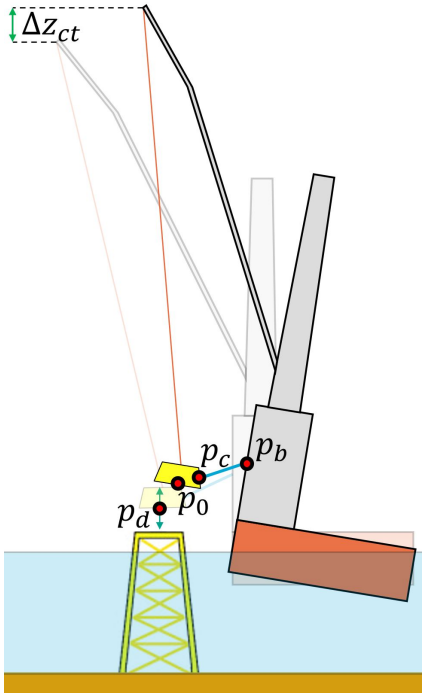

Figure 5.13: LC2 with control variables

Steady-state error
The proposed controller by Ren et al. [41] considers a heavy-lifting operation. Since the payload (in his study) has a significant mass, and tuggers are used to lift the payload, the wire elongation causes a steady-state error in the positional error. Therefore an integral gain is implemented in the control scheme (see Equation 2.21). However, since this study focuses on a relatively light payload, the tension and thus elongation in the lines are relatively small.

The maximum allowable tension in the lines tuggers lines is 220kN. The steel wire rope has a stiffness of 65E+03kN, so the maximum strain (ϵ) can be determined with Equation 2.10. This results in a strain of 3.38·10^{-3}. The tugger lines have a length of $\pm$16-23m (in static equilibrium), indicating maximum wire elongation of 0.05-0.08m.

In addition, the tuggers are used to correct the horizontal position and do not lift the payload; there are no constant (high) tensions and thus elongation in the wires. For the above reasons, the K_i term has been removed, and the control scheme obtains the desired connecting point (p_{cd}) as follows:

$$p_{cd}(t) = p_d + p_c - p_0 \tag{5.4}$$

Power limit
Since the winches have a power capacity, not all tension-velocity combinations are possible. Therefore, a power capacity filter is implemented when calculating the winch velocity (u) (Equation 2.22). The tension is monitored, and together with the calculated u, the needed P (Equation 2.1) is determined. When the required P exceeds the winch power limit (P_{limit}), the maximum winch velocity (u_{max}) that ensures the P_{limit} is not exceeded is determined by:

$$u_{max} = \frac{P_{max}}{T} \tag{5.5}$$

Tension limit
The system must operate within safe working limits (SWL) to guarantee a safe lifting operation. Tension is a limitation that should be considered. The positioning tuggers are actively trying to minimise the wires' length error, which is a direct consequence of the positional error. Ren et al.'s controller does not take into account the tension in the wires, which creates a high probability of the tension limits

being exceeded. For example, there may be moments when the controller wants to haul out while the tension is almost zero, causing the lines to fall slack.

As a solution, it is decided to combine the positioning controller with the damping controller. The result is a proportional controller that monitors two errors: the length error (e_l) and the tension error (e_T). The controller determines the winch velocity (u) based on both errors in the following way:

$$u = k_{P,l} \cdot e_l + k_{P,T} \cdot e_T \tag{5.6}$$

where $k_{P,l}$ and $k_{P,T}$ are two proportional gains which are to be tuned. The adjusted positioning controller tries to keep the payload at the desired position while simultaneously lowering the tension error. When error becomes larger or smaller, the winch will give it more or less priority accordingly. To what extent priority is given to both errors depends on the proportional gains. For example, if one gives the controller a $k_{P,l}$ of zero, the controller will ignore the length error (e_l), and the winch will behave as a damping tugger. Suitable proportional gains are to be obtained in an iterative data-driven way through time domain analyses.

Velocity limit
Finally, a velocity filter is implemented. This filter monitors whether the calculated winch velocity (u) exceeds the velocity limit (u_{max}). When $u > u_{max}$, the calculated u is rejected and automatically becomes u_{max}.

An overview of the control scheme of the proposed controller is given below in Figure 5.14

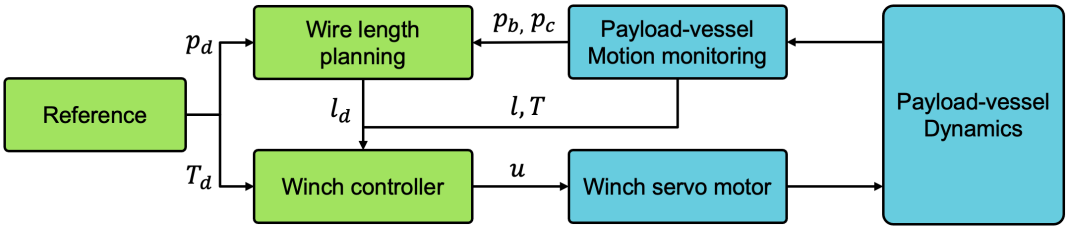

Figure 5.14: Overview of the damping-positioning controller

5.4.2. Tuning

The proposed controller uses two proportional gains ($k_{p,T}$ & $k_{p,l}$), which are to be tuned. A higher $k_{P,L}$ causes an increase in the speed of the control system response to positional errors (e_l). The same applies to $k_{P,l}$ and the tension error (e_T). The extent to which positioning and tension control is required depends on the environmental conditions. Therefore the influence of $k_{P,l}$ and $k_{P,l}$ is investigated for the challenging peak periods (9-10s). Again, $k_{P,T}$ is expressed by the means of the damping ratio (ζ) (see Equation 2.17) and a bow quartering sea (θ= 135 deg) environment is accessed. The pendulum mode in LC2 has a natural frequency of $\pm$0.068Hz, see Table 5.1, which results in a critical damping of 1.59E+05 $\frac{\text{kN·s}}{\text{m}}$.

Positional error
The standard deviation of positional errors using different control gains can be found in Figure 5.15. The relatively high STD of e_p values are shown in red and relatively low in green. As explained in Chapter 4, the positional error for a peak period of 10s is significantly higher due to the natural periods of the system. This can also be observed in the given heat maps. When θ= 135deg, the positional error is mainly caused by the pendular motions of the payload. Therefore just adding the tugger lines already causes a significant reduction in the positional error. This is confirmed by the scenario in which both control gains are zero. In this scenario, the controller does not correct for the errors; the tuggers remain at a fixed length. However, it can be seen that the positional error is already significantly reduced compared to the uncontrolled scenario (see Chapter 4). Furthermore, it can be seen that a higher $k_{p,l}$ leads to a decrease in positional error. However, this trend stops when $k_{p,l}$ becomes larger than 0.4. For a higher value of $k_{p,l}$, the controller will compensate more for a given error causing the controller

to respond with a higher velocity. At some point, this does not lead to a lower positional error as the controller will overshoot.

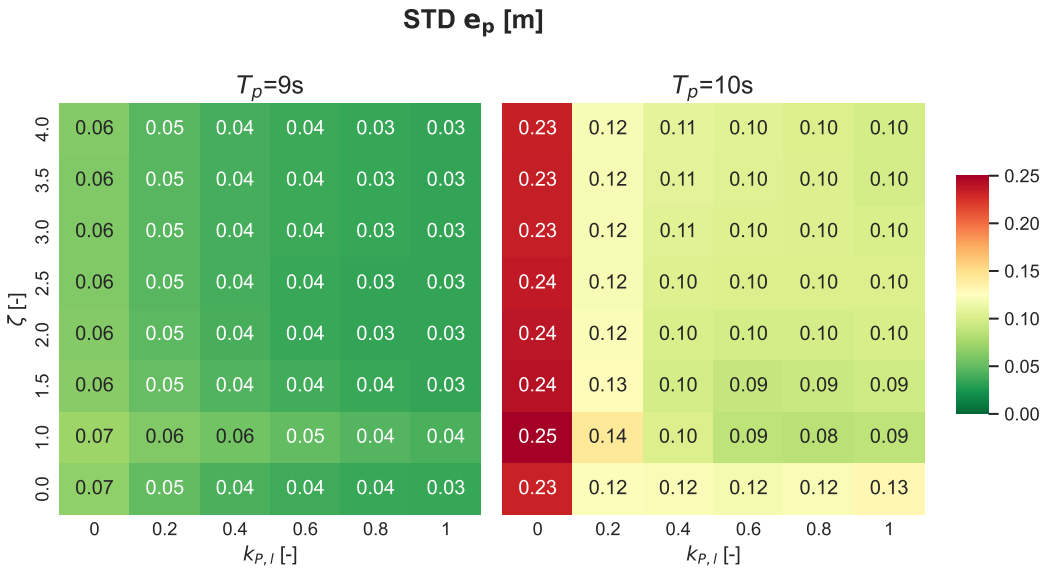

Figure 5.15: Influence of proportional gains on e_p

System limits

In addition, it has been investigated whether the controller exceeds the system limits. In Figure 5.16, two heat maps are given that indicate whether the systems' tension limits are exceeded and to what extent (in percentage time). When the cells are orange, the system's limits have been exceeded. As expected, when the damping part of the controller is disabled (i.e. ζ=0), the controller is very likely to exceed the system limitations. Furthermore, it can be seen that when the damping coefficient increases, the chance of exceeding the tugger limit increases. This is because when ζ gets higher, the range (R) of the tension velocity relationship becomes lower. A lower range means more tension build-up and increase the chance of exceeding the tension limit.

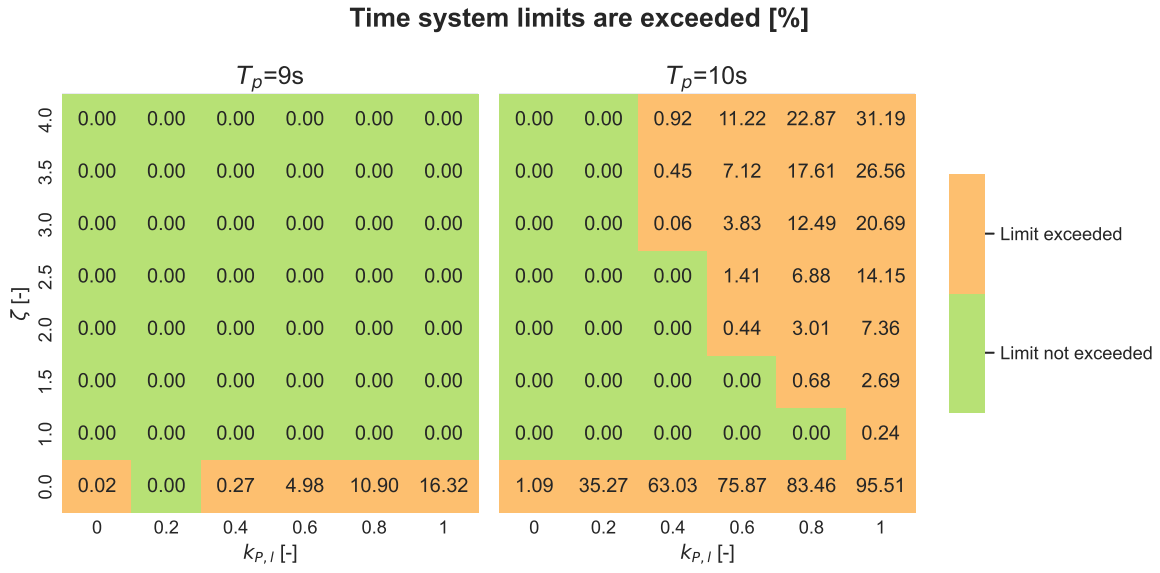

Figure 5.16: Percentage time of limits being exceeded for different control gains (LC2)

Total work

Finally, the influence of the control gains on the power consumption (total work) of the control strategy has been determined. The results are summarised in the heat maps shown in Figure 5.17. Similarly to LC1, the higher T_p results in more work due to the increased excitation of the system. In addition, it can be seen that an increase in $k_{P,l}$ results in a significant increase in work, which can be explained by the increase in responsiveness to the positional error. When both control gains are zero, there is no active response to the tension and length error, and the tugger lines remain at a fixed length. Logically, in this scenario, no energy is needed; therefore, the total work is zero.

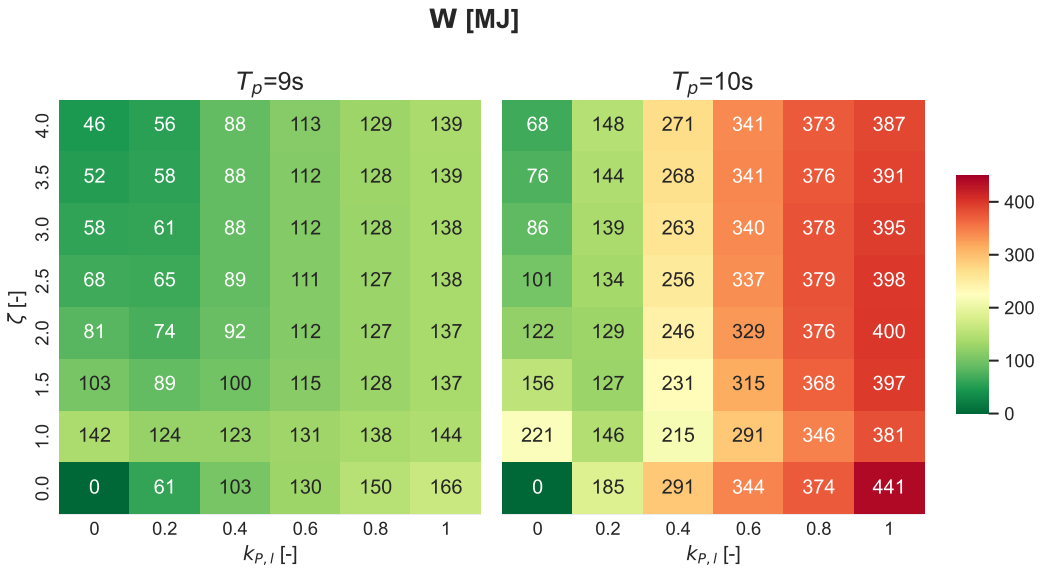

Figure 5.17: Total work for different control gains (LC2)

In short, a higher $k_{P,l}$ leads to a lower positional error, a greater chance that the system limitations are exceeded and an increase in work. An increase in ζ has no significant effect on the positional error, a lower probability of exceeding the system limits and a slight decrease in the work.

The lowest positional error can be found for $k_{P,l} \geq 0.4$. An increase in $k_{P,l}$ leads to an increase in work, and the chance of exceeding the system limitations increases. Therefore a $k_{P,l}$ of 0.4 has been chosen. Given the fact that a low ζ reduces the chance of system failure and leads to a lower workload, a ζ of 1 is chosen.

6

Results

This chapter evaluates the proposed control strategies based on multiple time domain simulations for different sea-states. The different wave particulars for which the control strategies are evaluated are given in Table 6.1. More general information about the simulation properties is given in Chapter 3.

Table 6.1: Wave particulars performance evaluation

H_s [m]	T_p [s]	γ [-]	θ [deg]
1.5	4	5	90-180 (step size 15)
1.5	5	2.87	
1.5	6	1.12	
1.5	7	1	
1.5	8	1	
1.5	9	1	
1.5	10	1	

6.1. Load Case 1

In Figure 6.1, the impact of the damping controller on LC1 is given. To put it in perspective, the results of the uncontrolled system (which were already given in Chapter 4) are presented next to the results of the damping tuggers.

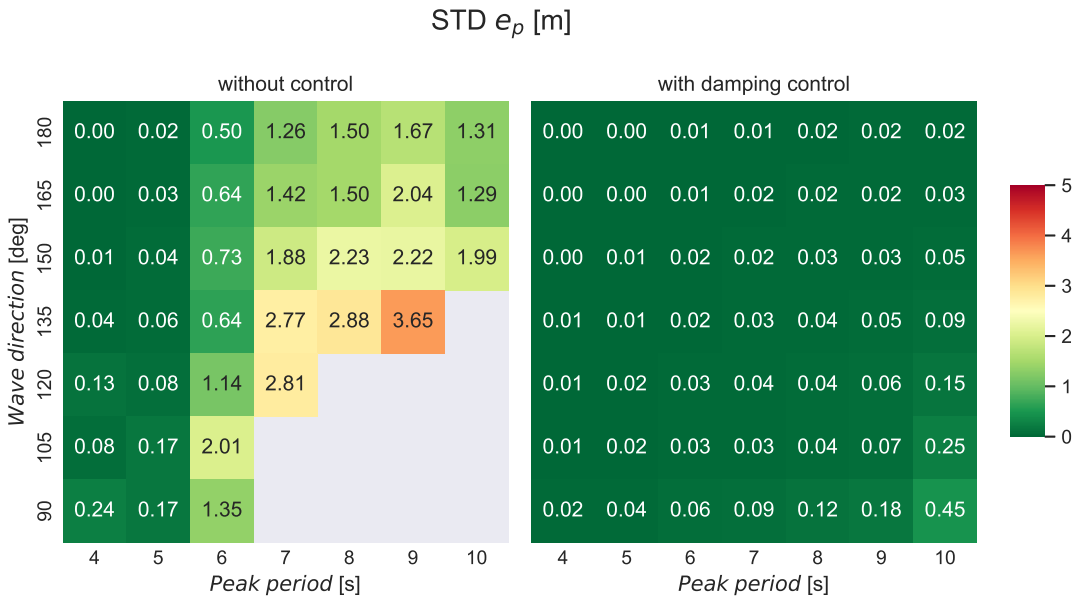

Figure 6.1: e_p results (no tuggers vs. standard damping tuggers)

When comparing both heat maps, the impact is clear. The tuggers prove to be very effective; not a single model has crashed, and e_p is considerably lower for every sea state. The most significant reduc-

tion in the positional error is achieved for the more challenging sea states (i.e. more beam-on wave directions and higher peak periods). However, the positional error is not eliminated. As the damping control scheme is a proportional controller, it does not track the reference input; hence over- and undershooting is unavoidable. For the higher peak periods, the chance of tuggers reaching the maximum tension (and then switch to constant tension mode) becomes higher. In the constant tension mode, the tugger winch follows the load's motion and can no longer hold the payload at the desired position. Therefore, the trend of greater positional error for more challenging sea states is still observed after implementing the damping tuggers.

To give a more detailed insight into the impact of the damping tuggers, several time history examples are given in Figure 6.2. The time history plots show the horizontal motions (X & Y) and positional error over time. Only the time-domain motions from 200-800s are shown to avoid crowding up. As the pendular motions cause the positional error, a fluctuating positional error can be observed in the uncontrolled scenario. The pendular motions in the horizontal plane can be observed by the fluctuation X and Y position of the bottom centre position of the JLT (p_0). After implementing the damping tuggers, a significant decrease in the payload's horizontal motions and desired position can be observed. The JLT follows the fluctuating desired position (p_d) very well, which can be seen in Figure 6.2d. The steeper the slope of the X & Y signal, the larger the velocity of the JLT. This ultimately leads to higher tensions, hence a greater positional error.

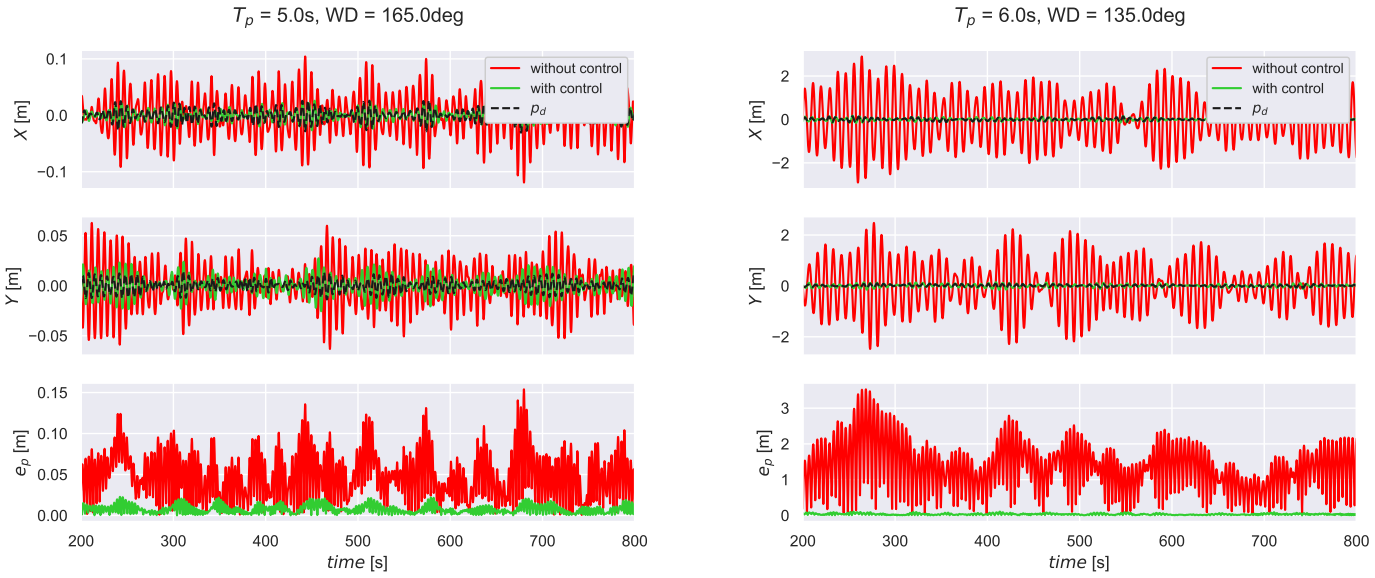

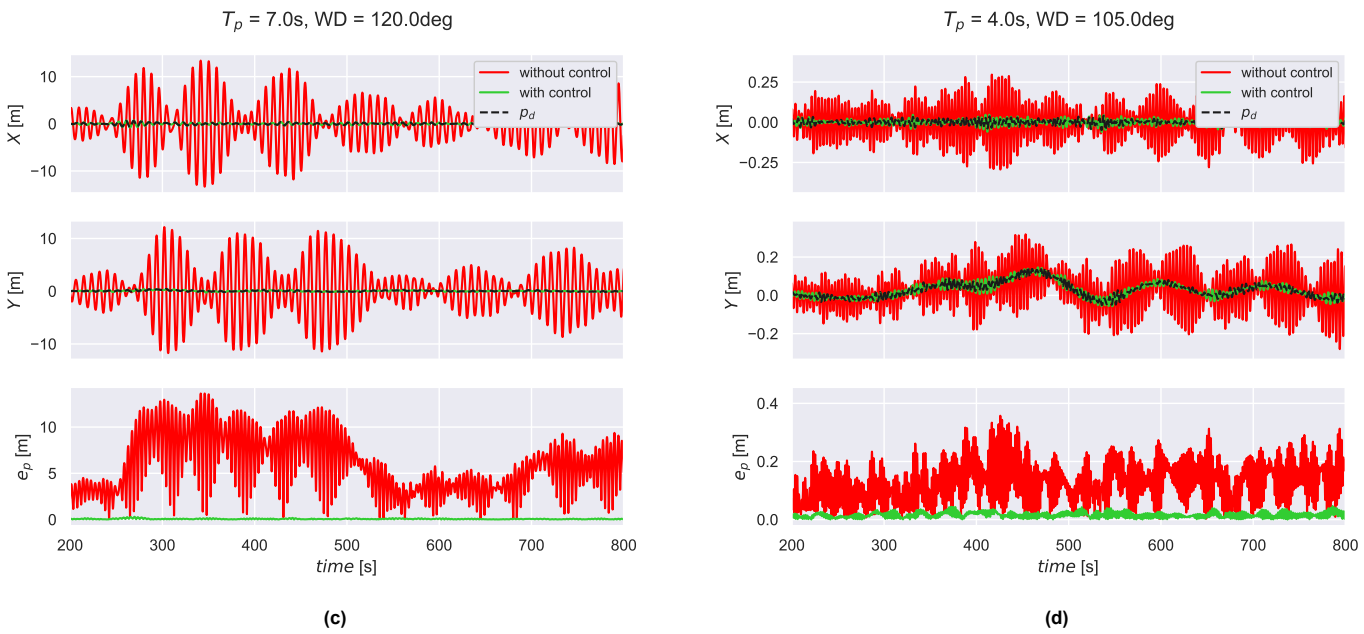

Figure 6.2: Example of motions at the JLT bottom center in different sea states (LC1)

6.2. Load Case 2

In Figure 6.3, the impact of the proposed controller for LC2 is given. In addition, the results when implementing the damping tuggers are shown. As damping tuggers are the current state state-of-the-art in offshore motion mitigation of suspended payloads, it can be determined how the proposed control scheme performs in comparison to the damping tuggers. The damping control scheme has been tuned in the same way as in LC1.

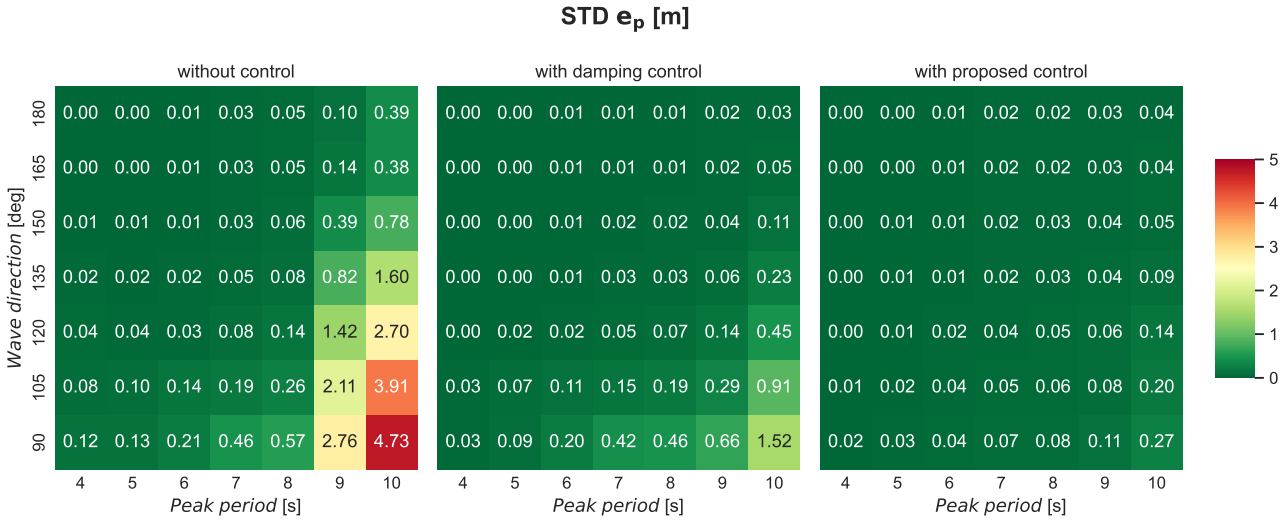

Figure 6.3: e_p results (no tuggers vs. positioning-damping tuggers)

Again the damping tuggers prove to be very effective. The standard deviation had decreased significantly. The data also indicates a higher STD of e_p in LC2 than LC1 for higher peak periods. This can be explained by the smaller natural roll period in combination with the crane tip excitation that contributes to the positional error in LC2. In these sea states, the proposed control scheme is more effective in reducing the positional error than the damping tuggers. In some sea states, the specific motion reduction is not very significant, e.g. sea state with T_p=6s and θ=165deg. It should be noted that the system's

motion in the corresponding sea states is minimal. These scenarios are thus not challenging, and a tugger winch control is redundant.

Figures 6.4 & 6.5 show some of the simulations' time history and trajectory plots. In LC2, the crane orientation is perpendicular to the vessel's stern. Therefore, the X- and Y-displacement are related to the payload's side- and off-lead motions. The desired position (p_d) is fixed in the global reference system and is constant over time. In LC2, the excitation of the crane tip also contributes to the positional error. As the crane is positioned more or less midships, the pitch has a significantly smaller effect on the crane tip motion than the roll motion of the vessel. For this reason, the Y-displacement is (in general) higher compared to the X-displacement.

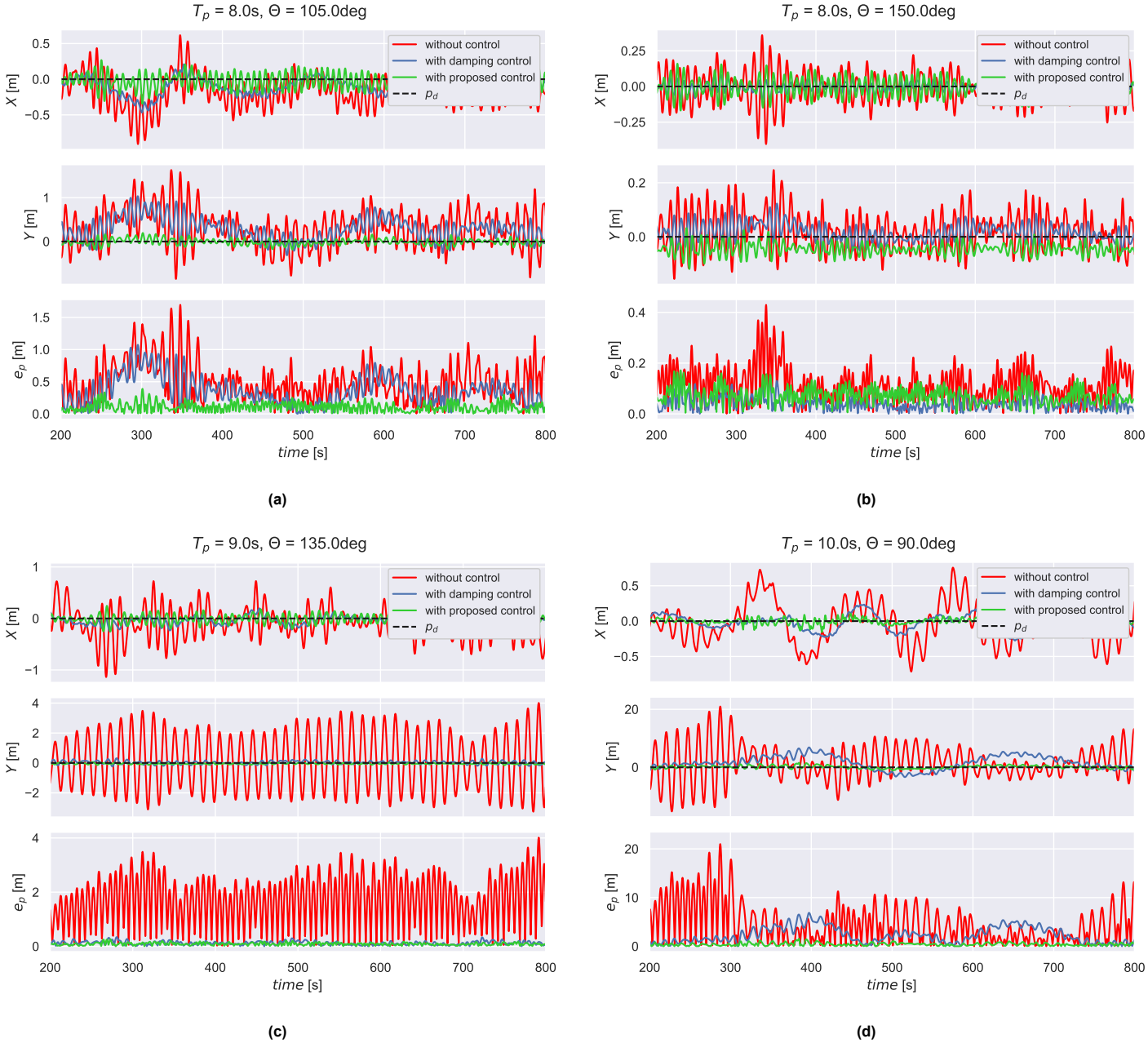

Figure 6.4: Example of motions at the JLT bottom center in different sea states (LC2)

The proposed control scheme causes the tuggers to dampen the system, resulting in a decrease in pendular motions, but at the same time corrects the positional error caused by the crane tip motions. Therefore, especially in sea states where the excitation of the crane tip is considerably (i.e. high roll motions), the tuggers operating with the proposed control scheme are better able to keep the payload in the desired position (compared to the damping tuggers). In sea-states with small roll motions of the vessel, no significant difference in the positional error between damping and proposed control tuggers can be observed (see Figure 6.4d).

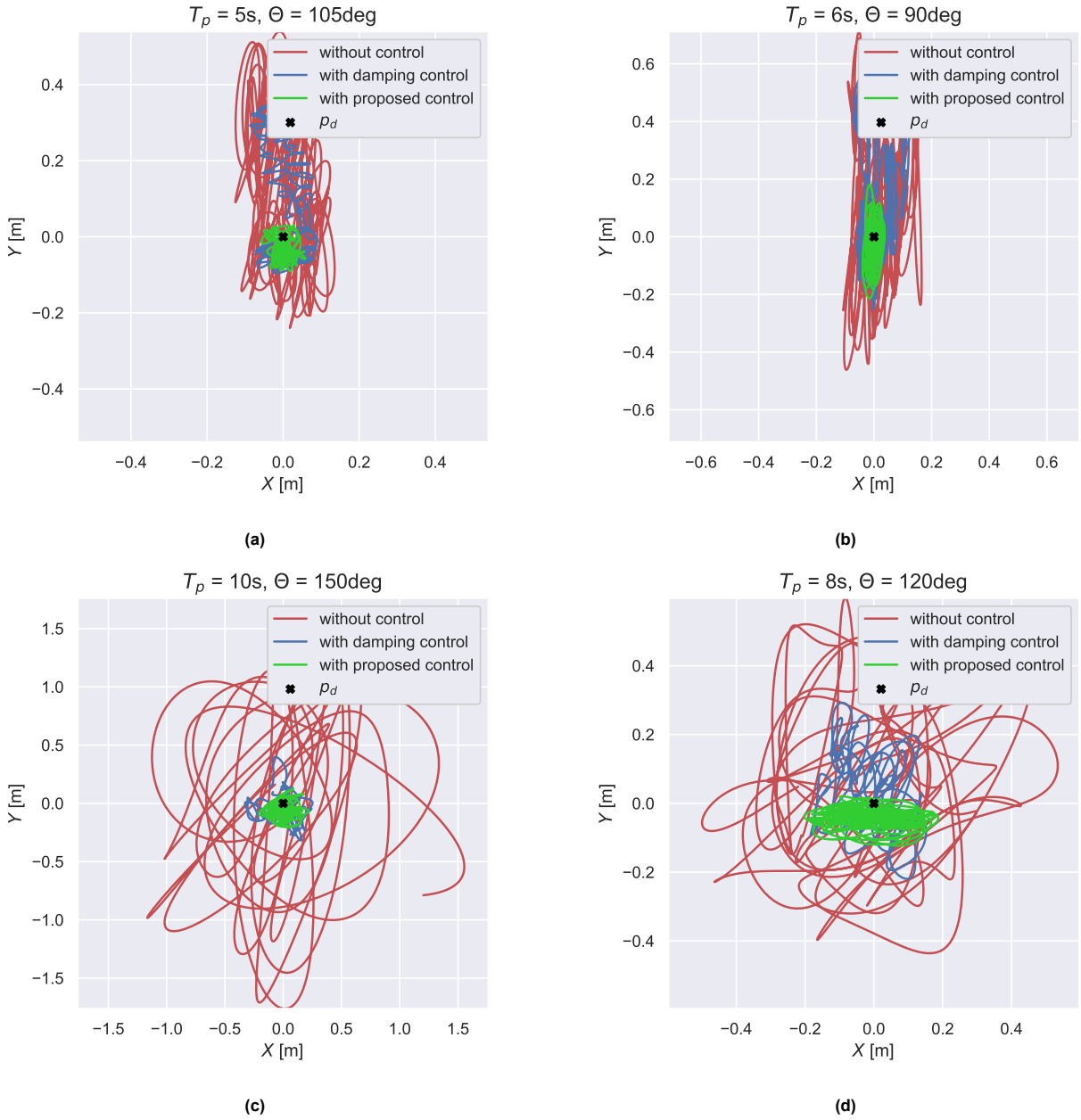

Figure 6.5: Trajectories of the bottom center of the JLT in the horizontal plane

The PSD plots provide information on how the energy is distributed among different frequencies for a given signal. For any dynamical system, acceleration is responsible for its motion. Therefore the spectra of the horizontal accelerations (X & Y) of the JLT have been analysed. Examples of spectra are presented in Figure 6.6. It can be noted that the magnitude of the peaks in the spectra is well reduced by the controlled tugger winches. The peaks in these plots can be explained by the sea state and the system's natural frequencies. For example, in Figure 6.6a the PSD response of a sea state with a peak

period of 7s and a wave direction of 135deg is given. The natural frequency of the pitch mode is 0.12 Hz (see Table 5.1), which explains the peak in the PSD in the X direction (=side-lead direction). The natural frequency of the roll mode is $\pm$0.075 Hz. In this case, however, no peak can be observed in the Y-direction (off-lead direction). This is because the concerned frequency falls outside the wave spectra of this sea-state (see Figure 4.2). Since the other example concerns a sea state where the roll mode does fall in the range of the wave spectra, a peak at $\pm$0.075Hz can be observed. It can also be observed that the peak is much more significant, which confirms the higher JLT resonance for the given sea state.

In both the scenarios without control, one can also observe a peak at 2.3Hz and 2.6Hz for the X and Y acceleration respectively. These peaks correspond to the double pendulum mode in the side- (X) and off-lead (Y) direction.

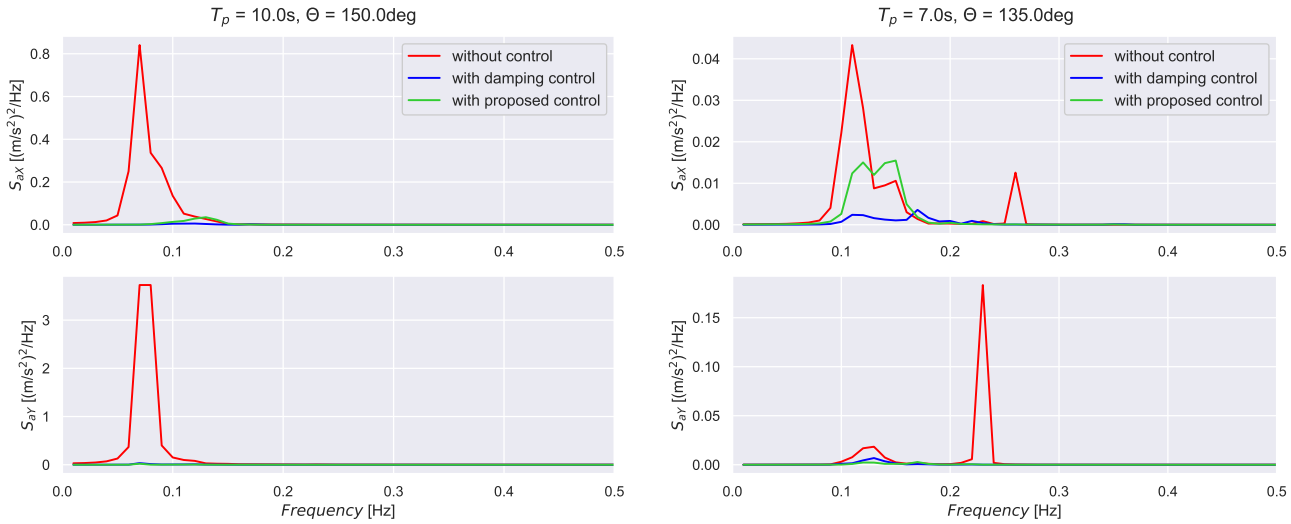

Figure 6.6: e_p results (Peak Spectral Density plot example of the JLT accelerations)

6.2.1. Measurement sensitivity analysis

It should be noted that it is assumed that the required values are well estimated by sensors and observers. However, in reality, there will be measurement errors that affects the performance of the control scheme. For this reason, a sensitivity study is conducted regarding this measurement accuracy.

Figure 6.7 shows the sensitivity of the proposed control scheme for a given sea state (θ=135deg and T_p=9s) in Load Case 2. The observers of the controller monitor three different variables: the locations of the payload, the location of the winch and tension in the lines. It is assumed that the winches can accurately measure the tension. To simulate a measurement noise, a measurement error, normalised to its actual length, has been added after obtaining the desired length (Equation 2.20) in the following way:

$$l_{d,noise} = l_d + l_d \cdot \beta \cdot \text{random number (in between -0.500 and 0.500)} \tag{6.1}$$

The measurement error is expressed using the measurement error ratio (β). When β=0.1, the accuracy of distance measurement is 90%. In this case, the inaccuracy of a 1m measured distance would be around 0.1m.

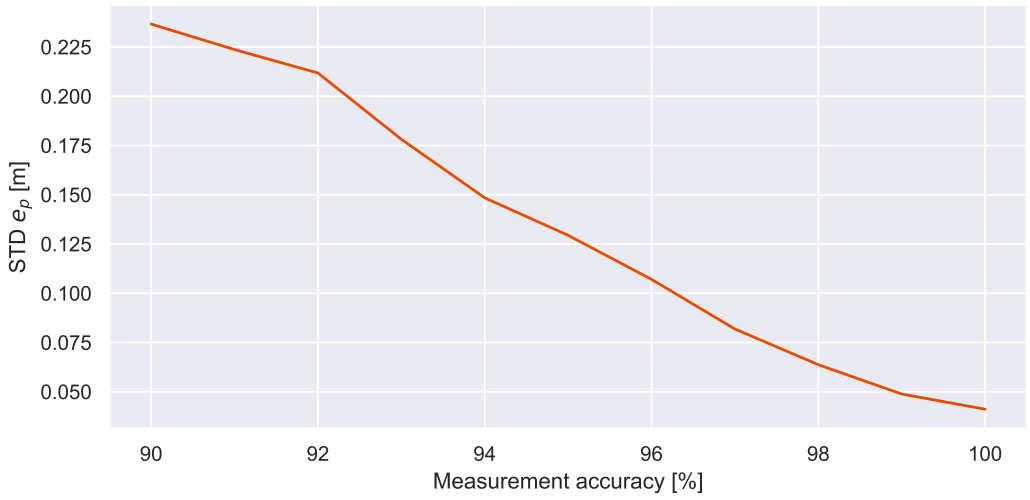

Figure 6.7: Measurement error sensitivity results

The sensitivity study shows the expected trend; a lower accuracy leads to a higher positional error. In addition, the controller remains stable and the trend is more or less linear. Therefore, it can be confirmed that the controller's performance is sensitive to measurement error and observers with high accuracy are crucial.

7

Conclusion & Discussion

7.1. Conclusions

In this study, a model-free control scheme has been proposed for a general offshore floating lifting operation with a complex-shaped payload. The controller uses tugger winches as an actuator to keep the payload at its desired horizontal position. The performance is evaluated by implementing the control scheme into a fully integrated simulation model and examining the dynamic behaviour of various sea states. The control strategy uses three tugger winches, in which two are placed on both ends of the outrigger, and the third one comes from the crane boom. Two load cases are considered, for which different control schemes are implemented. Load Case 1 considers the installation operation of a jacket foundation, for which the damping tuggers are the recommended model-free control scheme to be used. Load Case 2 is the scenario in which the jacket is to be decommissioned and makes use of a control scheme which is proposed by the author. The control scheme is inspired on the proven concept of the damping tuggers proposed by Meskers and Dijk [32] and a recent paper published by Ren et al. [41]. In doing so, a model-free control scheme is obtained, capable of both damping and positioning a suspended payload while considering the system's tension, velocity and power limitations.

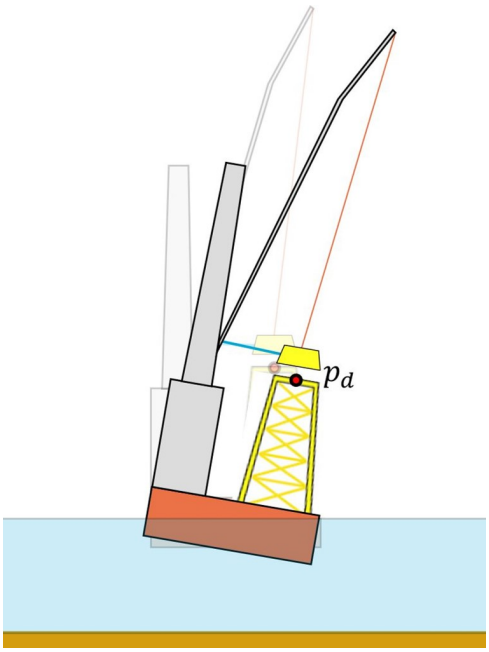

Figure 7.1: Load Case 1

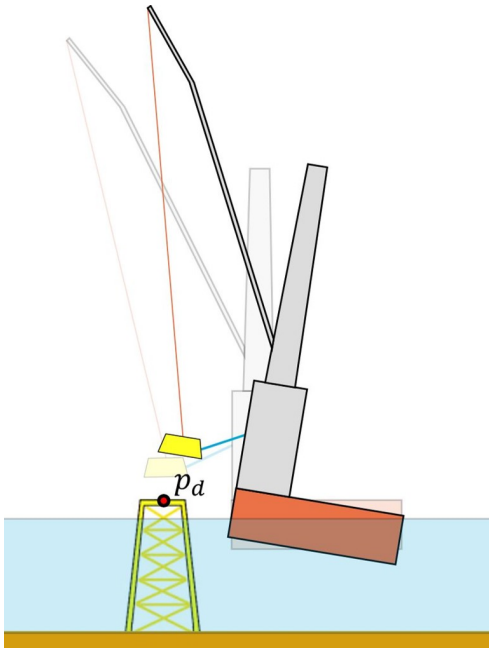

Figure 7.2: Load Case 2

Figure 7.3: Concerned load cases

The main research question states:

What is the impact of the proposed model-free control strategies on the dynamic behaviour of a complex-shaped 6-DOF payload?

It can be concluded that when no countermeasures are taken to deal with the payload's motions, it will have a strong impact on the workability of the operation in both load cases. The implementation of both model-free control schemes results in a significant decrease in the standard deviation of the positional error and therefore provides a more efficient and safe lifting operation.

In Load Case 1, the positional error is a result of the resonance motions of the payload. The damping tuggers are a highly effective measure for cancelling the pendular motions. Besides keeping the payload's position constant in the vessel's reference system, the control scheme also prevents the system from exceeding the tension, power and velocity limits when tuned correctly. The results confirm the effectiveness of the current state-of-the-art when it comes to motion mitigation of a suspended payload.

The desired position in Load Case 2 is, contrary to Load Case 1, variable in the vessel's reference system. As a result, besides the payload's motions, the crane tip excitation also contributes to the positional error. The damping tuggers and the proposed control scheme significantly reduce the positional error compared to the uncontrolled scenario. The proposed control scheme can better keep the payload at its desired position in both the X (side-lead) and Y-direction (off-lead) for sea states in which significant crane tip excitation takes place. The proposed control scheme has a simple form, but a adequate performance, which has been verified by multiple time domain simulations. Since the control scheme is model-free, the controller can be implemented in other configurations (e.g. different number of lift wires or type of payloads). Another advantage of the controller is that the setpoint (i.e. desired position) can be adjusted. This allows the controller to be used for various purposes (e.g. heave compensation).

The sub-questions are the following:

What are the relevant motion modes of the system and to what extent does the proposed configuration of tugger winches influence these?

The first-order wave-induced vessel motions cause the excitation of the payload. The wave frequency and natural frequency of the system's modes determine the severity of the excitation of the payload. The roll and (therefore the) pendulum mode cause the installation problems (i.e. high positional errors) for a wave frequency close to their resonant frequencies. The natural frequency of the pendulum mode depends on the hoist tackle length and is therefore highly dependent on the type of lifting operation. Implementing the winch configuration adds stiffness to the system, resulting in a significant reduction in the natural periods of the payload modes. As the considered payload is relatively light, the coupling between the payload and vessel is weak, and the impact on the natural periods of the vessel is less significant.

The vessel (and thus crane tip) motions become more significant when the sea is abeam and for a wave frequency close to the natural roll period. The pitch mode is less relevant for two reasons. First, the Bokalift 1 is a monohull vessel, hence less vulnerable to pitching. Secondly, the crane is positioned approximately midships, which causes pitching to have a smaller impact on the crane tip excitation (compared to rolling). In Load Case 1, more significant excitation of the crane tip leads to greater tension in the tugger lines and thus indirectly increases the positional error. In Load Case 2, the crane-tip excitation directly influences the positional error.

What are the system's limitations and how do they affect the tugger winch performance?

Important limitations to consider when using tugger winches are the tension, velocity and power limits. In the considered case study, the winch type is responsible for the maximum winch velocity and power. The padeyes on the crane boom are responsible for the maximum allowable tension in the tugger lines. The chance that the tension, velocity or power limit is exceeded depends on several factors, such as the payload type, winch configuration, desired control behaviour and environmental conditions. For example, as the power limitation of the winches restricts certain tension-velocity combinations, it will have more impact on the performance when lifting heavier payloads. In other words, a change in the system limits will not necessarily affect the performance of the tugger winches.

Considering the results of implemented model-free control schemes, several conclusions can be drawn:

Load Case 1

As the desired position is fixed in the vessel's reference system, a positional error of zero could theoretically be achieved if the tuggers were kept at a fixed length under a given pre-tension (if one would neglect the elongation of the wires). However, in this scenario, the tension in the lines would become too high; therefore, keeping the lines at a fixed length is impossible in the concerned case. The damping tuggers prevent exceeding these limits. The lower the damping ratio, and the more energy dissipation takes place and the lower the positional error and energy consumption of the winches. The power or tension limit of the system determine the maximum possible damping. When the maximum allowable tension is reached, the damping tuggers switch to constant-tension mode, and the chance arises that the velocity limits will be exceeded. Hence, the chance of exceeding the velocity limit depends on the tension limits. Therefore, the tension limits are a critical factor in the damping tuggers' performance (and reason for implementation). Enforcing the padeyes on the crane, thereby increasing the tension limits of the system, would significantly improve the controller's performance. If the tension limit is high enough, it will make the control scheme's implementation redundant as the tuggers can be kept at a fixed length. In this case, the pre-tension must be high enough to avoid slack.

Load Case 2

The damping part of the proposed controller has a significant impact on the positional error as it adds damping to the system, which significantly reduces the risk of exceeding the tension limits. The power filter prevents tension-velocity combinations that exceed the power capacity of the winch. When the correction takes place, it will be at the expense of the effectiveness of the controller. The same applies to the velocity filter. The required winch velocity depends on the speed at which the tugger line's base and connecting point move relative to each other.

7.2. Discussion & Recommendations

At the current stage, the positional error cannot be totally cancelled by the proposed control scheme. However, it must be noted that the cancellation of the positional error is not required for a successful operation. It is deemed likely that the imperfect configuration geometry and the inability to anticipate on the errors are factors that can be improved and reduce the positional error even more. The design of a configuration is a very general and complex problem. Besides the position of the payload's centre of gravity, it depends on the tugger line properties, winch capacities, payload shape, vessel type, etc. The design of an optimal configuration and arrangement of the base- and connecting points significantly impact the controller's performance and should be addressed and evaluated in future studies. Various optimisation methods can be applied for this, for example, the algorithm proposed by Deng et al. [11]. The performance of the proposed control scheme can be further improved by involving derivative control (the predicted future error) and considering payload motion prediction.

The winch velocity, tension and power limits are considered when tuning the control schemes. However, besides the limitations that directly influence the winch behaviour, there are more limitations that could hinder the performance of the proposed control strategy in the real system and should be investigated. Examples are the maximum side- and off-lead angles of the hoist wires.

Due to the model-free characteristic of the proposed control scheme, the controller can be used for

various purposes and different configurations. Research into suitable operations is recommended.

Given the sensitivity to measurement error, a system without complex measurement situations (including uncertainties and noise) is a prerequisite and ways to maximise the observers' accuracy should be investigated. Since the distance between the winches is constant, their position is fixed in the vessel's reference system and the position of the winches can probably be monitored more accurately than the payload's position. Therefore, a recommendation would be to investigate range-based localisation algorithms to determine the payload's position. Based on this knowledge, one can determine the position of a node (i.e. the payload) in three-dimensional space when the distances (i.e. wire length) and position of four anchor points (i.e. the winches) are known [50].

In this thesis, control delay (i.e. reaction time) effects are neglected. In reality, the control delay is unavoidable because of the motor inertia of the winches and the delay caused by the observers. As with the (investigated) measurement error, a control scheme's performance is also influenced by the time lag of the controller. Research into the impact and ways to minimise the reaction time is recommended.

Finally, wind loads are not taken into account and will influence the system's dynamics. In addition, although Orcaflex can calculate and predict the dynamics of the real system, there will be model errors. For example, the model neglects frictional forces and the mass of the winches. In addition, the crane is assumed to be rigid, but in reality, it can introduce additional oscillations to the payload's motion. It could appear that the proposed control scheme does not exhibit a similar performance in the real system. Or even worse, the system could be destabilised by the controller if the model error is not taken into account, even if the control scheme works perfectly for the Orcaflex model. However, it is deemed unlikely that this would happen as the sensitivity study regarding the measurement error indicates a stable response of the controller. Nevertheless, experimental testing is required to verify the effectiveness of the control scheme.

References

[1] Mahdieh Adeli et al. “Anti-swing control for a double-pendulum-type overhead crane via parallel distributed fuzzy LQR controller combined with genetic fuzzy rule set selection”. In: *2011 IEEE International Conference on Control System, Computing and Engineering*. IEEE. 2011, pp. 306–311.

[2] David G Alciatore. *Introduction to mechatronics and measurement systems*. Tata McGraw-Hill Education, 2007.

[3] Mathias H Andersson et al. *A framework for regulating underwater noise during pile driving*. 2017.

[4] Valentin Antoci, Michael Voor, and Craig Roberts. “Effect of wire tension on stiffness of tensioned fine wires in external fixation: a mechanical study”. In: *American journal of orthopedics (Belle Mead, N.J.)* 36 (Oct. 2007), pp. 473–6.

[5] M. F. Ashby. *Materials selection in mechanical design*. Oxford, OX Boston, MA: Butterworth-Heinemann, 1999. ISBN: 0750643579.

[6] BVG Associates. *Guide to an offshore wind farm*. Tech. rep. 2019.

[7] W Bolton. *Control systems*. Oxford: Newnes, 2002. ISBN: 0080529984.

[8] Boskalis. *Dynamic Lifting Analysis - Jacket Installation - HLV Bokalift 1*. Tech. rep. 034325-BOS-01PJI-ENG-RP-007-01. 2021.

[9] Boskalis. *Equipment Sheet Bokalift 1*. Available at `https://boskalis.com/about-us/fleet-and-equipment/offshore-vessels/heavy-lift-vessels.html`. 2021.

[10] Brian R Copeland. “The design of PID controllers using Ziegler Nichols tuning”. In: *Internet: http://educypedia. karadimov. info/library/Ziegler_Nichols. pdf* (2008).

[11] Wu Deng et al. “An Enhanced MSIQDE Algorithm With Novel Multiple Strategies for Global Optimization Problems”. In: *IEEE Transactions on Systems, Man, and Cybernetics: Systems* 52.3 (2022), pp. 1578–1587. DOI: `10.1109/TSMC.2020.3030792`.

[12] DNV. *Environmental conditions and environmental loads*. DNV DNVGLRPC205. Akershus, Norway: Det Norske Veritas group, 2019.

[13] Klaas Dokkum. *Ship knowledge : ship design, construction and operation*. The Netherlands: DOKMAR, 2013. ISBN: 907150025X.

[14] Eager One. *Jacket lifting tool for offshore wind farm installation*. Available at `https://eager.one/products/jacket-lifting-tool-for-offshore-wind-farm-installation/`. 2021.

[15] Thor Fossen. *Handbook of marine craft hydrodynamics and motion control*. Chichester, West Sussex, U.K. Hoboken N.J: Wiley, 2011. ISBN: 1119994128.

[16] Jocelyn Fréchot. “Realistic simulation of ocean surface using wave spectra”. In: *Proceedings of the first international conference on computer graphics theory and applications (GRAPP 2006)*. 2006, pp. 76–83.

[17] Pouria Hajikarimi and Fereidoon Moghadas Nejad. “Chapter 3 - Mechanical models of viscoelasticity”. In: *Applications of Viscoelasticity*. Ed. by Pouria Hajikarimi and Fereidoon Moghadas Nejad. Elsevier, 2021, pp. 27–61. ISBN: 978-0-12-821210-3. DOI: `https://doi.org/10.1016/B978-0-12-821210-3.00003-6`. URL: `https://www.sciencedirect.com/science/article/pii/B9780128212103000036`.

[18] KW Hermans and JM Peeringa. *Future XL monopile foundation design for a 10 MW wind turbine in deep water*. ECN, 2016.

[19] Huisman. *Technical specification 3000mt Offshore Mast Crane*. Tech. rep. A16-43000-C0-001. 2021.

[20] IEA. *World Energy Outlook 2021*. Available at https://www.iea.org/reports/world-energy-outlook-2021. 2021.

[21] IEC. *Wind energy generation systems - Part 3-1: Design requirements for fixed offshore wind turbines*. IEC 61400-3-1. Nordhavn, Denmark: Dansk Standards Association, 2019.

[22] IRENA. "Renewable power generation costs in 2018". In: *International Renewable Energy Agency* (2019).

[23] Zhiyu Jiang. "Installation of offshore wind turbines: A technical review". In: *Renewable and Sustainable Energy Reviews* 139 (2021), p. 110576.

[24] Zhiyu Jiang et al. "A parametric study on the final blade installation process for monopile wind turbines under rough environmental conditions". In: *Engineering Structures* 172 (2018), pp. 1042–1056. ISSN: 0141-0296. DOI: https://doi.org/10.1016/j.engstruct.2018.04.078. URL: https://www.sciencedirect.com/science/article/pii/S0141029617328456.

[25] J.M.J. Journée, W.W. Massie, and R.H.M. Huijsmans. *Offshore Hydromechanics (Third Edition)*. Sept. 2015.

[26] Robi Kelc et al. "The Physiology of Sports Injuries and Repair Processes". In: May 2013, pp. 43–86. ISBN: 978-953-51-1031-6. DOI: 10.5772/54234.

[27] Gi Bae Kim et al. "Machine learning applications in systems metabolic engineering". In: *Current Opinion in Biotechnology* 64 (2020). Analytical Biotechnology, pp. 1–9. ISSN: 0958-1669. DOI: https://doi.org/10.1016/j.copbio.2019.08.010. URL: https://www.sciencedirect.com/science/article/pii/S0958166919300643.

[28] Joyce Lee and Feng Zhao. *Global Offshore Wind Report*. Available at https://gwec.net/global-offshore-wind-report-2021/. 2021.

[29] Elmira Madadi. "Model-Free Control Design for Nonlinear Mechanical Systems". PhD thesis. Dissertation, Duisburg, Essen, Universität Duisburg-Essen, 2019.

[30] J Manwell. "Offshore Wind Energy Technology Trends, Challenges and Risks". In: *Renewable Energy Systems* (2013), pp. 1306–1338.

[31] Buckley C P Bucknall C B McCrum N. G. *No Title*. Oxford University Press, 1997. ISBN: 978-0-198565-26-0. URL: https://app.knovel.com/hotlink/toc/id:kpPPEE0023/principles-polymer-engineering/principles-polymer-engineering.

[32] Geert Meskers and Radboud van Dijk. *A Damping Tugger System for Offshore Heavy Lifts*. Tech. rep. 2012, pp. 315–323.

[33] Walt Musial. *Floating Wind Turbines on the Rise*. Available at https://www.nrel.gov/news/program/2020/floating-offshore-wind-rises.html. 2020.

[34] Tiago P. Nascimento and Martin Saska. "Position and attitude control of multi-rotor aerial vehicles: A survey". In: *Annual Reviews in Control* 48 (2019), pp. 129–146. ISSN: 1367-5788. DOI: https://doi.org/10.1016/j.arcontrol.2019.08.004. URL: https://www.sciencedirect.com/science/article/pii/S1367578819300483.

[35] Quang Hieu Ngo et al. "Fuzzy sliding mode control of an offshore container crane". In: *Ocean Engineering* 140 (2017), pp. 125–134. ISSN: 0029-8018. DOI: https://doi.org/10.1016/j.oceaneng.2017.05.019. URL: https://www.sciencedirect.com/science/article/pii/S0029801817302718.

[36] Michael O'Connor et al. "Weather windows analysis incorporating wave height, wave period, wind speed and tidal current with relevance to deployment and maintenance of marine renewables". In: (Oct. 2012).

[37] Ki-Yong Oh et al. "A review of foundations of offshore wind energy convertors: Current status and future perspectives". In: *Renewable and Sustainable Energy Reviews* 88 (2018), pp. 16–36.

[38] Antonio Pegalajar-Jurado et al. *Cascaded numerical models for offshore floating wind turbines*. DTU Vindenergi, 2018.

[39] Yuzhe Qian, Yongchun Fang, and Biao Lu. “Adaptive robust tracking control for an offshore ship-mounted crane subject to unmatched sea wave disturbances”. In: *Mechanical Systems and Signal Processing* 114 (2019), pp. 556–570. ISSN: 0888-3270. DOI: https://doi.org/10.1016/j.ymssp.2018.05.009. URL: https://www.sciencedirect.com/science/article/pii/S0888327018302577.

[40] Dongsheng Qiao et al. “Analysis on snap load characteristics of mooring line in slack-taut process”. In: *Ocean Engineering* 196 (2020), p. 106807.

[41] Zhengru Ren et al. “Model-free anti-swing control of complex-shaped payload with offshore floating cranes and a large number of lift wires”. In: *Ocean Engineering* 228 (2021), p. 108868.

[42] Hannah Ritchie and Max Roser. “CO2 and Greenhouse Gas Emissions”. In: *Our World in Data* (2020). https://ourworldindata.org/co2-and-other-greenhouse-gas-emissions.

[43] “Copyright”. In: *Marine Systems Identification, Modeling and Control*. Ed. by Tony Roskilly and Rikard Mikalsen. Oxford: Butterworth-Heinemann, 2015, p. iv. ISBN: 978-0-08-099996-8. DOI: https://doi.org/10.1016/B978-0-08-099996-8.09995-X. URL: https://www.sciencedirect.com/science/article/pii/B978008099996809995X.

[44] Sebastian Schreier. *Lecture notes Floating Structures and Offshore Moorings*. Feb. 2021.

[45] Mahmud Iwan Solihin, Ari Legowo, Rini Akmeliawati, et al. “Robust PID anti-swing control of automatic gantry crane based on Kharitonov’s stability”. In: *2009 4th IEEE Conference on Industrial Electronics and Applications*. IEEE. 2009, pp. 275–280.

[46] Asgeir J. Sørensen. *Marine Cybernetics lecture notes*. Aug. 2018.

[47] Paul Van der Valk. “Coupled Simulations of Wind Turbines and Offshore Support Structures: Strategies based on the Dynamic Substructuring Paradigm”. PhD thesis. TU Delft, Oct. 2014. DOI: 10.4233/uuid:ac619319-9eae-443d-8b94-d0246f80ffdb.

[48] WindEurope. *Offshore Wind in Europe. Key trends and statistics 2020*. Available at windeurope.org. 2021.

[49] Tong Yang et al. “Neural network-based adaptive antiswing control of an underactuated ship-mounted crane with roll motions and input dead zones”. In: *IEEE Transactions on Neural Networks and Learning Systems* 31.3 (2019), pp. 901–914.

[50] Reza Zekavat and R Michael Buehrer. *Handbook of position location: Theory, practice and advances*. Vol. 27. John Wiley & Sons, 2011.

[51] John G Ziegler, Nathaniel B Nichols, et al. “Optimum settings for automatic controllers”. In: *trans. ASME* 64.11 (1942).

A

Offshore wind Energy

A.1. Trends

The wind energy market is evolving and one can observe some noticeable trends. Trends of particular interest for this study will be discussed. These are: cumulative installations, wind turbine capacity, wind farm capacity and the distance to shore of wind farms.

A.1.1. Cumulative installations

Europe added 2,918 MW net offshore capacity in 2020. The decrease compared to 2019 was due to the impact of the COVID-19 pandemic on the offshore wind sector. Europe now has a total of 25,014 MW installed [48]. 79% of that installed capacity is installed in the North Sea. The remaining capacity

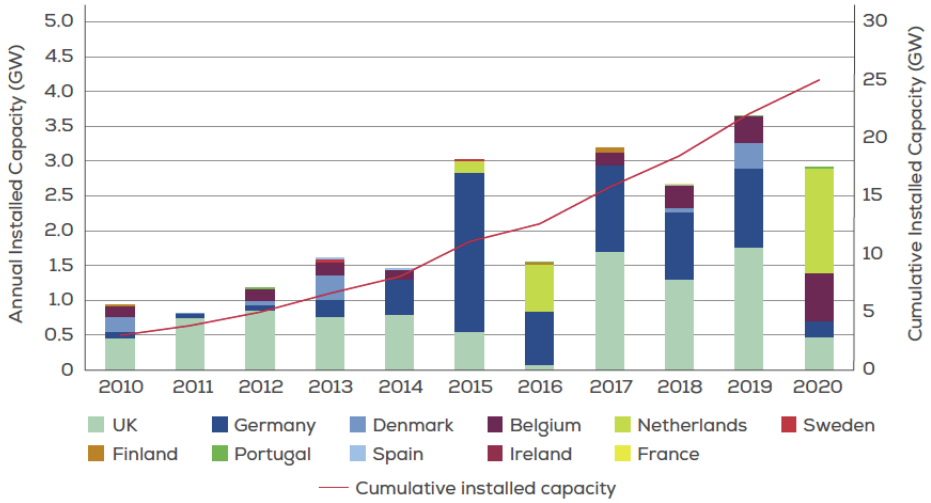

Figure A.1: Annual offshore wind installations by country (left axis) and cumulative capacity (right axis) [48]

is installed in the Irish Sea (12%) , Baltic sea (9%) and the Atlantic Ocean (<1%). The annual installed offshore wind turbines are expected to continue to increase in the coming years. Europe must install around 105 GW of new wind energy capacity over the next five years if Governments aim to reach the targets set in their National Energy and Climate Plans. An increase in offshore wind installations is also a trend outside Europe. Since 2019, China is leader in yearly installed wind capacity [28] and it is expected that other Asian countries and North America will also catch up in the coming years, see Figure A.2.

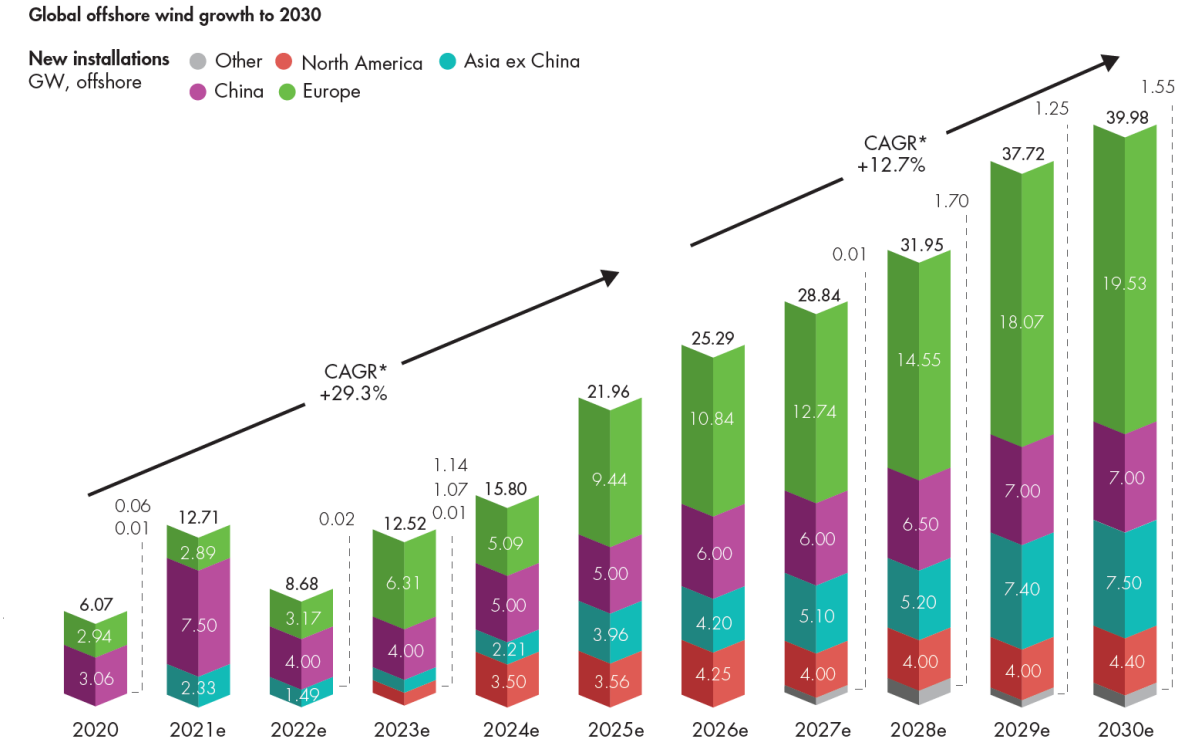

Figure A.2: Offshore market outlook to 2030 [28]

A.1.2. Wind turbine rated capacity

Offshore wind turbines continue to grow in size and power. Since 2015 OWTs have grown at a constant 16% rate. In 2020 the average rated capacity of OWTs installed was 8.2 MW. This trend is likely to continue in the coming years; in 2020, many next-generation OWTs, with a capacity of 10-13 MW, have already been ordered for projects in 2022. Figure A.3 shows the average turbine capacity trend. This trend can be explained by the fact that larger turbines require fewer turbines to produce the same amount of power compared to their smaller predecessors. This continued growth in rated power is one of the many factors that has led to lower offshore wind costs. The ever-growing turbines also affect the installation methods and costs.

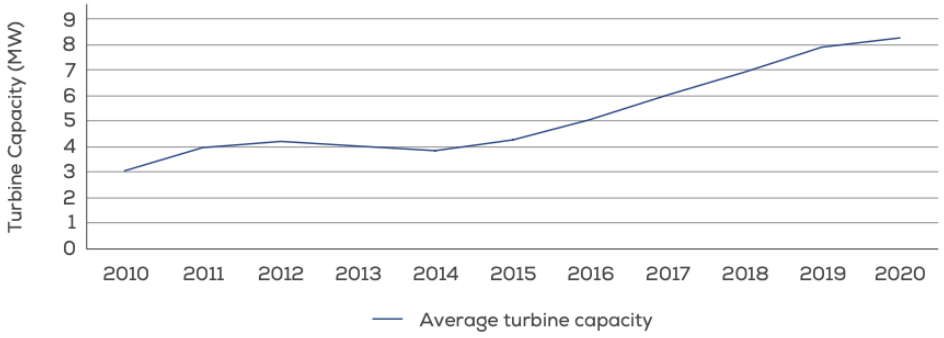

Figure A.3: Yearly average of newly installed offshore wind turbine rated capacity (MW) [48]

A.1.3. Wind farm capacity

In addition to the size of the wind turbines, there is also a trend in the size of the wind farms. Due to the larger wind turbines and the lower LCOE at larg(er) wind farms, the average wind farm capacity is growing the past years. The average wind farm in 2020 was 788 MW, which is 26% larger than the year before and more than two times as big as a decade ago, see Figure A.4.

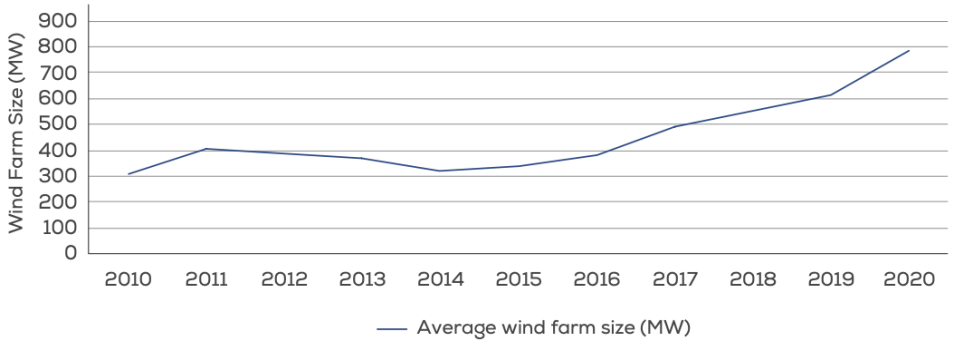

Figure A.4: Average size of commercial wind farm project in the year (MW) [48]

A.1.4. Water depth and distance to shore

Offshore wind farms have moved further from shore and into deeper waters. At the end of 2015, the average water depth of grid-connected wind farms was 27.1 m. In 2020 this average has increased to 36m. One of the reason of this is the better wind conditions further offshore. The average distance to shore of offshore wind farms under construction in 2020 was 44 km [48]. In Figure A.5 one can find the average water depth and distance to shore of offshore wind farms under construction in 2020. The size if the bubble indicates the capacity of the site. Most offshore wind platforms have been installed at depths less than 60 meters, which makes the current offshore wind energy market dominated by bottom-fixed OWTs [22]. This trend increases the installation costs; deeper waters require larger equipment (such as ships and foundations) and an increased distance to the shore increases the installation time.

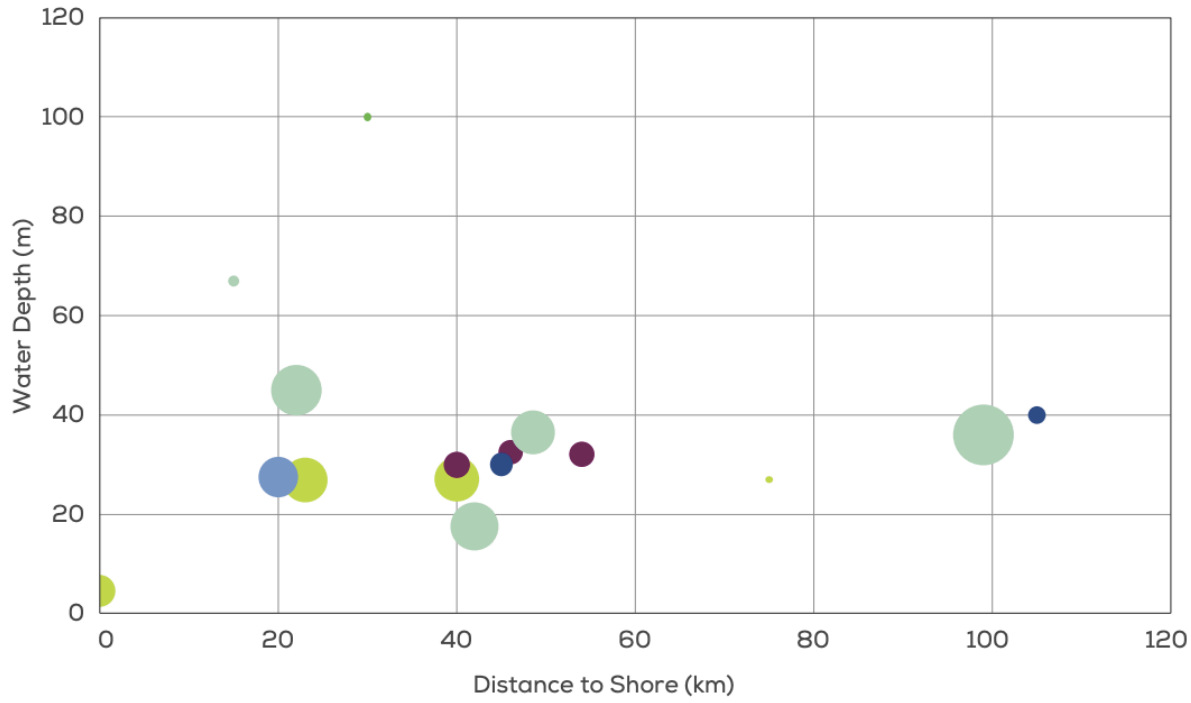

Figure A.5: Average water depth and distance to shore of offshore wind farms under construction during 2020 [48]

A.2. Common types of OWT substructures

Different types of marine substructures exist for installing OWTs, as is shown in Figure A.6 and A.7. There are two main type of substructures: bottom-fixed and floating. Bottom-fixed offshore wind turbines are rigidly connected to the seabed. The connection to the wind turbine tower is usually made with a transition piece, while the connection to the seabed can rely on gravity, penetration of the pile into the seabed, or suction buckets. Floating substructures rely on mooring and anchoring systems to fulfill their station-keeping purposes in deep water [23]. The mooring lines are generally chains, metallic wires or synthetic ropes, which are attached to the seabed through drag anchors, suction buckets or gravity anchors [38]. These different substructure types can be classified according to the water depths they are suited for [47].

Bottom-fixed substructures have the risk of excessive wind and wave induced motions during the installation of the substructure and the installation of the wind turbines. When using floating substructures the latter risk can be reduced by assembling the wind turbine components in a sheltered area (for example near to coast). Subsequently, the substructure with wind turbine can be towed to its final position for mooring connection [23].

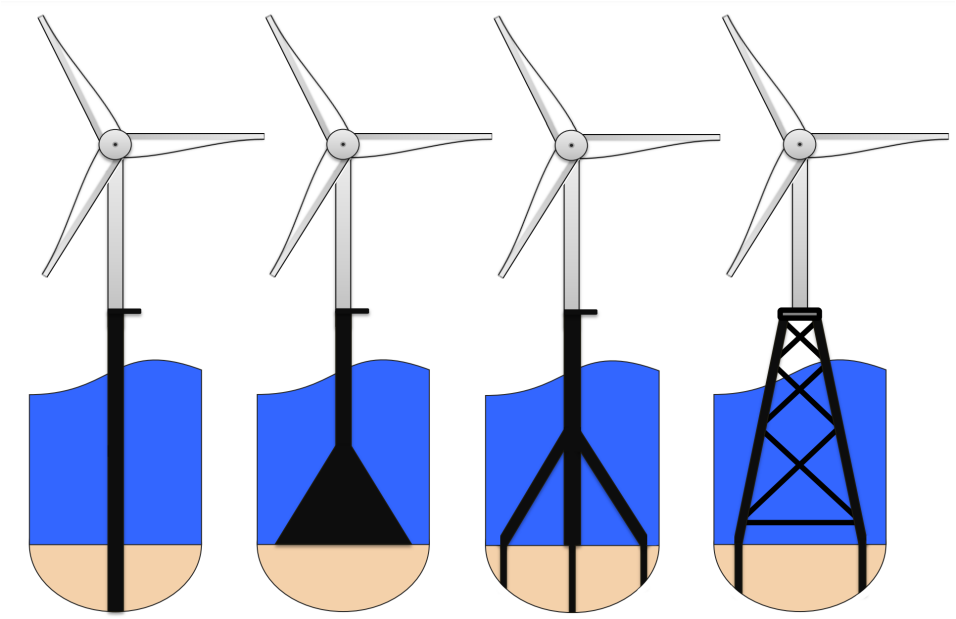

Figure A.6: Different bottom-fixed substructure types for OWTs. From left to right: monopile, gravity based, tripod and jacket [47]

A.2.1. Shallow waters: up to approximately 35 meters

Most OWTs are currently installed in water depths up to 35 meters. In shallow water, the most commonly used types of marine foundations are the following:

- **Monopile foundation**
  A long steel tubular structure with a large diameter that is hammered or vibrated into the seabed. Since monopiles are relatively simple to produce and install, they are the most used substructure type; over two-thirds of all installations in 2020 (80.5%) were monopile foundations [48]. Monopile OWTs commonly have a diameter of 3–8 m and are considered economic for water depths of 20-35 meter [23]. To extend the feasibility to larger wind turbine and greater water depths, so called 'XL-monopiles' with diameters up to 10 meters, are currently under development. The embedded length of the monopile is dependent on the soil conditions and the size of the turbine. Typically, embedded lengths of monopiles are between 20 and 50 m [30]. A large hydraulic hammer is used to drive the piles into the seabed. The impact of the pile driving is one of the considerations in the choice of wall thickness. Certain soil types are not suitable for pile driving. In those cases, a large diameter drill may be used to bore a socket into which the monopile is inserted.

Before the installation of the monopiles the substructures must first be transported to the site by a transportation barge. The installation is done by a jack-up vessel or heavy lift crane vessel. [18].

As described in Section A.1, turbines are getting larger which causes the use of monopiles for the support structures to become more problematic. This is because it is getting harder and harder to find seagoing hammers large enough to drive the very large monopiles [30].

- **Gravity based foundation (GBS)**
  This type of substructure is placed on the seabed and use its weight (1500-4500 tonnes [23]) to create a stable support for the OWT. Its stability comes from the added weight in the form of sand, rocks or iron. GBS structures are attractive alternatives to the monopile foundation when driving the monopile would present difficulties. GBS require a stable/firm seabed and are only economically feasible in very shallow waters (<10 meters), therefore this type of substructure is rarely used nowadays [47]. Gravity based structures have a cumulative share of 5% of all installed substructures [48]. The GBS are constructed on shore or in a dry dock and subsequently taken to tine wind farm site by ship or barge and lowered into place by a large crane.

  The weight of the foundation makes finding vessel to transport and install them a potential challenge. Some companies are therefore investigating the possibility of constructing a GBS which can be floated out to the installation site and then sunk into place [30]. Such a solution would eliminate the need for large vessels or cranes.

A.2.2. Medium water depths: approximately 30 to 60 meters

As discussed in Section A.1, the current trends in the offshore wind industry are to install larger wind turbines in deeper waters. The substructure solutions for shallow waters can become economically and/or technically infeasible in medium water depths. At water depths beyond 30 meters multi-member support structures are used. These come in a variety of designs, depending on the application. The most commonly used multi-member support structure are the tripod and jacket. The production costs of multi-member support structures are relatively high they are composed of many tubular elements that are (generally) connected in the welded nodes. On the other hand, the substructure require relatively little steel to manufacture them.

the most commonly used substructure types are:

- **Tripod foundation.**
  As the name implies, this substructure has three legs. Tripods consists of a central vertical tube, connected to three legs that form a wide base at the seabed. At the seabed the legs are connected to small diameter piles that are driven into the soil in order to anchor the tripods to the seabed. The wide base provides a stable footing which makes it able to withstand large overturning moments [47]. According to WindEurope is the current cumulative share of tripods 2.2%.
- **Jacket foundation**
  A multi-membered construction which is generally built from three or four legs that are connected by bracing. Jacket foundations used for OWT are based on designs adapted from the offshore petroleum industry Manwell. Jackets are fabricated on shore, brought to the site, and lowered, by crane, into place. The legs of the substructure can be attached to small diameter suction buckets or soil-piles to anchor the structure to the seabed [47]. Because of the ”see-through” appearance of the substructure, they are less sensitive to hydrodynamic loads compared to other substructure types. The cross-braced structure and its large footprint result in a stiff foundation type. Despite storage and logistics challenges [23], a jacket-supported OWTs is the second most used foundation (9.9%) and its share is increasing the past years [48].

A.2.3. Deep waters: 60 meters and beyond

According to Musial [33] depths of around 60 meters represent the offshore wind cutoff where bottom-fixed support structures end and floating substructures begin. Regardless of the type of floating support structure for OWTs, lateral movement of the structure must be prevented. This is done by station-keeping facilities, which consist of anchor and mooring lines or tendons. Many different floating concepts are under development, only the three types shown in Figure A.7 are briefly described. Note that most of these types of substructures are still in a testing or prototype phase. All floating foundations

together represents a cumulative 0.2% [48].

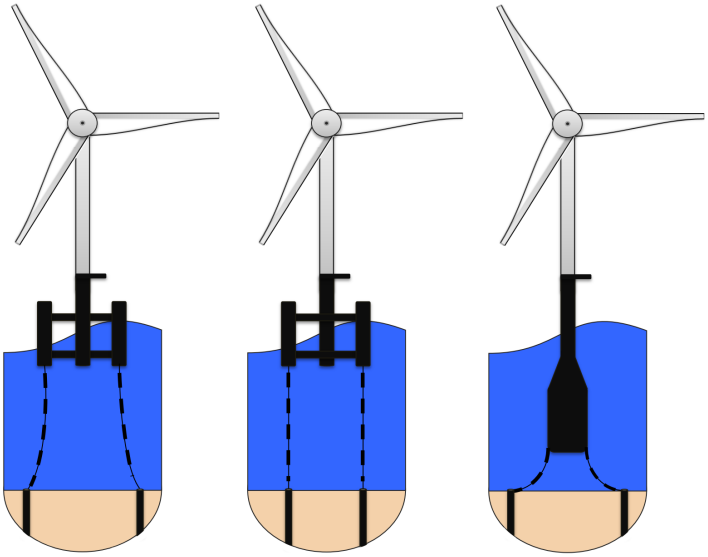

Figure A.7: Different floating substructure types for OWTs. From left to right: semi-submersible, tension leg platform and floating spar buoy [47]

- **Semi-submersibles**
  The floating substructure is partly submerged with a wide base to provide a stable support base for the OWT. The center of mass is higher than the center of buoyancy in these substructures. The stability is maintained through lateral movement of the center of buoyancy when the substructure start to tilt. To achieve this, the water plane area of the semi-submersibles must be quite large. Therefore, they are generally heavy and complex to manufacture. Semisubs are moored with catenary lines and normally use drag anchors.
- **Tension leg platform**
  A vertically moored floating structure. A tension leg platform has a very large buoyancy and uses it to tension the mooring lines between the floater and the seabed in order to stay stable. These tensioned mooring lines, also called taut lines, are connected to the seabed by gravity anchors or suction buckets. This substructure reduces the floater motions but also introduces higher demands on mooring design and soil conditions.
- **Spar-buoy foundation**
  A large slender cylindrical buoy that float upright. Its center of gravity is below sea-level and below the center of buoyancy, which helps stabilise the wind turbine during operation. Spars are moored with catenary lines and normally use drag anchors.

B

Motion control systems

”Control engineering is the science of altering the behaviour of a dynamic process in a beneficial way”[43]. A dynamic process is defined as a process whose output(s) change as a continuous, time-varying function of the input(s). A simple example is the cruise control of a car. The input to the system is the desired speed and the manner in which the actual speed responds is a dynamic function dependent on the physical parameters associated with the engine, car and the external conditions. The use of a control system may have various reasons, however the highest importance is to ensure system stability [43]; they are used to maintain a desired result or value [7].

B.1. Control systems models

Control systems can be classified as an open-loop or closed-loop.

B.1.1. Open-loop system

In this kind of control systems the output may be controlled by a varying input, but the actual output does not influence the input. So the output is determined solely by the initial setting. The advantage of these systems is that are a relatively simple and therefore cheap with a generally good reliability. The disadvantage is that they are often inaccurate since there is no correction for errors. Figure B.1 shows the basic block diagram of such a system. Each block in a block diagram represents a component of the

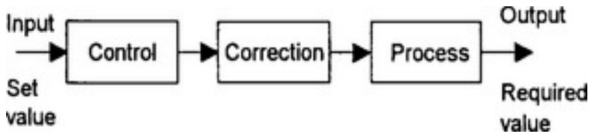

Figure B.1: Open-loop control system [7]

system whereas the connecting arrows represent a system state or signal. An open-loop control system has three basic elements: control, correction and the process which a variable is being controlled [].

1. **Control element**: determines the action to be taken based on the given input to the system
2. **Correction element**: receives input from the controller and gives the action designed to change the variable being controlled as an output.
3. **Process element**: represents the process of which a variable is being controlled.

B.1.2. Closed-loop systems

Unlike the open-loop systems, closed loop systems are able to give feedback to the system to achieve a desired output [43]. The term *closed-loop* refers to the loop created by the feedback path. A closed-loop control system continuously compares the actual output with the desired output value, in order to have the controller compensate for the differences (called an ”error signal”) between the two. This error signal is used as input for the controller. Closed-loop systems have therefore the advantage of being

relatively accurate in the matching the real and desired values. The disadvantage is that the systems are more complex, therefore more costly and have greater chance of breakdown [7]. A standard block representation of a basic closed loop system is illustrated in Figure B.2.

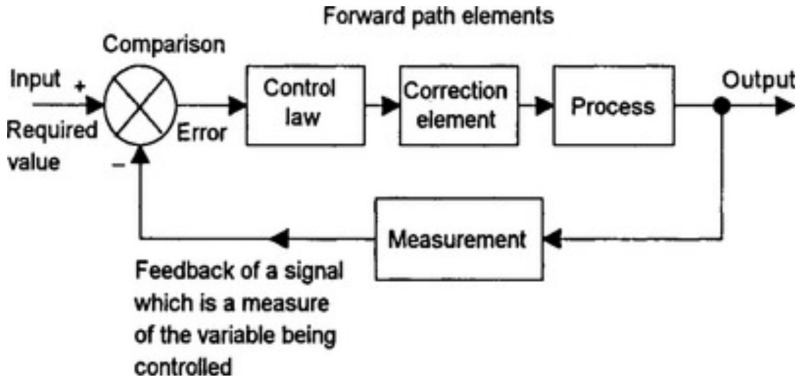

Figure B.2: Closed-loop control system [7]

An closed-loop control system has 5 basic elements:

1. **Comparison element**: compares the desired value of the variable being controlled with the measured value and produces an error signal:

$$error = reference\ value\ signal - measured\ actual\ value\ signal \tag{B.1}$$

   Thus, only when there is a difference between the desired value and the actual value of the variable, there will be an error signal and control action will be initiated.
2. **Control law implementation element**: determined the needed action when an error signal is received. Three different control laws can be implemented: proportional, integral and derivative control. These will be discussed in Section B.2.
3. **Correction element**: often called the *final control element*, corrects/change the controlled condition. A correction unit that has the power to carry out the control action is often called the *actuator*.
4. **Process element**: the system in which the variable is being controlled.
5. **Measurement element**: this element generates a signal related to the variable condition of the process that is being controlled.

In modern marine systems, control systems play and essential part. There are numerous examples of maritime control systems. The focus of this study is on motion reduction. An example of a control system to reduce ship motion is an fin roll stabilisation systems. The system is commonly used to

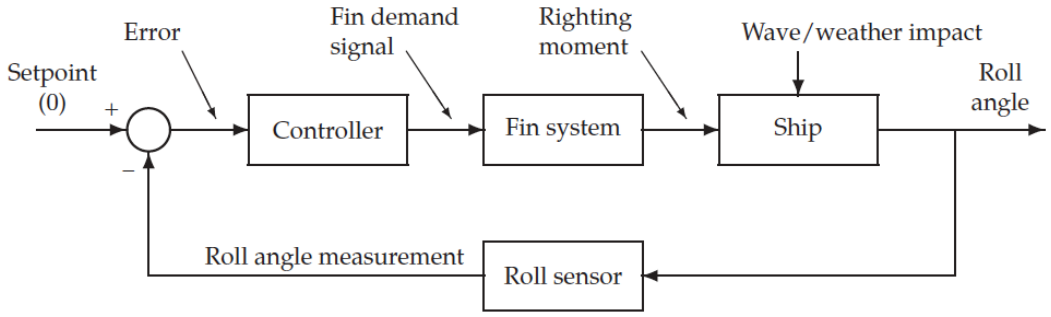

Figure B.3: Fin roll stabilisation control block diagram [43]

improve the behaviour of a ship under the impact of wave loads. In such a system a moment is produced by means of the a fin angle to correct the (undesired) measured roll angle of the ship. The feedback is loop of this system is shown in Figure B.3.

B.2. Process control

As already shown and said in the previous section, a feedback controller is a mechanism that controls the output of a system by adjusting the input. This is done by continuously measuring the output, comparing it to the desired output (the setpoint) and adjusting the input depending on the calculated error. A PID-controller is the most common used feedback controller. It adjusts the control variable depending on three types of errors:

- The present error (P-proportional control)
- The accumulated error in the past (I-integral control)
- The predicted future error (D-derivative control)

As shown in Figure B.2, the output/correction of the controller (u) is equal to the control input to the plant. It is calculated in the time domain and equal to the proportional gain (K_p) multiplied with the magnitude of the error (e) plus the integral gain (K_i) multiplied with the integral of the error plus the derivative gain (K_d) multiplied with the derivative of the error).

$$u(t) = K_p e(t) + K_i \int e(t)dt + K_p \frac{de}{dt} \tag{B.2}$$

B.2.1. Proportional control (P-control)

A proportional controller multiplies the error by a constant gain term (Kp) to get the controller output. In other words, the output is proportional to the input, so if the error value is zero, then the output is zero. Also a value of Kp which is too high will result in oscillation of PV. The disadvantage of a P-controller is that it is not able to track the reference input, so therefore will always be steady-state error.

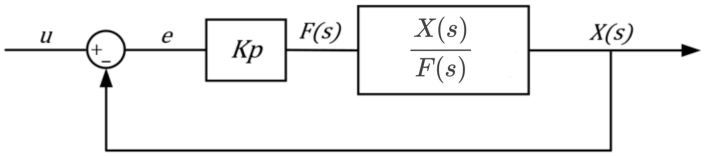

Figure B.4: P-controller block diagram

B.2.2. Proportional and integral control (PI-control)

PI control results in a good speed of response because of the proportional element. The integral element get rid of any steady-state error. PI control fits a system well when it is predominantly first order.

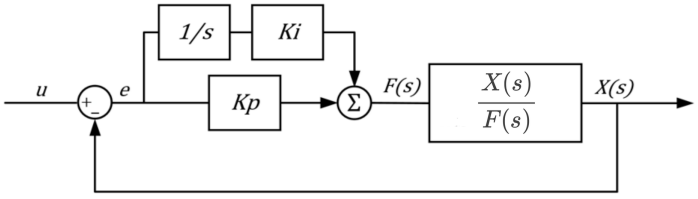

Figure B.5: PI-controller block diagram

B.2.3. Proportional integral and derivative control (PID-control)

For second- or higher order systems a PID controller fits well. A PID controller is a common type of feedback controller. It is furthermore used when a good transient response is desired. The integral term eliminates any steady-state error, while the derivative action fives a fast response without the output becoming oscillatory. The disadvantage of the PID controller is that the derivative action is susceptible to noise on the error signal.

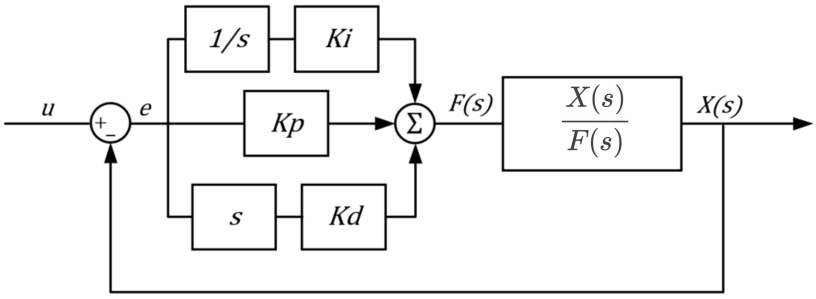

Figure B.6: PID-controller block diagram

B.2.4. The characteristics of the P, I and D terms

There are four major characteristics of a closed-loop step response:

1. **Rise time**: the time it takes for the plant output y to become larger than 90% of the setpoint for the first time.
2. **Overshoot**: the difference between the peak level and steady-state, normalised against the steady-state.
3. **Settling time**: the time it takes for the system to reach its steady-steate.
4. **Steady-state error**: the difference between the steady-state and the setpoint.

A higher value for K_p has the effect of increasing the control signal proportionally for the same level of error. The controller will compensate more for a given level of error causes the closed-loop system to react faster, but also to overshoot more. Besides that, K_p reduces, but not eliminate, the steady-state error. The addition of K_d term to a controller, adds the ability of the controller to 'anticipate' error. This anticipation adds damping to the system, thereby decreasing overshoot. K_d has no effect on the steady state error. The addition of K_i helps to reduce the steady-state error. In case of a persistent steady state error, the integrator increases the control signal over time and driving the error down. A disadvantage of the integral term is that it can make the system more sluggish; when the error signal changes sign, it sometimes takes some time for the integrator to 'unwind'.

A summary of the general effect of each controller parameter (K_p, K_d and K_i) on a closed-loop system can found in Table B.1. Note, these guidelines hold a most cases, but not all. To investigate the effect of turning the individual gains, one has to do more analysis, or have to perform testing on the actual system.

Table B.1: all parameters and equations needed for the EOM of a floating crane vessel

Response	Rise time	Overshoot	Settling time	S-S error
K_p	Decrease	Increase	Small change	Decrease
K_i	Decrease	Increase	Increase	Decrease
K_d	Small change	Decrease	Decrease	No change

B.3. PID tuning

B.3.1. PID pole placement algorithm

Fossen suggests the PID pole placement algorithm when tuning a PID controller for a linear mass-damper-spring system ($m\ddot{x} + d\dot{x} + kx = 0$). When a PID-controller (Equation B.2), is added to a mass-damper-spring system, the closed loop system in Equation B.3 is found. For simplicity, $K_i = 0$ is assumed.

$$m\ddot{x} + (d + K_d)\,\dot{x} + (k + K_p)\,x = 0 \tag{B.3}$$

The natural frequency (ω_n) and damping ratio (ζ) of this system are therefore:

$$\zeta = \frac{d + K_d}{2m\omega_n}, \quad \omega_n = \sqrt{\frac{k + K_p}{m}} \tag{B.4}$$

To specify the controller parameters, the following six steps of the pole placement algorithm can be used [15]:

1. Specify the bandwidth $\omega_b > 0$ and the relative daming ratio $\zeta > 0$
2. Compute the natural frequency with

$$\omega_n = \frac{1}{\sqrt{1 - 2\zeta^2 + \sqrt{4\zeta^4 - 4\zeta^2 + 2}}}\omega_b, \tag{B.5}$$

   (ζ = 0: not damped, ζ < 1: under damped, ζ = 1: critical damped, ζ > 1: over damped).
3. Specify the gain: $K_m \geq 0$
4. Compute the P gain:

$$K_p = m + \omega_n^2 - k \tag{B.6}$$

5. Compute the D gain:

$$K_d = 2\zeta\omega_n m - d \tag{B.7}$$

6. Compute the I gain:

$$K_i = \frac{\omega_n}{10} K_p \tag{B.8}$$

A linear mass-spring-damper system is given by:

$$m\ddot{x} + d\dot{x} + kx = 0 \tag{B.9}$$

this system is equivalent to:

$$\ddot{x} + 2\zeta\omega_n\dot{x} + \omega_n^2 x = 0 \tag{B.10}$$

where the relative damping ratio (ζ) and the natural frequency (ω_n) are defined as:

$$2\zeta\omega_n = \frac{d}{m}, \quad \omega_n^2 = \frac{k}{m} \tag{B.11}$$

From Equation B.11, Fossen[15] derived the linear damping formulae for a mass-damper-spring system:

$$d = 2\zeta\sqrt{km}, \quad \zeta = \sqrt{1 - r^2} \tag{B.12}$$

Where r a reduction factor denoting the ratio between the natural frequency (ω_n) and the frequency (ω) of the linearly damped system. According to Fossen, marine craft commonly have a reduction of 0.5% in the natural frequency (thus r=0.995). This formula can be used to determine the linear damping in heave, roll and pitch of a marine vessel. Linear damping for surge, sway and yaw can be determined with different equation, since this is a mass-damper system:

$$d = \frac{m}{T} \tag{B.13}$$

T is defined as the time constant. A step response can be used to estimate the numerical value.

B.3.2. Ziegler Nichols Tuning

Ziegler and Nichols [51] provided a technique for tuning the PID gains for a large class of industrial system. The method proposed rules for determining values of proportional gain K_p, integral time T_i, and derivative time T_d based on the transient response characteristic of a given plant. Ziegler and Nichols provided two methods, a step response method and a frequency response method. These procedures are nowadays accepted as standard in control system practice.

The transfer function of PID controller is found by taking the Laplace transform of Equation B.2:

$$C(s) = K_p + \frac{K_i}{s} + K_d s \tag{B.14}$$

which can be rewritten to

$$C(s) = K_p \left(1 + \frac{1}{T_i s} + T_d s\right) \tag{B.15}$$

where T_i is the reset time (=$\frac{K_p}{K_i}$) and T_d is the rate time or derivative time.

The reset time is the time used by the integrator term output to equal the proportional term output due to a step change in input applied to a PI-controller [10].

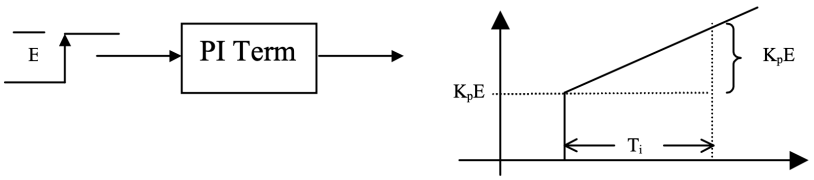

Figure B.7: reset time [10]

The rate time is the amount of time used by a proportional term output in response to a ramp change input applied to a PD-controller.

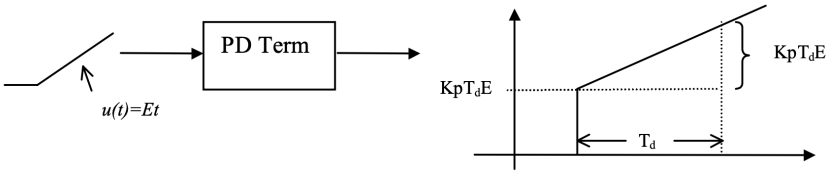

Figure B.8: rate time [10]

The first method

The first method is applied to plants with responses illustrated in Figure B.9.

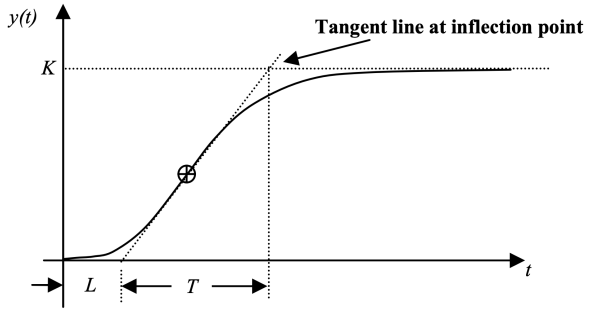

Figure B.9: Response Curve for Ziegler-Nichols First Method [10]

This is typical first order system response with a delay. This type of response is characterised by two parameters, the delay time (L) and the time constant (T). Both parameters are found by drawing a tangent to the step response at its point on inflection and noting its intersections with the steady-state values and the time axis. The plant model is given by Equation B.16.

$$G(s) = \frac{Ke^{-sL}}{Ts+1} \tag{B.16}$$

The control parameters are given in Table B.2. The values in the table were obtained based on many simulations and experiments. Tuning, i.e. substituting Table B.2 in Equation B.15, the PID-controller

Table B.2: Ziegler-Nichols Recipe – First Method

PID type	K_p	$T_i = K_p/K_i$	$T_d = K_d/K_p$
P	T/L	∞	0
PI	$0.9T/L$	L/0.3	0
PID	$1.2T/L$	2L	$0.5L$

by the first method of Ziegler and Nichols gives the following transfer function:

$$\begin{aligned} G_{c1}(s) &= K_p\left(1 + \frac{1}{T_i s} + T_d s\right) \\ &= 1.2\frac{T}{L}(1 + \frac{1}{2Ls} + 0.5Ls) \\ &= 0.6T\frac{(s+\frac{1}{L})^2}{s} \end{aligned} \tag{B.17}$$

Second method
The second method proposed by Ziegler and Nichols targets plants that can be rendered unstable under proportional control. The desired result of this technique is a closed loop system with 25% overshoot. In reality, this results is rarely achieved since Ziegler and Nichols determined the adjustments based on a specific plant model. Using the second method, the values for K_p, T_i and T_d are set according to Table B.3, where K_{cr} and P_{cr} are the critical gain and critical period, respectively.

Table B.3: Ziegler-Nichols Recipe – Second Method

PID type	K_p	$T_i = K_p/K_i$	$T_d = K_d/K_p$
P	$0.5K_{cr}$	∞	0
PI	$0.45K_{cr}$	P_{cr}/1.2	0
PID	$0.6K_{cr}$	$P_{cr}/2$	$P_{cr}/8$

Tuning, i.e. substituting Table B.3 in Equation B.15, the PID-controller by the second method of Ziegler and Nichols gives the following transfer function:

$$\begin{aligned} G_{c2}(s) &= K_p\left(1 + \frac{1}{T_i s} + T_d s\right) \\ &= 0.6K_{\text{cr}}\left(1 + \frac{1}{0.5P_{\text{cr}}s} + 0.125P_{\text{cr}}s\right) \\ &= 0.075K_{\text{cr}}P_{\text{cr}}\frac{\left(s+\frac{4}{P_{\text{cr}}}\right)^2}{s} \end{aligned} \tag{B.18}$$

C

Tugger line materials

According to Dokkum[13], high grade cables, polyamide, polyester, polyolefines and steel wire ropes are cable types that are commonly used on ships.

High-grade cable
High Module Poly-Ethylene (HMPE) and Aramide are high grade cables. Based on weight, aramide is 5 times a strong as steel. It is also a very stiff material, it hardly creeps and is fire resistant. The difference between the 2 materials is that aramide sinks, where HPME floats. Strength wise high grade cables are comparable to steel. The price is however 5-10 time higher than steel cables. The advantages of high grade cables compared to steel cables are: light weight, low elasticity, easy to handle, small backlash and non-conductive.

Polyamide
Polyamide, better known as nylon is a dense material and absorbs water after being in contact with water a few days. This significantly ($\approx$ 20%) reduces the minimum breaking force of the material. Finally, polyamide has a large elasticity which can cause unwanted backlash.

Polyester
A material which is very resistant to wear and is very durable in both wet and dry conditions. The mechanical properties of this material resemble polyamide, except that it is more resistant to wear. Furthermore, the material is more expensive, has a higher density and the energy absorbing capacity is lower compared to polyamide. The high energy absorbing capacity of polyamide is therefore often used as shock absorber, to protect steel cables from large shocks.

Polyolefines
Polyolefine rope are mixtures of the compounds polypropylene and polyethylene. The advantages of this type of cable is that its relatively cheap and light. The material is on the other hand not very resistant to war, has a low TCLL-value and a short life span.

Steel wire ropes
Steel wire ropes are strong, cheap and have little elongation under tension, have a high wear resistance. The downsides of these ropes is that they are heavy and they rust. These cables are made of a number of strands, turned in a long spiral around the core. The strands are usually galvanised, but untreated steel wires also exist. For special purpose stainless steel is used. Regular greasing of these types of wires is essential.

D

Figures

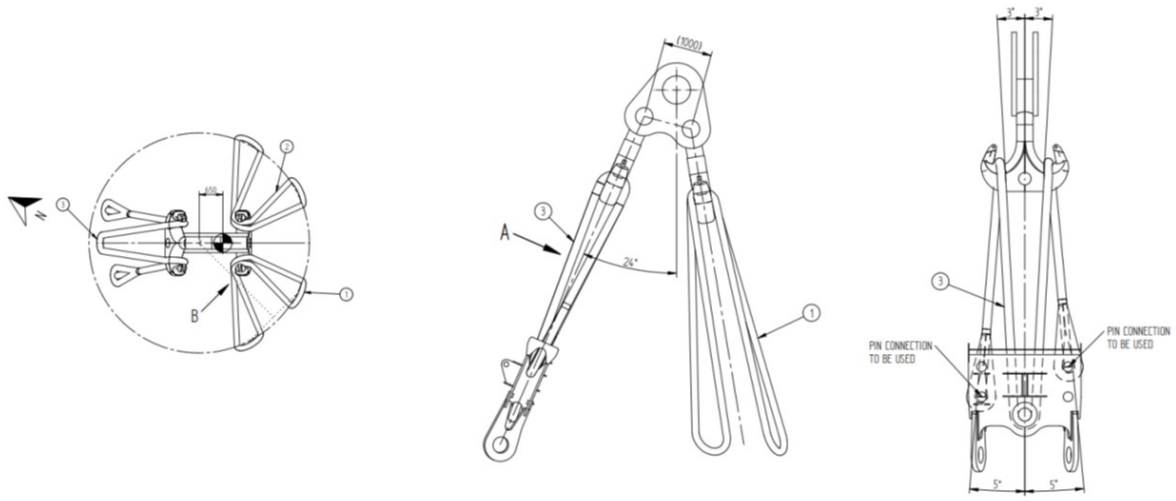

Figure D.1: Rigging schematic [8]

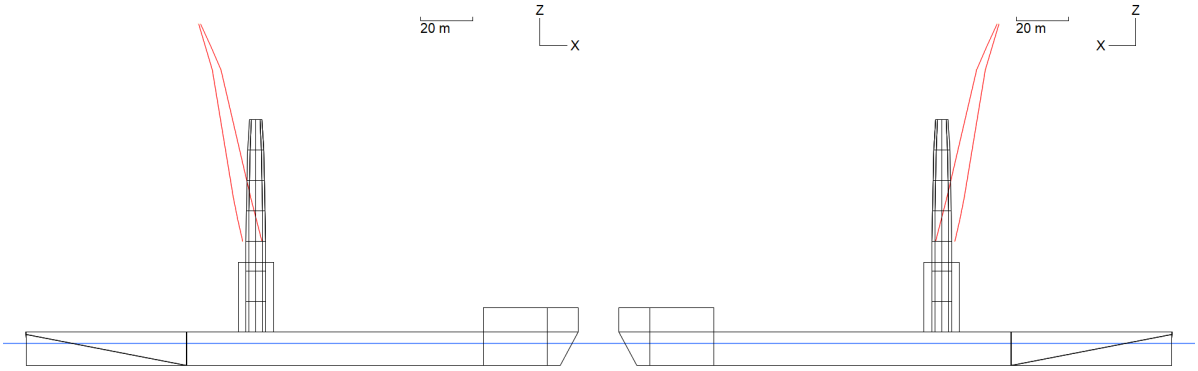

(a) Side view (positive y)

(b) Side view (negative y)

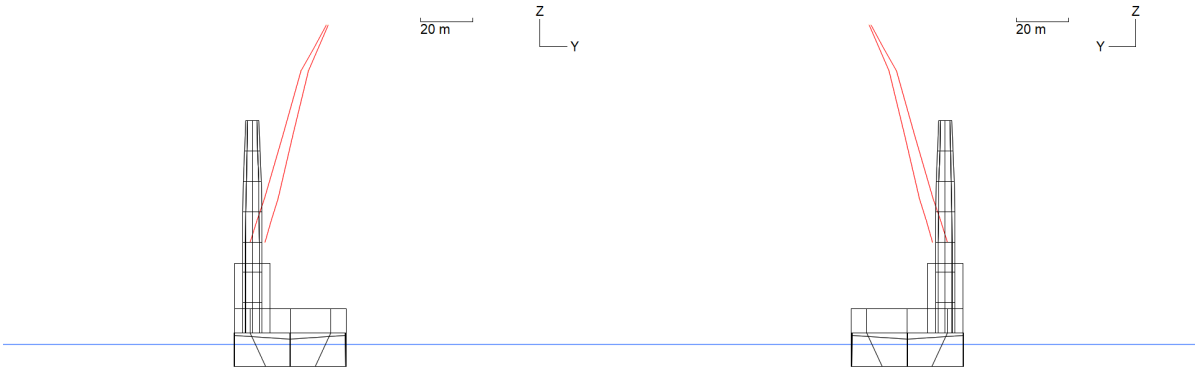

(c) Front view

(d) Back view

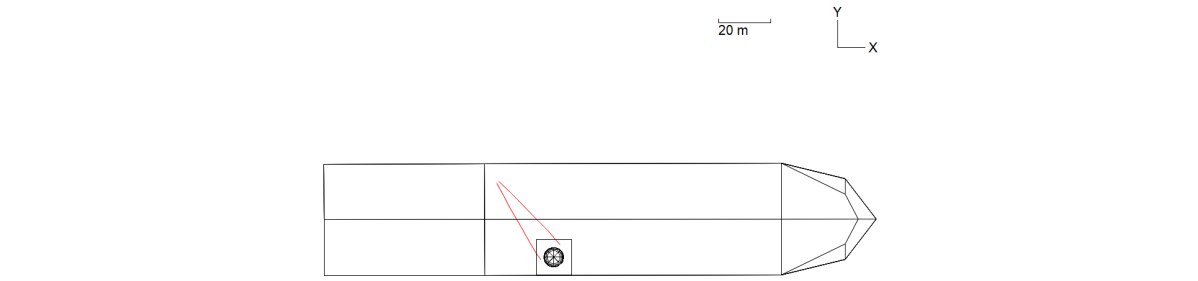

(e) Top view

Figure D.2: Different views of the Bokalift 1

E

Derivation of Equation 5.1

The power function is given by the following function:

$$T = \frac{-P_{max}}{u} \tag{E.1}$$

where the tension-velocity profile is given by:

$$T = \underbrace{\frac{A}{R}}_{\text{Slope}} u + T_d \tag{E.2}$$

First, the expression is given for which the functions are equal to each other (i.e. Equation E.1 = Equation E.2):

$$-\frac{P_{max}}{u} = \frac{A}{R}u + T_d \quad \longrightarrow \quad \frac{A}{R} = -\frac{P_{max}}{u^2} - \frac{T_d}{u} \tag{E.3}$$

To find the maximum slope of the tension velocity profile which prevents the tension velocity slope of exceeding the power limits, the derivative of the power function should be equal to the slope of the tension-velocity profile. Taking the derivative of Equation E.1 results in:

$$T' = \frac{P_{max}}{u^2} \tag{E.4}$$

Substituting Equation E.4 in Equation E.2 one obtains the following equation:

$$T = \frac{P_{max}}{u} + T_d \tag{E.5}$$

setting the above equation equal to Equation E.1, the winch velocity for which the slope of Equation E.1 and Equation E.2 are equal is found:

$$-\frac{P_{max}}{u} = \frac{P_{max}}{u} + T_d \quad \longrightarrow \quad u = -\frac{2P_{max}}{T_d} \tag{E.6}$$

Substituting this equation into Equation E.3, one obtain the minimum slope which ensures the tension-velocity profile does not exceeds the power limit:

$$\frac{A}{R} = \frac{T_d^2}{4P_{max}} \tag{E.7}$$

Because the slope is the inverse of the proportional gain of the damping control scheme (see Equation 2.16), the minimum proportional gain is given by:

$$k_{P,T} = \frac{4P_{max}}{T_d^2} \tag{E.8}$$

F

Equipment Sheet Bokalift 1

Boskalis

EQUIPMENT SHEET

BOKALIFT 1
TRANSPORTATION & INSTALLATION VESSEL

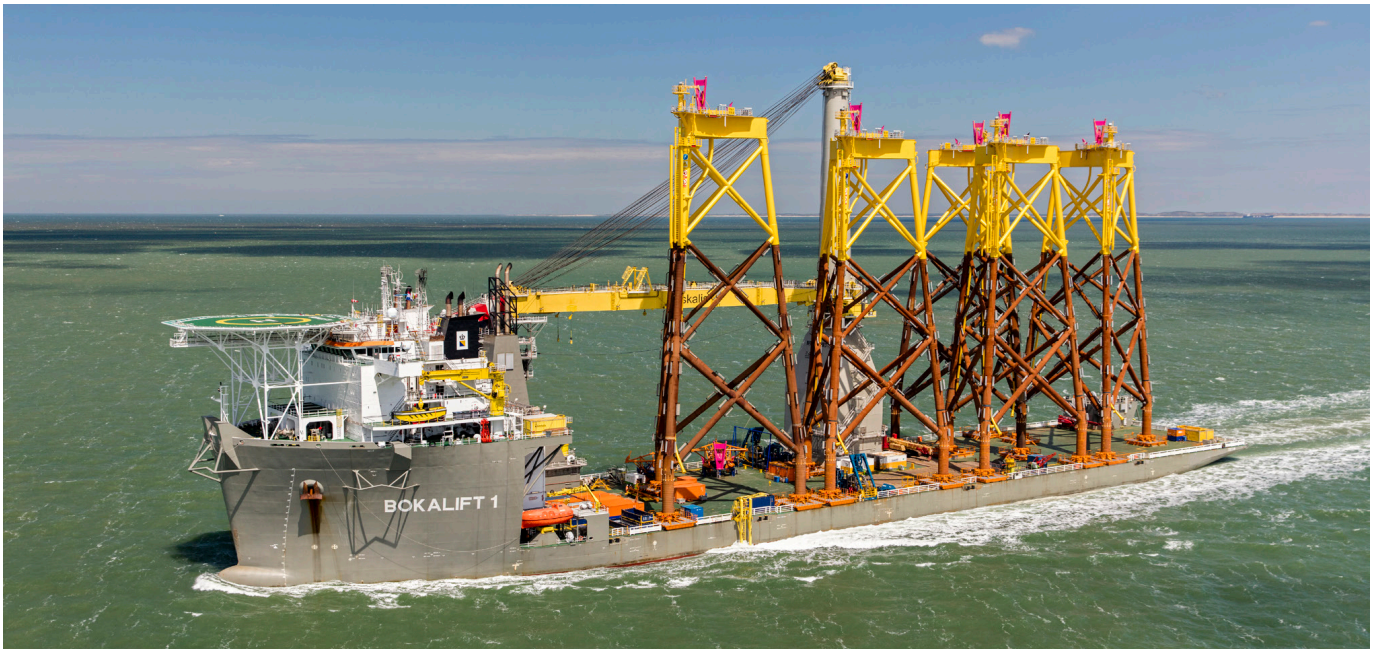

CONSTRUCTION / CLASSIFICATION

Vessel built by	Keppel Singapore 2017
Year of conversion	2017
Classification	BV | ✠ Hull ✠ Mach, Cleanship Ice, Class 1D
IMO	9592850
Call sign (flag)	5BVH4 (Cyprus)

FEATURES

Accommodation	150 persons SPS compliant
Main crane	Huisman OMC 3,000 t
Cargo deck: Size Rated Max deck load	 6,300 m^2 25 t/m^2 15,000 t
Max. transit speed	12.5 kn
Store crane	2 x 30 t at 10 m radius 20 t at 16.5 m radius
Air draft	85 m
Helideck	Suitable for S-61N and S-92 max take-off weight: 12.8 t

MAIN VESSEL DATA

DP system	Kongsberg DP-2
Reference systems	DGPS, HiPaP
Length overall	216 m
Breadth	43 m
Depth moulded	13 m
Operating draft	8.0 - 9.0 m
Installed power	
Main engines	4 x 3,840 kW, 2 x 4,800 kW
Auxiliary engine	1,110 kW

PROPULSION

Main sailing	2 x 5,250 kW
Retractables	4 x 3,500 kW
Bow thrusters	2 x 1,200 kW
Mooring system	Optional 8-point mooring system
Ballast capacity	2 x 1,500 m^3/hr
Anti-heeling system	8 x 2,000 m^3/hr

Boskalis

BOKALIFT 1 - WITH STANDARD BOOM
TRANSPORTATION & INSTALLATION VESSEL

MAIN CRANE
LIFTING CAPACITY

Main block	3,000 t up to 28 m radius 800 t up to 72 m radius
Auxiliary hoist	1,200 t up to 50 m radius 600 t up to 81 m radius
Whip hoist (double fall)	200 t up to 92 m radius
Whip hoist (single fall)	80 t up to 94 m radius

LIFT HEIGHT ABOVE DECK

Main block	90 m at 30 m radius
Auxiliary block	99 m at 35 m radius

DEPTH RANGE

Auxiliary block	1,128 t at 230 m water depth 330 t at 900 m water depth
Whip hoist	Single line 1,900 m water depth

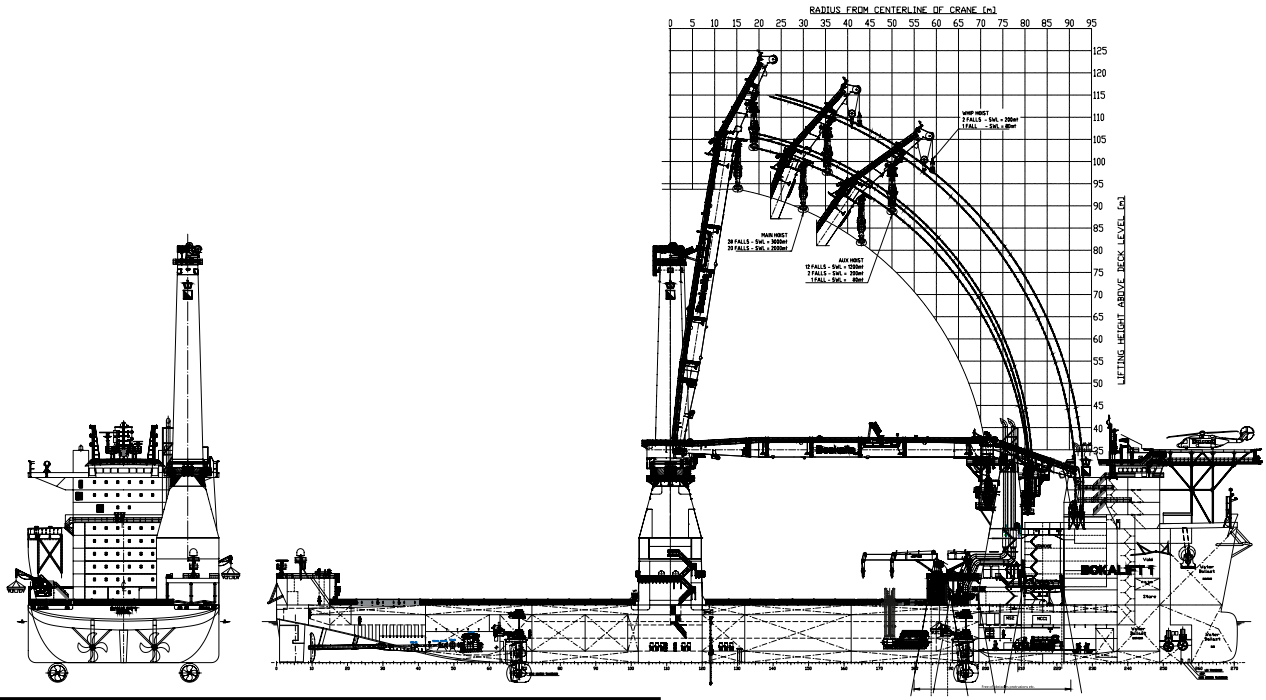

SIDE VIEW

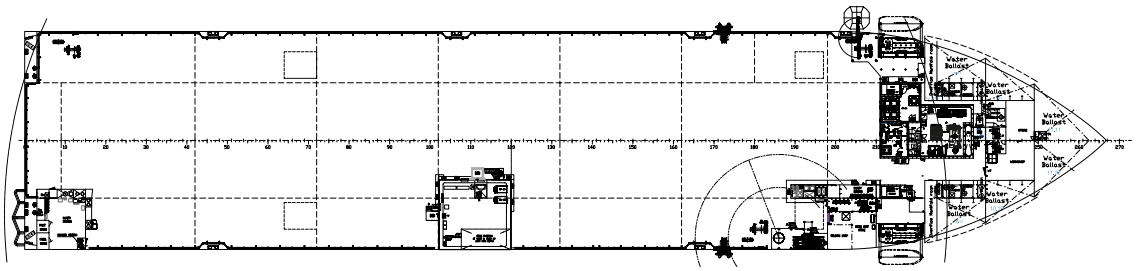

TOP VIEW

Boskalis
PO Box 43
3350 AA Papendrecht
The Netherlands
T +31 78 69 69 000
offshore.energy@boskalis.com

www.boskalis.com/offshore

Boskalis

BOKALIFT 1 - WITH LONG BOOM
TRANSPORTATION & INSTALLATION VESSEL

MAIN CRANE
LIFTING CAPACITY

Main block	2,300 t up to 28 m radius
	600 t up to 92 m radius
Whip hoist (double fall)	200 t up to 101 m radius
Whip hoist (single fall)	80 t up to 103 m radius

LIFT HEIGHT ABOVE DECK

Main block	113 m at 21 m radius 107 m at 35 m radius
Whip hoist	124 m at 24 m radius

DEPTH RANGE

Whip hoist	Single line 1,900 m water depth

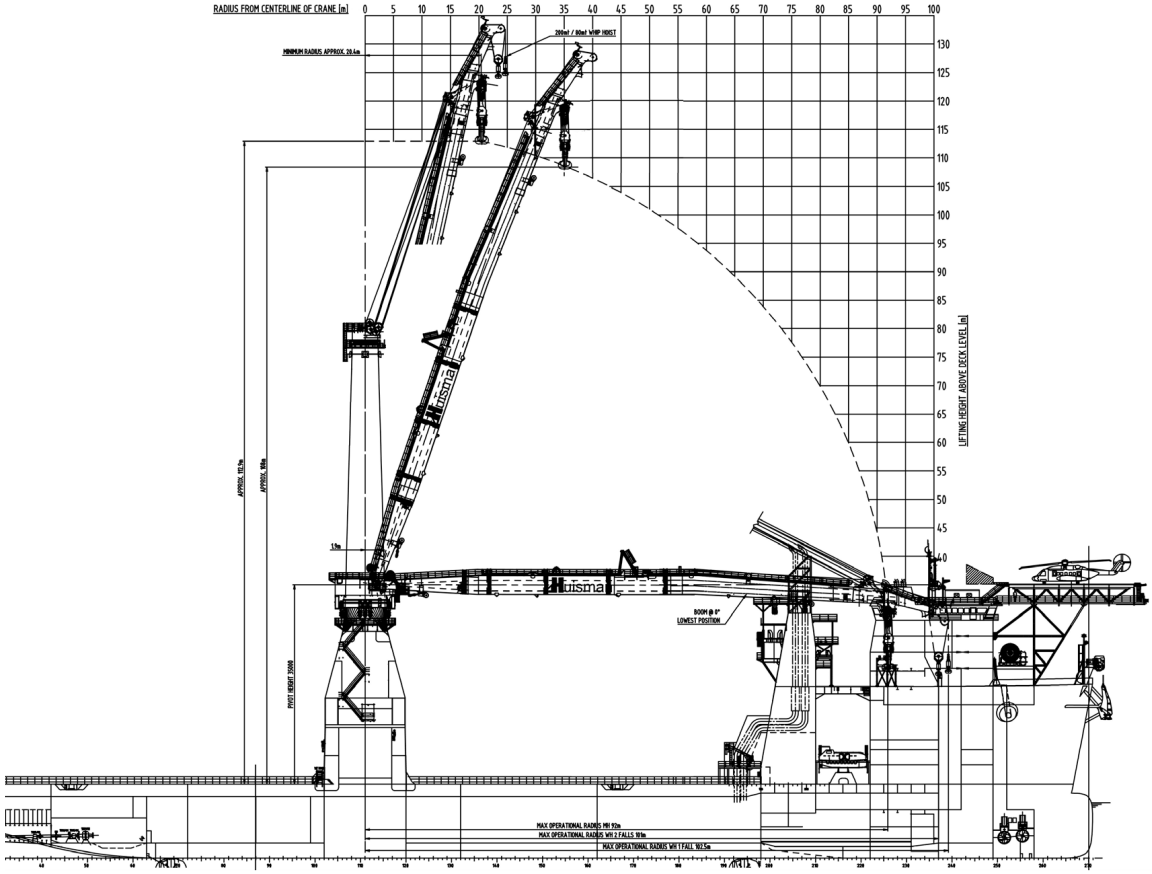

SIDE VIEW

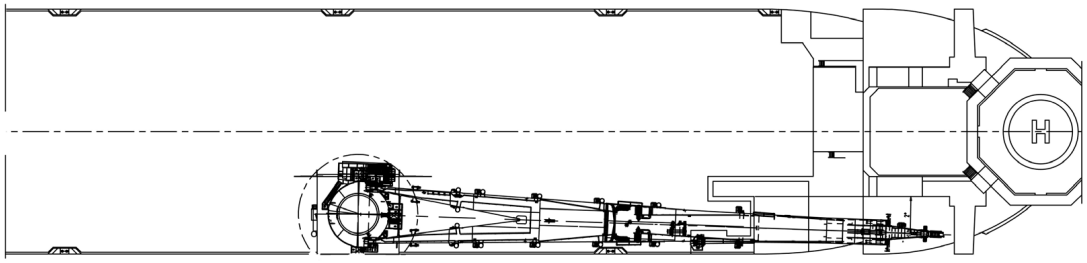

TOP VIEW

Boskalis
PO Box 43
3350 AA Papendrecht
The Netherlands
T +31 78 69 69 000
offshore.energy@boskalis.com

www.boskalis.com/offshore